

FUNCTIONALIZED GRAPHENE: CHARACTERIZATION AND MECHANICAL
REINFORCEMENT

by

Brandon Gene Henderson, A.A., B.S., M.S.

A dissertation submitted to the Graduate Council of
Texas State University in partial fulfillment
of the requirements for the degree of
Doctor of Philosophy
with a Major in Materials Science, Engineering, and Commercialization
August 2015

Committee Members:

Gary W. Beall, Chair

William J. Brittain

Christopher P. Rhodes

Clois E. Powell

Mary S. Spaeth

COPYRIGHT

by

Brandon Gene Henderson

2015

FAIR USE AND AUTHOR'S PERMISSION STATEMENT

Fair Use

This work is protected by the Copyright Laws of the United States (Public Law 94-553, section 107). Consistent with fair use as defined in the Copyright Laws, brief quotations from this material are allowed with proper acknowledgment. Use of this material for financial gain without the author's express written permission is not allowed.

Duplication Permission

As the copyright holder of this work I, Brandon Gene Henderson, authorize duplication of this work, in whole or in part, for educational or scholarly purposes only.

ACKNOWLEDGEMENTS

I would like to thank Dr. Gary Beall for mentoring me during my graduate studies. His patience and insights have been invaluable to me and I am indebted to him for his constant help and guidance. I am grateful to have had him as my mentor. I would also like to thank Dr. Clois Powell for all his help. He would say he's just doing his job but the dedication with which he performs it and willingness to discuss a wide variety of subjects has been critical in helping me develop a deeper level of understanding. I would like to thank Dr. Christopher Rhodes for taking the time to discuss issues, ideas, and solutions with me. I would like to thank Dr. William Brittain for taking the time to be on my committee and give his input. Dr. Mary Spaeth also has my gratitude for providing valuable advice and input. I would like to the members of the Beall research group, past and present, with whom I've worked for their help and assistance.

My greatest thanks go, of course, to my wife Ana. She has been supportive, patient, and encouraging. I would like to thank and recognize my parents who have always believed in me and encouraged me. I won't ever be able to repay their kindness and sacrifice. I would like to thank my grandmother, Muggie, who also has helped me all my life. I would like to offer my thanks to my brother and my sister for their support and encouragement. Finally, I would like to dedicate this accomplishment to my daughter, Brianna. Maybe someday you will read this and I want you to know I love you. You and our family are the most important things in my life.

TABLE OF CONTENTS

	Page
ACKNOWLEDGEMENTS	iv
LIST OF TABLES	viii
LIST OF FIGURES	ix
ABSTRACT	xii
CHAPTER	
1: INTRODUCTION.....	1
1.1 Introduction.....	1
1.2 Review of Literature	7
1.2.1 Epitaxial growth on Silicon Carbide	7
1.2.2 Chemical Vapor Deposition on Metals	9
1.2.3 Synthesis via Polycyclic Aromatic Hydrocarbons.....	11
1.2.4 Micromechanical Cleavage	12
1.2.5 Solvent-based Exfoliation	12
1.2.6 Exfoliation via Intercalation Compounds	13
1.2.7 Electrochemical Exfoliation.....	14
1.2.8 Arc Discharge	15
1.2.9 Exfoliation of Graphite Oxide.....	16
1.2.9.1 Structure of Graphite Oxide	16
1.2.9.2 Chemical Reduction of Graphite Oxide	18
1.2.9.3 Photocatalytic Reduction of Graphite Oxide.....	19
1.2.9.4 Electrochemical Reduction of Graphite Oxide	20
1.2.9.5 Solvothermal Reduction of Graphite Oxide	20
1.2.9.6 Thermal Annealing of Graphite Oxide.....	21
1.2.9.7 Microwave and Photo-Irradiation of Graphite Oxide	23
1.2.10 Commercial Outlook for Graphene and Graphite Oxide	
Production Methods.....	23
1.2.10.1 Commercial Outlook for Graphene from Epitaxial Growth on SiC	24
1.2.10.2 Commercial Outlook for Graphene from CVD.....	24
1.2.10.3 Commercial Outlook for Graphene from Liquid-phase and	
Thermal Exfoliation	25
1.3 Dissertation Efforts	26
1.4 Technical Relevance	27

2: EXPERIMENTAL METHODS	29
2.1 Materials Used	29
2.2 Equipment Used.....	29
2.3 Preparations and Methods.....	30
2.3.1 Preparation of SEM samples.....	30
2.3.2 Preparation of AFM samples	30
2.3.3 Preparation of FTIR samples	30
2.3.4 Preparation of XPS samples.....	31
2.3.5 Preparation of Raman samples.....	31
2.3.6 Preparation of Humic Acid	31
2.3.7 Extrusion of HA-PS Nanocomposites.....	31
2.3.8 Extrusion of HA-MAfPP Nanocomposites.....	32
2.3.9 Injection Molding of HA-PS Nanocomposites	32
2.3.10 Injection Molding of HA-MAfPP Nanocomposites	33
2.3.11 Solvent Casting FG-PU Nanocomposites	33
2.3.12 DMA of PS and HA-PS Nanocomposites.....	34
2.3.13 DMA of MAfPP and HA-MAfPP Nanocomposites	34
2.3.14 DMA of PU and PU/-FG Nanocomposites.....	35
3: RESULTS AND DISCUSSION	36
3.1 Characterization of Functionalized Graphene	36
3.1.1 SEM of FG.....	36
3.1.2 AFM of FG.....	37
3.1.3 FT-IR of FG and HA.....	38
3.1.4 Raman of FG and HA	39
3.1.5 XPS of FG and HA	42
3.2 Characterization of Polymers and Nanocomposites	44
3.2.1 DMA of MAfPP and HA-MAfPP Nanocomposites	44
3.2.2 DMA of PS and HA-PS Nanocomposites.....	45
3.2.3 DMA of PU and FG-PU Nanocomposites.....	47
3.2.4 XRD of HA	51
3.2.5 XRD of FG and PU	53
4: CONCLUSIONS	56
4.1 Summary.....	56
4.2 Future Work.....	57

APPENDIX SECTION.....	59
REFERENCES	97

LIST OF TABLES

Table	Page
1: Weight and volume of PU and FG solutions used.....	33
2: Mechanical reinforcement of polymer-graphene nanocomposites.....	50
3: Abbreviations and Definitions.....	59
4: Calculations of average storage modulus and standard deviation in MAfPP and HA-MAfPP samples.....	66
5: Calculations of average storage modulus and standard deviation in PS and HA-PS samples.....	73
6: Calculations of average storage modulus and standard deviation in PU and FG-PU samples.....	84
7: Variables used in Halpin-Tsai Equation with references.....	85

LIST OF FIGURES

Figure	Page
1: Direction that stress is applied in compression, tensile, and shear testing.	2
2: Graph of sinusoidal stress function and strain function for an ideal elastic material, ideal viscous material, and viscoelastic material.	3
3: Graphical representation of Bernal (A-B) stacking of two sheets of graphene.	9
4: The Lerf-Klinowski model of the structure of graphene oxide.	17
5: Scholz-Boehm model of GO.....	17
6: Structure of GO proposed by Dekaney and colleagues.	18
7: SEM image of FG.....	36
8: SEM image of FG.....	37
9: AFM of FG sheet.	38
10: FT-IR of FG and HA.	39
11: Raman spectrum of HA.	40
12: Raman spectrum of FG.....	40
13: XPS of the C1s region for HA and FG.	42
14: XPS of the O1s region for HA and FG.....	43
15: DMA of MAfPP and HA-MAfPP samples.	44
16: Average storage modulus of HA-MAfPP samples at 30° C.....	45
17: DMA of PS and HA-PS samples.	46
18: Average storage modulus of HA-PS samples at 30° C.....	47

19: DMA of PU and FG-PU samples.	48
20: Average storage modulus of FG-PU samples at 30° C.....	49
21: XRD of HA powder.	51
22: XRD of HA, MAfPP, 1.0% HA-MAfPP, and 2.0%HA-MAfPP.....	52
23: XRD of HA, PS, 1.0% HA-PS, and 2.0%HA-PS.....	53
24: XRD of FG powder.....	54
25: XRD of FG and FG-PU samples.	55
26: DMA of neat MAfPP samples.	60
27: DMA results for neat MAfPP showing storage modulus at 30° C.	61
28: DMA of MAfPP - 1.0% HA samples.	62
29: DMA results for MAfPP - 1.0% HA showing storage modulus at 30° C.	63
30: DMA of MAfPP - 2.0% HA samples.	64
31: DMA results for MAfPP - 2.0% HA showing storage modulus at 30° C.	65
32: DMA of neat PS samples.....	67
33: DMA results for neat PS showing storage modulus at 30° C.....	68
34: DMA of PS - 1.0% HA samples.....	69
35: DMA results for PS - 1.0% HA showing storage modulus at 30° C.	70
36: DMA of PS - 2.0% HA samples.....	71
37: DMA results for PS - 2.0% HA showing storage modulus at 30° C.	72
38: DMA of neat PU samples.	74
39: DMA results for neat PU showing storage modulus at 30° C.	75

40: DMA of PU - 0.1% FG samples.....	76
41: DMA results for PU - 0.1% FG showing storage modulus at 30° C.....	77
42: DMA of PU - 0.5% FG samples.....	78
43: DMA results for PU - 0.5% FG showing storage modulus at 30° C.....	79
44: DMA of PU - 1.0% FG samples.....	80
45: DMA results for PU - 1.0% FG showing storage modulus at 30° C.....	81
46: DMA of PU - 2.0% FG samples.....	82
47: DMA results for PU - 2.0% FG showing storage modulus at 30° C.....	83
48: XRD of neat MAfPP.....	86
49: XRD of MAfPP - 1.0% HA sample.....	87
50: XRD of MAfPP - 2.0% HA sample.....	88
51: XRD of neat PS sample.....	89
52: XRD of PS - 1.0% HA sample.....	90
53: XRD of PS - 2.0% HA sample.....	91
54: XRD of neat PU sample.....	92
55: XRD of PU - 0.1% FG sample.....	93
56: XRD of PU - 0.5% FG sample.....	94
57: XRD of PU - 1.0% FG sample.....	95
58: XRD of PU - 2.0% FG sample.....	96

ABSTRACT

Polymer nanocomposites with better performance and lower cost are in constant demand. One of the challenges inherent in this field is balancing these two factors. Graphene provides the possibility of producing high performance polymer nanocomposites but is too expensive for adoption in a variety of commercial applications. Currently, oxidation of graphite followed by reduction is the most cost effective method for providing graphene like material for use in polymer nanocomposites. This method often requires the use of organic solvents, which are expensive and harmful, or surfactants, which are not easily removed and affect the properties of the resulting material. The results shown here demonstrate that functionalized graphene, derived from humic acid, provides mechanical reinforcement in polymer nanocomposites. This provides a novel source for graphene-like material and eliminates the need for an oxidative step currently used to exfoliate graphite. Functionalized graphene has properties similar to that of graphene including being atomically thin. It also has the compatibility necessary for inclusion in a water dispersible polyurethane matrix. Functionalized graphene was well dispersed in these systems and provided storage modulus mechanical reinforcement of 150% at 1.0% loading which is higher than the level of reinforcement reported in comparable materials. This level of storage modulus mechanical reinforcement would require a 4% loading level of montmorillonite nanoclay to get an equivalent amount of reinforcement and is 45% of the storage modulus reinforcement predicted with the Halpin-Tsai theoretical model.

CHAPTER 1: INTRODUCTION

1.1 Introduction

There is a constant demand for new materials that have better properties and lower cost. Nanocomposites are answering these demands by providing a lightweight material with corrosion resistance, high fatigue strength, and facile processibility.¹ They are used in multiple commercial applications including aircraft components, electronic packaging, medical equipment, and home building materials.² Nanocomposites are blends of two materials with distinct structure-property relationships. Each material in the nanocomposite retains its separate identity but they work in combination to give bulk nanocomposite material characteristics with synergistic properties of each individual material. Polymer nanocomposites have discrete phases consisting of a polymer matrix phase and at least one dispersed phase. The matrix phase is sometimes referred to as the primary phase because it is continuous and encases the dispersed phase. In polymer nanocomposites it is usually the less hard phase. The dispersed phase is embedded in the matrix phase and is discontinuous. In polymer nanocomposites it is usually stronger than the matrix phase and, for this reason, is sometimes referred to as the reinforcing phase.¹

The strength of a material is how well it withstands an applied stress without failing. Adding a reinforcing phase to a nanocomposite increases the strength or toughness of a material by providing mechanical reinforcement. Mechanical reinforcement can be described in various terms depending on what kind of stress is applied to the material. Examples of direction that stress may be applied are shown in Figure 1 which shows compressive, tensile, and shear stresses.

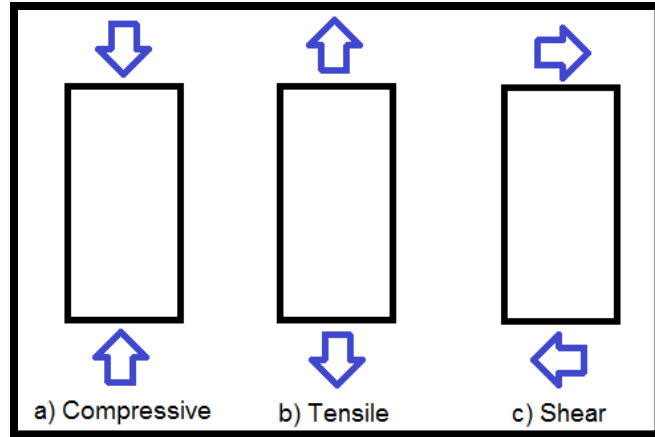


Figure 1: Direction that stress is applied in compression (a), tensile (b), and shear (c) testing.

Modulus is the term used to describing how well a material resists deformation under an applied stress. How well a material resists deformation under compressive stress is called the compressive modulus, under tensile stress is called tensile modulus or Young's modulus, and under shear stress is called shear modulus. Materials also have storage and loss moduli which are useful for evaluating mechanical reinforcement of a reinforcing phase in a nanocomposite material. Storage and loss moduli are properties of viscoelastic materials. They can be measured by placing a sample in several configurations, including tensile and/or single cantilever configurations, in a dynamic mechanical analysis (DMA) instrument. The DMA applies stress and releases the stress in an oscillatory, sinusoidal manner. If the strain of the sample occurs in phase with the applied stress the material is exhibiting an elastic response. If the strain of the sample lags the applied stress at an angle of 90° the material is exhibiting a viscous response. Most materials have elastic and viscous behavior as a function of temperature. Graphs of sinusoidal stress functions plotted with strain functions corresponding to elastic, viscous, and viscoelastic properties are shown in Figure 2.

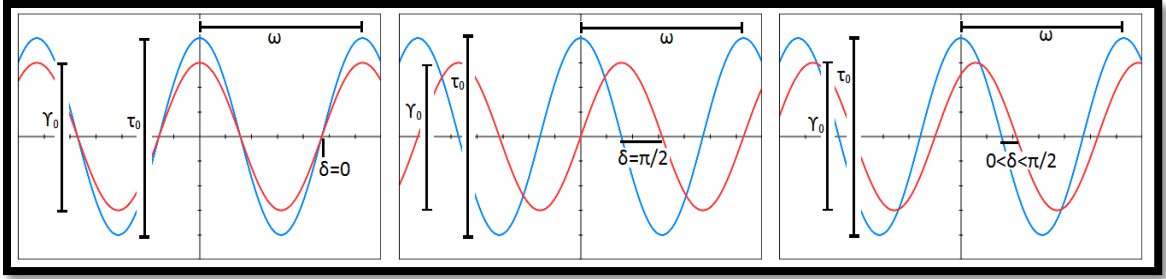


Figure 2: Graph of sinusoidal stress function (blue) and strain function (red) for an ideal elastic material (left), ideal viscous material (middle) and viscoelastic material (right). Time is represented on the horizontal axis and amplitude is represented on the vertical axis.

In Figure 2 the amplitude of the dynamic stress function is τ_0 , the amplitude of the shear strain function is γ_0 , the imposed oscillation frequency is ω , and the shift angle between the dynamic stress function and shear strain function is δ . The response of the material to the stress sine wave yields a complex modulus which is the sum of the elastic (storage) modulus and imaginary (loss) modulus. The storage modulus measures how much energy is stored in a material when stress is applied and the loss modulus measures how much of the energy is lost, most commonly as heat. Adding a dispersed phase to a polymer matrix to increase the storage modulus of the material is one type of mechanical reinforcement and can be used to evaluate and quantify the reinforcement imparted by the dispersed phase. An increase in the storage modulus of a nanocomposite material as compared to the pure polymer is an increase in mechanical reinforcement. DMA is a non-destructive test method that measures modulus as a function of temperature every time a sine wave stress is applied. Thus, the complex modulus as well as the calculated storage and loss moduli of a material can be determined while sweeping across a range of frequencies and/or temperatures.³

The magnitude of mechanical reinforcement in a nanocomposite material depends on many factors including the morphology of the dispersed phase, dispersed phase/matrix

phase interfacial interaction, percent loading (often given in weight of dispersed phase/weight of matrix percent or wt/wt %), and properties of the matrix and dispersed phases.⁴ If all other factors are equal then adding a dispersed phase with a higher tensile modulus will increase the tensile modulus of the resulting nanocomposite more than adding a dispersed phase with a lower tensile modulus. In order to produce a nanocomposite material with a high modulus one would want to use a dispersed phase with a high modulus. A common example of this is the use of glass fiber to reinforce polyester resin. The tensile modulus of a typical polyester resin with no reinforcement is ~55 MPa and the tensile modulus of a common (E-type) glass fiber is 80 GPa.⁵ However, when this type of glass fiber is chopped and dispersed in the polyester at a 30% wt/wt loading, the tensile modulus of the resulting fiberglass is ~100 MPa.⁶ If one were to add glass fibers with a higher tensile modulus than E-type glass fibers (e.g. S-type glass fibers, 89 GPa tensile modulus⁵) under the same conditions, the tensile modulus of the resulting fiberglass composite would be higher.⁵

Graphene has the highest tensile modulus of any known material making it an appealing filler for increasing the mechanical strength of polymer nanocomposite materials. Graphene is a single sheet of sp²-hybridized carbon atoms and has a tensile modulus of 1,000 GPa.⁷ The significance of the modulus of graphene may be highlighted by comparing it to the tensile modulus of structural steel (ASTM-A36) which has a tensile modulus of 200 GPa.⁸ Thus, graphene would provide a large increase in mechanical strength in polymer nanocomposites. However, graphene does not have functionalities conducive to favorable matrix-filler interactions. Lack of these favorable interactions not only limit the dispersion of graphene in most polymers, but also prevent

the transfer of applied force from matrix to filler. These are critical to mechanical reinforcement in nanocomposite materials.

Morphology is another important consideration of dispersed phase materials because it affects the degree to which they will interact with the matrix phase. In order to maximize the interfacial interaction between the matrix and dispersed phases the surface area of the dispersed phase should be maximized. Assuming complete exfoliation, a sufficiently low level of loading, and favorable compatibility, a dispersed phase with a higher surface area will interact with a matrix phase more than a dispersed phase with a low surface area. Dispersed phases with a plate like morphology have higher surface areas and higher aspect ratios than dispersed phases of equal volume with a spherical morphology enabling them greater interaction with the matrix phase. The chemical inertness of graphene makes dispersion challenging whereas functionalized graphene has improved interaction with many polymer matrices due to its high surface area and increased compatibility with the polymer matrix. The small dimensions of graphene and functionalized graphene meet the criteria (at least one dimension less than 100 nm)⁹ for them to qualify as nanoparticles and the nanocomposites that incorporate them as a dispersed phase are known as nanocomposites. The high surface area and resulting high interfacial interaction of nanoparticles with matrix phases produce nanocomposites that demonstrate mechanical reinforcement at loading levels as low as 0.5% (wt/wt).

Graphene is often described to be of a certain quality. It is important to note that quality in this sense refers to the degree to which the product resembles a perfect graphene-like structure and not its suitability for a specific use. Higher quality graphene is more useful for some applications while lower quality graphene is better suited to other

applications. Most methods for producing graphene leave some defects and/or functionalities on the material. Therefore, the terms graphene and functionalized graphene (FG) used here refer to similarity of the materials to pristine graphene with the understanding that they bear resemblance to each other, and the point at which one term is more applicable than the other is not well defined.

There have been a variety of ways of making graphene and FG reported. These methods are covered in more detail in Section 2: Review of Literature. All of these methods have drawbacks, the primary one being cost. Currently, exfoliation of graphite is one of the most cost effective techniques of producing one type of FG known as reduced graphene oxide (rGO).¹⁰ There have been multiple methods developed to accomplish this including various methods for the exfoliation of graphite. These exfoliation methods, while capable of mass production, are still rather expensive and require the use of reagents that are difficult to work with and dispose of. Therefore, it would be of economic benefit to develop a method of producing functionalized graphene at a lower cost using reagents more amenable to industrial and commercial use.

Production of rGO on an industrial scale involves two steps. The first step is to oxidize graphite in order to exfoliate it in an appropriate, usually aqueous solution. The second step is a reduction which is usually done via chemical methods. Another starting material recently used to make FG material is humic acid (HA) which is a highly conjugated carbonaceous material that can be suspended in basic aqueous solutions. It is found in soil, coal, and marine environments.¹¹ Using HA as a starting material to prepare FG eliminates the need for an oxidation step.

1.2 Review of Literature

There have been many methods utilized to synthesize graphene and FG. They can be generally divided into two different subgroups. Some methods separate layers of graphite to produce graphene and FG and can be referred to as top-down methods. Other methods utilize a carbon containing source in order to produce graphene and can be referred to as bottom-up methods. Bottom-up approaches include epitaxial growth on silicon carbide, chemical vapor deposition (CVD), and synthesis via polycyclic aromatic hydrocarbons. Top-down approaches include micromechanical cleavage, solvent-based exfoliation, exfoliation via intercalation compounds, electrochemical exfoliation, arc discharge, unzipping carbon nanotubes, and exfoliation of graphite oxide (GO). Each approach will be discussed individually.

1.2.1 Epitaxial growth on Silicon Carbide

In ultrahigh vacuum at around 1000 °C the silicon in silicon carbide (SiC) sublimates causing carbon atoms and their bonds to rearrange resulting in either a single layer or multiple layers of graphene.¹²⁻¹⁴ Formation of graphene starts at the outer layer and continues inward consuming approximately three layers of SiC to form one sheet of graphene.^{15,16} First, a carbon layer is formed that is isostructural with graphene but lacks sp^2 character and is still bonded to silicon atoms in the lower layer. When silicon in the lower layer begins to desorb the upper layer is converted to graphene and carbon in the lower layer is again isostructural with graphene but lacking sp^2 character and bonded to the silicon in the next lower layer.¹⁵ Graphene layers continue to form in this way, slowing with each layer produced. The layers of graphene slow desorption of silicon in

lower SiC layers as the silicon must diffuse to the sample edges or to a defect in graphene (e.g. a grain boundary or pinhole) to escape the layer. Therefore, graphene with fewer defects leads to fewer layers being formed. The quality of graphene grown from SiC can be improved by increasing pressure with an inert gas (e.g. argon) and increasing the temperature to 1450-1500 °C. The improved mobility of the carbon atoms under these conditions enhances the quality of the graphene formed and subsequently limits the number of graphene layers formed to one or two.^{15,17-19} In addition to thermal annealing, pulsed electron irradiation has also been used to promote the preferential sublimation of silicon from SiC.²⁰ Research into epitaxial growth of graphene on SiC has primarily focused on the silicon rich (0001) and carbon rich (000 $\bar{1}$) surfaces of hexagonal silicon of the 4H and 6H polytypes though it has also been demonstrated on cubic phase SiC.²¹⁻²³ The growth mode of graphene on both the silicon and carbon rich faces is the same, however their stacking arrangement is different. Graphene sheets grown on the silicon rich face stack in a Bernal (i.e. A-B) configuration (see Figure 3), whereas, graphene sheets grown on the carbon rich face stack rotationally in layers rotated 30°, or $\pm 2.20^\circ$ with regard to the direction of the SiC on which they are grown. The three orientations are interleaved which results in a high density of fault boundaries between the layers. This causes electronic decoupling of the layers in such a way that the electronic properties of single layer graphene (SLG) are predominant in the stacked system.²⁴

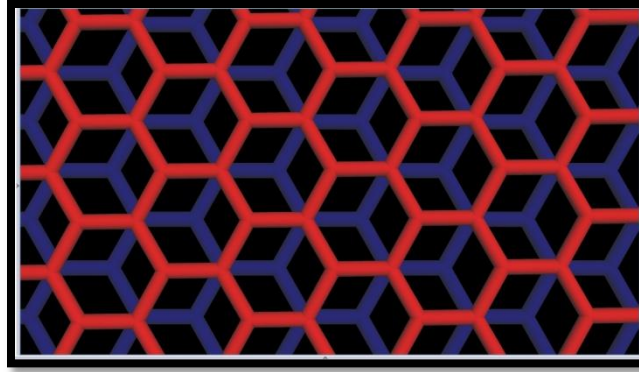


Figure 3: Graphical representation of Bernal (A-B) stacking of two sheets of graphene.

This method of producing graphene is used primarily in electronic applications because it has the advantage of producing conductive graphene on a non-conductive SiC substrate. Graphene produced using this method is of high quality with individual crystallites reaching lateral dimensions in the hundreds of micrometers.²⁵ The demanding conditions required and the cost of SiC wafers are two challenges that must be addressed in order to make this method commercially viable. One possible solution to reduce the temperature required involves applying a thin layer of nickel as a catalyst to promote graphene growth at temperatures in the range of 700-800 °C.²⁶⁻²⁸ The cost of this method may also be reduced by using cheaper cubic SiC as a substrate but research regarding this possibility is still ongoing and has not yet proven effective.¹⁰

1.2.2 Chemical Vapor Deposition on Metals

CVD involves pyrolysis of gases containing carbon, usually at high temperatures. Graphene is produced on various transition metal substrates following pyrolysis. The method of graphene growth proceeds via surface catalysis, segregation effect or some combination of both. In surface catalysis the carbon-containing gas decomposes and graphene formation takes place on the metal surface. This mechanism tends to be self-

limiting because graphene layers deposited on the substrate passivate the surface of the metal. In the segregation mechanism, carbon is dissolved in the bulk metal at elevated temperatures. When the metal is cooled carbon becomes less soluble in the metal and diffuses to the surface forming graphene.²⁹⁻³¹ However, it is difficult to control the number of layers of graphene in the segregation process. This method has significant independent variables that must be controlled including the amount of carbon diffusing into the metal, thickness of the substrate, composition of the substrate, time, and temperature. The type of metal substrate is also an important consideration.³⁰ For example, a nickel (111) substrate with an atomically smooth surface that is a single crystal (i.e. no grain boundaries) tends to produce few layer graphene (FLG) whereas polycrystalline nickel tends to produce layers of graphene (graphite) of variable thickness containing significant levels of imperfections. The grain boundaries act as nucleation sites for the formation of graphene and differences in cooling rates between the crystals produce variations in thickness.³²

CVD has produced graphene on a number of transition metals (Fe,^{33,34} Ru,³⁵ Co,³⁶⁻³⁸ Rh,^{39,40} Ir,^{41,42} Ni,^{32,43-46} Pd,^{47,48} Pt,⁴⁹ Cu,⁵⁰⁻⁵⁶ Au⁵⁷) and metal alloys (Cu-Ni,⁵⁸⁻⁶¹ Au-Ni,⁶² Ni-Mo,⁶³ stainless steel,^{64,65} Mn-Cu⁶⁶). Much of CVD research has focused on copper as a substrate because carbon is insoluble in copper (below 0.001 atomic % at 1000° C⁶¹). This insolubility limits CVD on copper exclusively to the surface catalysis mechanism. Thus, under controlled conditions, CVD on copper can result in a monolayer of layer of graphene. For electronic applications it is often necessary to transfer the graphene sheet(s) to an insulating substrate. Such transfers have been developed^{32,44,51,67}

yet still suffer from issues that must be controlled including grain size, wrinkles, ripples and doping levels.^{10,68}

It has been shown that CVD can be accomplished at lower temperatures (300-600° C) if the carbon source is introduced as a plasma. These methods are known as plasma-enhanced CVD or PECVD. This method has been demonstrated using microwave and radiofrequency excited plasma on substrates including nickel, copper, and stainless steel.⁶⁹⁻⁷² Although this lowers the temperature required for the process, new problems are introduced. The electrical field produced by the interaction of plasma with substrate promotes growth of graphene sheets perpendicular to the substrate.⁷³ It has been demonstrated that this shortcoming may be remedied by moving the plasma generation upstream of the substrate, but the temperature required was increased to 650-750° C.⁷⁴

The commercial viability of this method would be revolutionized if it was able to being applied to arbitrary substrates and/or modified in such a way that it could be applied at low temperatures and produced material with very few defects. If this were achieved it would eliminate the need for a transfer step in the former case, and improve the compatibility of this method with microelectronic technologies in the latter case.¹⁰ Substrate free CVD, which might be suitable for application to an arbitrary surface, has been accomplished in the laboratory but has not demonstrated commercial viability.⁷⁵⁻⁷⁷

1.2.3 Synthesis via Polycyclic Aromatic Hydrocarbons

Synthesis of planar sheets of sp^2 hybridized carbon with lateral dimensions up to ~3.2 nm has been known for some time.⁷⁸⁻⁸⁴ This bottom-up synthetic approach is based on the chemistry of polycyclic aromatic hydrocarbons (PAHs) and ranges from multiple ring molecules up to a structure consisting of 222 carbon atoms (C₂₂₂-PAH).⁸⁴ This

approach is capable of producing sp^2 hybridized ring systems of specific sizes, shapes, symmetries, functionalities, and edges. Molecules consisting of a hybridized core with pendant groups that sterically bend the molecule away from planarity and graphene molecules with zigzag edges have been produced.^{85,86} These structures and PAHs containing heteroatoms show potential for small graphene-like molecules with tunable optoelectronic properties.^{86,87} One problem with this approach is the size of the PAH is limited by a lack of solubility in organic solvents.³¹ This may be remedied to some degree by attaching pendant aliphatic groups but solubility still decreases with the size of the molecule.^{10,88}

1.2.4 Micromechanical Cleavage

This is the first method by which a single sheet of graphene was isolated and characterized and consists of repeatedly peeling apart the graphene sheets in graphite using tape until a single layer is obtained.⁸⁹ It is also known as the ‘scotch tape’ or ‘peel off’ method. This method is capable of producing single-, double-, and few layer graphene (SLG, DLG, and FLG respectively). The SLG, DLG and FLG sheets are of high quality because there is little processing involved. However, the procedure is labor intensive and impractical on a large scale. Therefore, the samples produced by this method are generally limited to research applications for the study of fundamental properties of graphene.^{29,89}

1.2.5 Solvent-based Exfoliation

Graphite is a good source of high quality graphene sheets. Separating the sheets from the bulk is not a simple undertaking and the number of processing steps must be

minimized to produce graphene sheets of higher quality. Solvent-based exfoliation begins with graphite as the starting material and utilizes a solvent to separate the sheets of graphene, thereby minimizing the number of processing steps.⁹⁰ However, sonication is sometimes used to promote separation which reduces the size of the graphene sheets.

An array of solvents and methods have been studied to exfoliate graphite to graphene.⁹¹ It was found that n-methyl pyrrolidone (NMP) gave the most SLG sheets in solution at a weight percent of ~1%.⁹⁰ NMP has a high boiling point (205° C) and is not easily removed following solvation.⁹¹ Other solvents have been evaluated yet none produced as many SLG sheets as NMP. It was, however, found that many solvents produced FLG containing less than five stacked sheets.⁹¹ The probability of this method being used to produce bulk graphene for commercial use is unlikely because of its reliance on organic solvents as well as the additional processing that would be required to separate SLG, DLG, and FLG from each other and the remaining graphite. However, it may provide a viable method for producing high quality graphene for fundamental studies.^{10,31}

1.2.6 Exfoliation via Intercalation Compounds

Exfoliation via graphite intercalation compounds (GICs) has been accomplished by either generating gas to exfoliate graphene sheets or reducing graphene sheets to exfoliate them in solution.^{29,31,88} Thermal expansion is an example of the former and was first reported in 1916 where it was demonstrated that exfoliated graphite could be produced by heating graphite-bromine intercalation compounds.⁹² It was originally referred to as expanded graphite and later exfoliated graphite.^{92,93} Interest in exfoliated graphite increased in the 1960's for use in gaskets, seals, fire extinguisher agents, thermal

insulators, and a variety of other applications.⁹³ This approach has also been reported via intercalation of ionic liquid crystals (ILCs) where heat is used to assist in intercalation of the ILCs (100° C). The material is then heated until gas is produced by ILC decomposition (700° C).⁹⁴ A lower temperature approach (~100° C) has been demonstrated using iron chloride (FeCl₃) and nitromethane (CH₃NO₂). Iron chloride assists in intercalation of nitromethane which is subsequently decomposed via microwave radiation.⁹⁵ Supercritical carbon dioxide (CO₂) has also been used where it is first intercalated and then depressurized, generating gaseous carbon dioxide in the interstices.⁹⁶

Exfoliation of reduced graphene sheets began when ternary compounds consisting of graphite, an alkali metal, and a polar organic solvent were demonstrated in the late 1960's.⁹⁷ It was later shown that tetrahydrofuran (THF) could be reversibly intercalated in graphite that had been reduced with a mixture of potassium and naphthalene.⁹⁸ This led to spontaneous exfoliation of graphite using potassium-based GICs in NMP.⁹⁹

1.2.7 Electrochemical Exfoliation

Due to its electronic structure graphene can act as an electron acceptor (oxidizing agent) and an electron donor (reducing agent) and has both an electron affinity and ionization potential of 4.6 eV.^{88,100} Initial examples of electrochemical exfoliation involved exfoliation of graphene from sacrificial graphite anodes. In one example of this method poly(sodium-4-styrenesulfonate) (PSS) was used as an electrolyte and surfactant with two graphite electrodes.¹⁰¹ The hydrophobic portion of PSS served to interact with the π -orbitals of graphene sheets and the hydrophilic portion stabilized them in water and prevented restacking.¹⁰² However, surfactants are difficult to remove and have been

shown to affect the electrical properties of graphene.^{101,103} In another study, a variety of electrolytes (HBr, HCl, HNO₃, and H₂SO₄) were used in the presence of a graphite anode.¹⁰⁴ It was found that only H₂SO₄-KOH solutions provided adequate efficiency for electrolytic production of graphene.¹⁰⁴ More recently it has been shown that graphene can be exfoliated electrochemically from the cathode with lithium GICs followed by sonication of the expanded electrode.^{105,106} In these studies sonication produces thermal shock followed by ultrasonic cavitation in the interstitial GICs which acts to expand the distance between layers of graphene.¹⁰⁷ Graphite intercalation of a lithium salt in a dimethylformamide-propylene carbonate solution with sonication has been shown to produce >70% FLG exfoliation.¹⁰⁵ A similar experiment using an aqueous solvent in which the lithium GIC reacts with water to form an interstitial hydrogen gas microexplosion has produced ~80% FLG.¹⁰⁶

1.2.8 Arc Discharge

Arc discharge between two graphite electrodes of high purity has been used to produce a variety of fullerenes and carbon nanotubes.¹⁰⁸ It has since been shown that FLG can be produced via arc discharge using H₂-He buffer gases of various proportions,¹⁰⁹ and buffer gases of H₂-Ar, H₂-N₂,¹¹⁰ H₂, and H₂-He-N₂.¹¹¹ Attempts to make graphene sheets were made using air and N₂ but were largely unsuccessful.¹¹¹ Hydrogen is necessary in the buffer gas to terminate the carbon bonds at the edges of the sheets and prevent the graphitic sheets from rolling up and closing.^{109,110} A study of the effects of various buffer gases showed that material with the highest crystallinity was produced by arc discharge in an atmosphere of hydrogen and helium.¹¹¹

1.2.9 Exfoliation of Graphite Oxide

Exfoliation of GO has garnered recent attention as a possible large-scale method of producing functionalized graphene and involves the oxidation of graphite, exfoliation in a solvent, and a reduction step to recover graphene-like characteristics.¹¹² However, the history of GO began over a century ago with studies of the chemistry of graphite including one well-known publication on the reactivity of graphite done by B. C. Brodie in 1859.¹¹³⁻¹¹⁵ He developed a multi-step method of oxidizing graphite using potassium chlorate (KClO₃) and fuming nitric acid (HNO₃). A one-pot version of this method was later developed by Staudenmaier.¹¹⁶ The Staudenmaier method, along with the Hummers method using potassium permanganate (KMnO₄) and sulfuric acid (H₂SO₄) published in 1958,¹¹⁷ are still the most common chemical methods used to oxidize graphite, often with modifications.^{29,31,118}

1.2.9.1 Structure of Graphite Oxide

To this point graphite oxide (GO) has been used to describe graphite that has been oxidized but a distinction should be made between GO and graphene oxide. Graphite oxide is oxidized graphite where there is interaction between sheets, i.e. the sheets are stacked or intercalated. When this order is disrupted, in a solvent for example, and the sheets are far enough apart that there is no interaction it is effectively an exfoliated system. When graphite oxide is dispersed in this manner it is referred to as graphene oxide (eGO).¹¹⁸

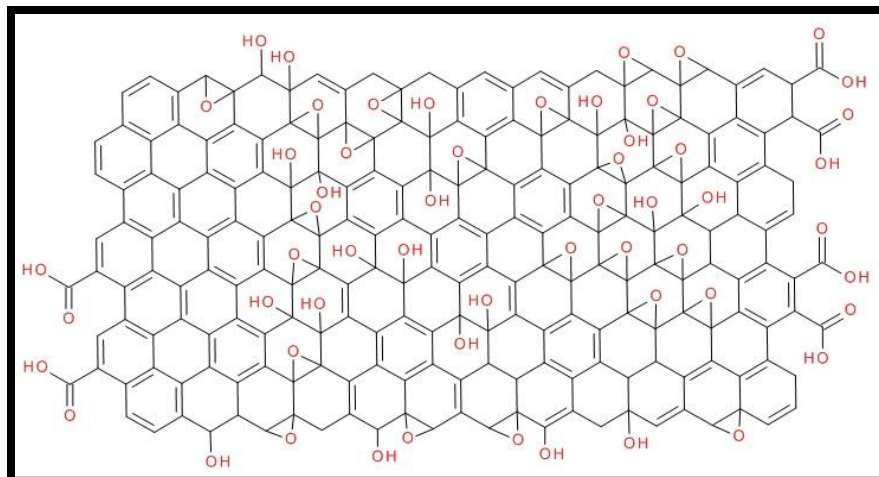


Figure 4: The Lerf-Klinowski model of the structure of graphene oxide.

There have been multiple structural models of GO and eGO proposed but the one that has found the widest acceptance was proposed by Lerf and Klinowski based on solid state nuclear magnetic resonance (NMR) experiments and is shown in Figure 4.^{118,119} A second publication by the same authors

proposed a similar structure for graphene oxide but without carboxylic acid functionalities on the edges of the sheet.¹²⁰ A more recent proposed structure by Dekany and colleagues is based on the Scholz-Boehm model where there are ribbon regions of carbon-carbon double bonds and oxidized chair regions that resemble hexane-like chairs (Figure 5). Dekany and colleagues expanded this proposed structure of GO to a larger scale,

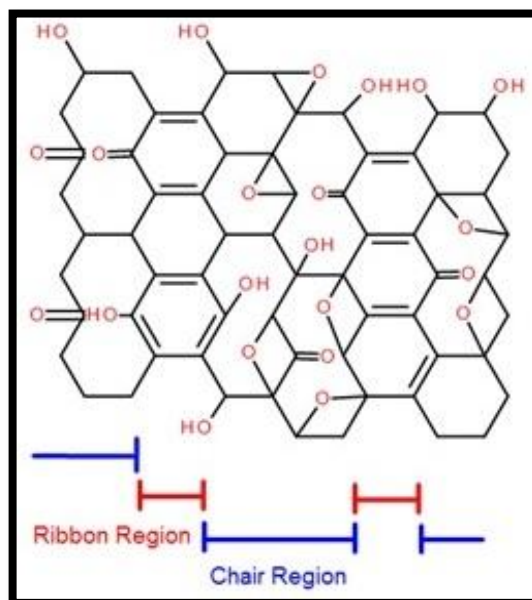


Figure 5: Scholz-Boehm model of GO.

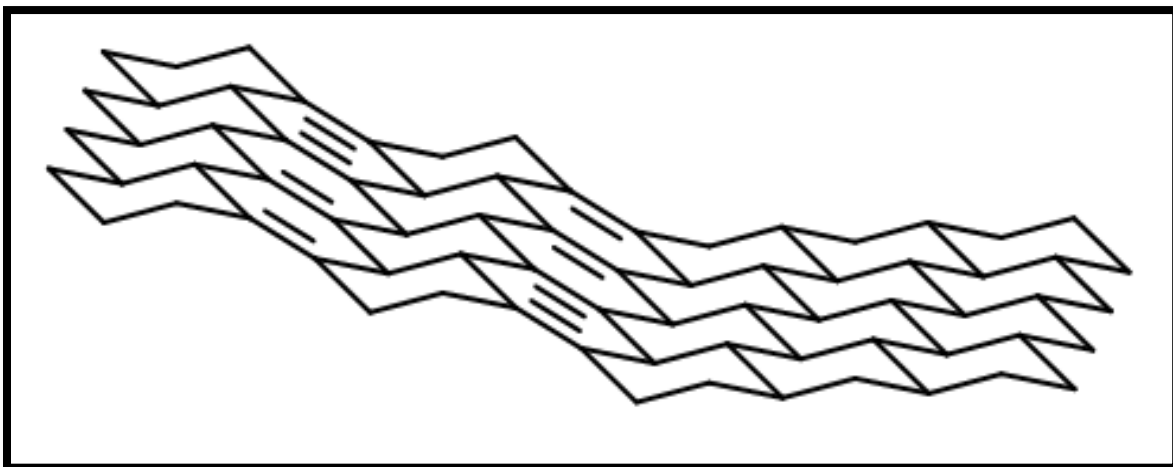


Figure 6: Structure of GO proposed by Dekaney and colleagues.

hypothesizing that the ribbon and chair regions would be randomly distributed. There would be a tilt angle between the boundaries of these two regions (shown in Figure 6) and would explain the macroscopic wrinkling shown in TEM images of GO.¹²¹

GO and eGO are not electrically conductive due to the disruption in the sp^2 bonding networks of the sheets.¹¹⁸ While this may be useful for some applications it is often the case that restoring the electrical properties to that of graphene is desirable. There have been many reduction techniques employed to achieve this goal including chemical, thermal, and electrochemical reductions.¹¹⁸ This reduced form of graphene oxide is often referred to, and will be referred to here, as reduced graphene oxide (rGO).

1.2.9.2 Chemical Reduction of Graphite Oxide

One of the most common chemical reduction techniques (as well as the first reported) is hydrazine monohydrate.¹²² While many chemical oxidizing agents react strongly with water, hydrazine monohydrate does not and this makes it especially useful for reducing aqueous dispersions of eGO.¹¹⁸ There have been proposals for the mechanism of reduction of eGO with hydrazine¹²² but it is not yet known.¹¹⁸ Ascorbic

acid (Vitamin C) has also been used to reduce eGO, This reduction method produces rGO with similar carbon to oxygen (C/O) ratios as hydrazine, and avoids the toxicity concerns of hydrazine use.¹²³ Metal hydrides (e.g. sodium hydride and lithium aluminum hydride) are strong reducing agents that react with water and are therefore unsuitable for use with aqueous dispersions of eGO. However, the kinetics of the sodium borohydride (NaBH₄) reaction with water are such that the reaction is slow enough to allow reduction of aqueous eGO with NaBH₄ when reducing solutions are made and used immediately.¹²⁴ This reduction was shown to be more effective than the reduction of eGO with hydrazine.¹²⁴ NaBH₄ is most effective at reducing C=O species and less so with epoxide and carboxylic acid functionalities.¹²⁵ In order to reduce any residual hydroxyl functionalities on the eGO surface the NaBH₄ reduction is sometimes followed by a dehydration step using concentrated sulfuric acid (H₂SO₄) which shows an increase in conductivity in the resulting rGO.¹²⁶ Hydroiodic acid (HI) has also been used as a reductant and results in rGO with higher C/O ratio and better conductivity than other chemical reductions. HI also affords flexibility in the reduction parameters and can be used on GO in colloid, powder, and film forms in gaseous or solution environments.^{127,128} Other chemical reductants have been used to reduce GO include hydroquinone,¹²⁹ pyrogallol,¹²³ strong alkaline solutions,¹³⁰ hydroxylamine,¹³¹ urea, thiourea,¹³² sodium hydrosulfite,¹³³ and thiourea dioxide¹³⁴ but have not proven to be as effective as those previously mentioned.¹³²

1.2.9.3 Photocatalytic Reduction of Graphite Oxide

GO has been reduced with ultraviolet (UV) radiation and photocatalysts like TiO₂,¹³⁵ ZnO,¹³⁶ and BiVO₄.¹³⁷ The resulting material is a photocatalyst-rGO

nanocomposite with photocatalyst anchored to the rGO sheet. This prevents collapsing of the sheets when solvent is removed and allows for facile redispersion in solvent.¹³⁵ These nanocomposite materials are currently being pursued for use in photovoltaic devices such as photocatalysis devices¹³⁸ and dye-sensitized solar cells.^{139,140}

1.2.9.4 Electrochemical Reduction of Graphite Oxide

GO has been reduced in an electrochemical cell and is carried out by an exchange of electrons between GO and the electrodes.¹⁴¹⁻¹⁴⁴ It can be done at room temperature and does not rely on the use of hazardous reactants. The potential needed to reduce GO is dependent on the pH of the buffer solution and it has therefore been proposed that H⁺ ions participate in the mechanism of the reaction.¹⁴¹ In one study the reduction of GO was found to start at -0.6 V at reached a maximum at -0.87 V and the reduction was electrochemically irreversible at these voltages.¹⁴⁴ Electrophoretic deposition (EPD) has been used to make rGO films. The mechanism is unclear but it was found that when a direct current was applied to the cell the GO sheets would stack in an overlapping configuration on the positive electrode.¹⁴³ Conductive rGO films were isolated from the electrode by air drying at room temperature.¹⁴³

1.2.9.5 Solvothermal Reduction of Graphite Oxide

In a sealed container solvents can be brought to a temperature well above their boiling point.¹⁴⁵ This solvothermal process has been used to react super critical (SC) water with carbohydrates to produce carbon nanospheres¹⁴⁶ and poly (vinyl alcohol) to produce carbon nanotubes.¹⁴⁷ The hydrothermal process has also been used on eGO to produce rGO and showed that the process removed oxygen from the eGO platelets and

simultaneously restored some conjugation.¹⁴⁸ It was also found that this hydrothermal process yielded rGO solution under basic conditions (pH=11) and aggregated rGO sheets under acidic conditions (pH=3) and that the latter were not easily exfoliated.¹⁴⁸

A solvothermal reduction of GO has been reported using N,N-dimethylformamide (DMF).¹⁴⁹ The reducing agent in this process was a small amount of hydrazine added to the solvent. While reduction took place, as indicated by an increase in C/O ratio, it was found that the resulting rGO was not conductive and had a sheet resistance of 10^5 - 10^6 Ω /sq. It has been suggested that this poor conductivity is the result of nitrogen-doping caused by the hydrazine.¹⁴⁹

A solvothermal reduction of eGO with N-methyl-2-pyrrolidone (NMP) has been reported.¹⁵⁰ This solvothermal reduction does not take place in a sealed container and is instead carried out via refluxing. The rGO produced in this manner had only moderate increases in C/O ratio and conductivity.¹⁵⁰ However this method, along with the other solvothermal reductions, produces stable solutions of rGO which are useful for some applications.¹³²

1.2.9.6 Thermal Annealing of Graphite Oxide

Thermal annealing is often used in conjunction with GICs. As mentioned previously, GICs are often intercalated in graphite with heating and evolve gas between the graphene sheets when heated further in order to exfoliate the sheets. The eGO produced using this method can be reduced at still higher temperatures in order to remove the oxygen but so far this multi-step heating method has yielded only small, wrinkles sheets.¹⁵¹ Carbon from the sheets is removed along with oxygen during the thermal

reduction step in this process in the form of CO₂, reducing the mass of the rGO by up to 30%.¹⁵¹ This causes both wrinkling in the sheets as well as breaking them apart.^{151,152}

An alternative method of thermal annealing involves a separate liquid exfoliation step followed by thermal annealing.¹³² In this method the annealing temperature has a great affect on the reduction of GO.^{151,153–157} When annealed at temperatures lower than 500 °C the C/O ratio was less than 7 and when annealed at 750 °C it was in excess of 13.¹⁵¹ It was found that the conductivity of thin rGO films was 50 S/ cm when annealed at 500 °C, 100 S/cm when annealed at 700 °C, and 550 S/cm when annealed at 1100 °C.¹⁵⁶ Another important consideration of the thermal reduction method is the atmosphere in which the GO is reduced. Thermal reduction of GO has been performed under vacuum,¹⁵³ in an inert atmosphere,¹⁵⁶ and in reducing atmospheres.^{156,158–160} It is important that oxygen be excluded from the process because it leads to oxygen etching at elevated temperatures.¹³² In fact, it has been reported that any residual oxygen during thermal annealing of GO under vacuum results in a rapid loss of material and a high quality vacuum (<10⁻⁵ Torr) is therefore required.¹⁵³ Thermal reduction of GO in atmospheres containing some amount of hydrogen serve the dual purpose scavenging any remaining oxygen as well as participating in the reduction of GO.¹⁵⁶ With hydrogen included in the process temperatures as low as 450 °C were used to produce rGO with a C/O ratio of 14.9.¹⁵⁶ It has also been demonstrated that an atmosphere containing argon and ammonia (NH₃) can be used to produce rGO doped with nitrogen.¹⁶⁰

It has been shown that the structure of rGO can be restored and the conductivity of the resulting material increased (~ 350 S/cm) when annealed at 800 °C in the presence of a carbon source such as ethylene.¹⁶¹ Another study showed an even higher level of

conductivity (~ 1314 S/cm) could be attained when rGO is functionalized with aromatic molecules and pyrolyzed.¹⁶²

1.2.9.7 Microwave and Photo-Irradiation of Graphite Oxide

Thermal annealing is the most common technique used for the thermal reduction of GO.¹³² However, alternative heating sources have been used including microwave^{163,164} and photo-irradiation.^{165,166}

There are many advantages of microwave irradiation to exfoliate and reduce GO including rapid preparation (≤ 1 minute depending on microwave power and mass of sample), uniform heating, and the use of commercially available microwave ovens.^{132,163} However, the rGO prepared using this method had a C/O ratio of 2.75 and a powder conductivity of 274 S/m (0.0275 S/cm).¹⁶³

Xenon lamps of the variety found on commercially available cameras emit about 9 times the thermal energy (< 2 mm: ~ 1 J/cm²) needed to heat GO films with a thickness of ~ 1 μ m to 100 °C. In one study it was found that a xenon lamp at a distance of less than 1 cm was capable of generating the required thermal energy of 0.1-2 J/cm² necessary to reduce GO films.¹⁶⁵ It was found that the C/O ratio in these samples went from 1.15 in the starting GO to 4.23 in the rGO and the conductivity of the resulting rGO was ~ 10 S/cm.¹⁶⁵

1.2.10 Commercial Outlook for Graphene and Graphite Oxide Production

Methods

The class of graphene and GO is determined by a number of factors such as the quality of the material, type, number and location of defects, and substrate to which it

is/may be applied. In order for a production method to be commercially viable it should also be scalable. There are a number of production methods that have been discussed that meet these requirements including epitaxial growth on SiC, CVD, liquid-phase, and thermal exfoliation of GO.¹⁰

1.2.10.1 Commercial Outlook for Graphene from Epitaxial Growth on SiC

Epitaxial growth of graphene on SiC produces graphene of very high quality with crystallite size in the range of hundreds of micrometers.²⁵ However, the high temperatures required (> 1,000 °C) are not convenient for use with silicon electronics. This, along with the high cost of SiC substrates and small wafer size, limits the use of SiC grown graphene to niche applications. One application to which this method lends itself is high-frequency transistors based on III-IV materials (e.g. InGaAs and GaN).¹⁶⁷ Another promising application is meteorological resistance standards which have already been demonstrated to be more sensitive at higher temperatures than conventional GaAs based standards.¹⁶⁸ Currently the high temperatures required for this method is an intractable problem and this needs to be addressed for use of this method in a wider range of applications. Other issues with this method that need to be addressed in the future include improving the quality of the product (e.g. eliminating terraces and improving control over the number of layers grown), increasing the size of graphene sheets, and elimination of unintentional doping.¹⁰

1.2.10.2 Commercial Outlook for Graphene from CVD

Polycrystalline graphene with large lateral dimensions (up to 30 inches) has been grown on copper via CVD.^{51,169} The high quality and large dimensions of CVD grown

graphene make it promising for many applications.¹⁰ Metals with graphene layers have high thermal and electrical conduction and enhance the performance of integrated circuit connections.¹⁰ Since graphene is impermeable and inert, graphene-coated metals also show excellent corrosion resistance, even on complex topographies.¹⁰ Currently, growing graphene via CVD is expensive due to the large energy consumption and need to remove the copper substrate.¹⁰ Although a roll-to-roll substrate removal process has been demonstrated¹⁶⁹ the transfer process must be optimized in order to make it cost effective.¹⁰ The temperature required for this process must also be reduced. Plasma-enhanced CVD is currently being developed which addresses this issue but it needs further refinement.¹⁰ Application of CVD grown graphene to arbitrary substrates would be a major boost to the viability of this method and, although substrate-CVD is being pursued,^{76,77,170} it does not yet allow enough control over the number of layers deposited, distribution, or sheet size. Other issues that must be addressed for this method to be commercially successful include CVD growth on thin metal sheets (<100 nm), better control of grain size, ripples and doping, and fine control over the number of layers.¹⁰

1.2.10.3 Commercial Outlook for Graphene from Liquid-phase and Thermal Exfoliation

Liquid-phase and thermal exfoliation include solvent-based exfoliation, exfoliation via GICs, and chemical reduction of graphite oxide methods mentioned previously. These methods may be implemented individually or in combination to achieve the desired degree of exfoliation and/or properties. Solvent-based exfoliation requires a solvent with a surface tension that favors intercalation followed by exfoliation of the graphene sheets in bulk graphite. The most appropriate solvents discovered to date

are organic solvents⁹⁰ which are often expensive and harmful.²⁹ An alternative is the use of surfactants in aqueous solutions which has been demonstrated^{171,172} but subsequent removal of the surfactants is difficult and can affect the properties of the resulting material.²⁹ In addition, both of these methods utilize sonication to increase the yields of SLG and FLG which fractures the sheets and increases the amount of defects.¹⁷³ Exfoliation via GICs, which as mentioned previously is usually done in conjunction with thermal shock, generally results in FLG which are still useful as they exhibit many of the appealing properties of graphene.¹⁰ Oxidation of graphite provides an efficient method for exfoliation in aqueous solution which can then be deposited as a thin film on almost any surface.¹⁰ GO can then be reduced using a variety of methods (as previously discussed) but complete reduction has proved difficult and elimination of all defects caused by oxidation is unlikely. Thus, rGO has many desirable properties but they do not match those of graphene.^{10,29}

Bulk grades of graphene produced using these methods are currently available commercially on the ton scale and being evaluated for numerous applications.¹⁰ The products in which these grades of graphene can be incorporated are numerous and include paints, inks, electromagnetic shielding, barrier coatings, heat dissipation, supercapacitors, etc. Commercial conductive inks have already been demonstrated and it is likely that other products based on these grades of graphene will be commercially available within a matter of years.¹⁰

1.3 Dissertation Efforts

The efforts of this study were threefold. The first was to characterize the FG derived from HA via scanning electron microscopy (SEM), atomic force microscopy

(AFM), fourier transform infrared spectroscopy (FT-IR), x-ray photoelectron spectroscopy (XPS), and raman spectroscopy. The second was to prepare nanocomposite films using polyurethane (PU) as a matrix that was compatible with an aqueous solvent. FG was added as a dispersed phase at a variety of loading levels. These samples were used to determine if FG provides mechanical reinforcement in nanocomposites using storage modulus as a measure of mechanical reinforcement. The third was to prepare polymer nanocomposite samples of the FG precursor material, HA. These samples were used to determine if HA also provides mechanical reinforcement in nanocomposites. HA is insoluble in neutral aqueous solutions so it was not possible to make PU-HA nanocomposite films in the same way FG-PU nanocomposite films were made. Therefore, two alternate matrices were selected for testing of mechanical reinforcement of HA in nanocomposites. The first HA nanocomposite matrix material was polystyrene (PS) which was selected to determine if the conjugated carbon ring systems in this polymer interact favorably with those in the proposed structure of HA. The second HA nanocomposite matrix was Exxelor™ PO 1020, a maleic anhydride functionalized polypropylene polymer (MAfPP) designed to interact favorably with polar fillers.¹⁷⁴ The dispersion of FG in PU was evaluated via x-ray diffraction (XRD).

1.4 Technical Relevance

FG is currently commercially available and is being evaluated for many applications. FG derived from HA provides the possibility of an alternative source of FG requiring fewer preparation steps. However, initial characterization of this material must be completed. The impact of FG derived from HA on nanocomposite properties must also be established. The research reported in this work was conducted to provide initial

characterization of FG derived from HA and elucidate the impact of this material on mechanical properties in nanocomposites via a polyurethane matrix test case.

CHAPTER 2: EXPERIMENTAL METHODS

2.1 Materials Used

National Nanomaterials, Inc. provided the FG used as an aqueous dispersion. A magnetic separation was performed on the aqueous dispersion and, unless otherwise noted, was then used without further treatment. Humic acid was derived from Agro-Lig® leonardite supplied by American Colloid Company. The polyurethane, Bahydrol® 124 was supplied by Bayer MaterialScience, LLC. as an aqueous dispersion and used as received. Exxelor™ PO 1020 (MAfPP) was supplied by Exxon Mobile Corporation and used as received. All other materials and chemicals were purchased from various sources prior to this project and used as received.

2.2 Equipment Used

SEM testing was performed with a FEI Company Helios Nanolab™ 400 DualBeam scanning electron microscope. AFM testing was performed with a Veeco Dimension 3100 atomic force microscope and a BudgetSensors® Tap190-AI-G cantilever in tapping mode. FT-IR testing was done with a Perkin Elmer Spectrum One FT-IR spectrophotometer. XPS testing was performed with a custom molecular beam epitaxy (MBE) system in the Advanced Functional Materials Laboratory at Texas State University. Raman was performed with a Thermo Scientific DXR Raman Microscope. An excitation wavelength of 532 nm was used on all samples. DMA testing was performed with a TA instruments Q800 dynamic mechanical analyzer. Extrusion was done with a Thermo Scientific HAAKE MiniLab II twin screw extruder in co-rotating mode. Injection molding was done with a Thermo Scientific HAAKE MiniJet II

injection molder. All XRD testing was performed with a Bruker D8 Advance Eco with a $\text{CuK}\alpha$ (1.5418 Å) source. All XRD samples were dried at 70° C under vacuum for 48 hours prior to testing.

2.3 Preparations and Methods

2.3.1 Preparation of SEM samples

FG solution was filtered using Whatman filter paper with a 0.20 micrometer pore size. The solid collected on the filter paper was rinsed once with deionized water (diH_2O). The solid was redispersed into diH_2O . The resulting dilute FG solution was spin coated on a silicon wafer substrate. The samples were dried under vacuum overnight in a vacuum oven at 70° C prior to SEM testing.

2.3.2 Preparation of AFM samples

Dilute FG solution was prepared as the SEM sample above except it was spin coated on a freshly cleaved mica substrate. The samples were dried under vacuum overnight at 70° C prior to AFM testing.

2.3.3 Preparation of FTIR samples

FG solution was filtered and washed as the SEM sample above. The solid recovered from the filter paper was collected and dried under vacuum overnight in a vacuum oven at 70° C. The solid was ground with a mortar and pestle and dried under vacuum overnight in a vacuum oven at 70° C. The powder was then mixed with dry potassium bromide powder and pressed into a pellet. The pellet was then used for FTIR testing.

2.3.4 Preparation of XPS samples

FG solution was filtered and washed as the SEM sample above. The solid from the filter paper was collected and dried under vacuum overnight in a vacuum oven at 70° C. The solid material was pressed into a pellet. The FG pellet was affixed to a silicon wafer substrate and used for XPS testing.

2.3.5 Preparation of Raman samples

FG solution was filtered and washed as the SEM sample above. The solid from the filter paper was collected and dried. FG powder was used for Raman testing.

2.3.6 Preparation of Humic Acid

20 g of leonardite powder was placed in a 1 liter beaker. 400 mL diH₂O was added to the beaker. Ammonium hydroxide was then added, with stirring, until a stable pH of ~10 was reached. The solution was gravity filtered overnight with VWR 415 filter paper (pore size 25 micrometers). The filtrate was collected and dried under air flow. The resulting solid was collected and dried under vacuum overnight in a vacuum oven at 70° C before use.

2.3.7 Extrusion of HA-PS Nanocomposites

Polystyrene pellets were dried overnight under vacuum in a vacuum oven at 70° C. 2.97 g of PS pellets and 0.03 g of HA powder were combined in an extruder heated to 200° C at 60 rpm and mixed for 5 minutes. This process was repeated 7 times to yield approximately 21 g of 1% (wt/wt) HA-PS nanocomposite material.

The 2% (wt/wt) nanocomposite was made as above except 2.94 g of PS pellets was combined with 0.06 g HA powder in the extruder. All other portions of the procedure were unchanged.

Neat PS material was made as above except 3.00 g of PS pellets was placed in the extruder. All other portions of the procedure were unchanged.

2.3.8 Extrusion of HA-MAfPP Nanocomposites

MAfPP pellets were dried overnight under vacuum in a vacuum oven at 70° C. 2.97 g of MAfPP pellets and 0.03 g of HA powder were combined in an extruder heated to 175° C at 200 rpm for 5 minutes. This process was repeated 7 times to yield approximately 21 g of 1% (wt/wt) HA-MAfPP nanocomposite material.

The 2% (wt/wt) nanocomposite was made as above except 2.94 g of MAfPP pellets were combined with 0.06 g HA powder in the extruder. All other portions of the procedure were unchanged.

Neat MAfPP material was made as above except 3.00 g of MAfPP pellets was placed in the extruder. All other portions of the procedure were unchanged.

2.3.9 Injection Molding of HA-PS Nanocomposites

Approximately 1.1 g of the HA-PS nanocomposite material was taken from the extruder and allowed to cool to room temperature. 1.1 g of the nanocomposite was weighed and placed in the injection molder heating barrel at 210° C. The injection pressure was 250 bar for 5 seconds and post pressure of 210 bar for 2 seconds with a tensile bar mold heated to 140° C. The mold was then allowed to cool and the sample

removed. 30 mm of the neck region was removed and used for DMA testing. This procedure was used on the neat PS, 1% (wt/wt) PS/HA, and 2% (wt/wt) PS/HA materials.

2.3.10 Injection Molding of HA-MAfPP Nanocomposites

Approximately 1.1 g of the HA-MAfPP nanocomposites was taken from the extruder and allowed to cool to room temperature. 1.1 g of the nanocomposite was weighed and placed in the injection molder heating barrel at 185° C. The injection pressure was 250 bar for 5 seconds and post pressure of 200 bar for 2 seconds with a tensile bar mold heated to 130° C. The mold was then allowed to cool and the sample removed. 30 mm of the neck region was removed and used for DMA testing. This procedure was used on the neat MAfPP, 1% (wt/wt) HA-MAfPP, and 2% (wt/wt) HA-MAfPP materials.

2.3.11 Solvent Casting FG-PU Nanocomposites

The PU dispersion was 37% (wt/wt) PU in water. The FG dispersion concentration was determined to be 5.44 mg/mL in water. The following table was used to mix aqueous solutions of PU with FG concentrations of 0%, 0.1%, 0.5%, 1.0%, and 2.0%:

Table 1: Weight and volume of PU and FG solutions used.

Percent FG/PU	PU Solution (g)	PU (g)	FG Solution (mL)	FG (mg)
0	20	7.4	0	0
0.1	19.98	7.393	1.36	7.4
0.5	19.9	7.363	6.8	37
1	19.8	7.326	13.6	74
2	19.6	7.252	27.21	148

Based on Table 1, the appropriate mass of PU solution and volume of FG solution were placed in a plastic 150 mL beaker. DI water was added to each beaker to bring the total volume to 100 mL. The solutions were mixed with a mechanical mixer for 5 minutes each. The solutions were poured into a Teflon® coated pan well (measuring ~6.5x6.5x3cm) and allowed to dry under ambient conditions. After drying under ambient conditions the films were placed on a glass substrate and dried in an oven overnight at 60° C. A cutting die and press were used to excise specimens for tensile testing.

2.3.12 DMA of PS and HA-PS Nanocomposites

DMA of PS and HA-PS samples was performed in single cantilever configuration from room temperature to 105° C. Amplitude was 15 micrometers with a ramp rate of 3° C per minute and a frequency of 1 Hz. Each sample size was measured individually with typical length, width, and thickness of approximately 17.5 mm, 5 mm, and 1.55 mm, respectively.

2.3.13 DMA of MAfPP and HA-MAfPP Nanocomposites

DMA of MAfPP and HA-MAfPP samples was performed in single cantilever configuration from room temperature to 142° C. Amplitude was 15 micrometers with a ramp rate of 3° C per minute and a frequency of 1 Hz. Each sample size was measured individually with a typical length, width, and thickness of approximately 17.5 mm, 4.9 mm, and 1.6 mm, respectively.

2.3.14 DMA of PU and PU/-FG Nanocomposites

DMA of PU and FG-PU samples was performed in film tension configuration from room temperature to 100° C. Amplitude was 50 micrometers with a ramp rate of 5° C per minute and a frequency of 1 Hz. Each sample size was measured individually with a typical length, width, and thickness of approximately 18 mm, 6 mm, and 0.95 mm, respectively.

CHAPTER 3: RESULTS AND DISCUSSION

3.1 Characterization of Functionalized Graphene

3.1.1 SEM of FG

SEM images of FG samples spin coated on a silicon substrate were taken to determine their morphology. Two representative SEM images are shown in Figures 7 and 8.

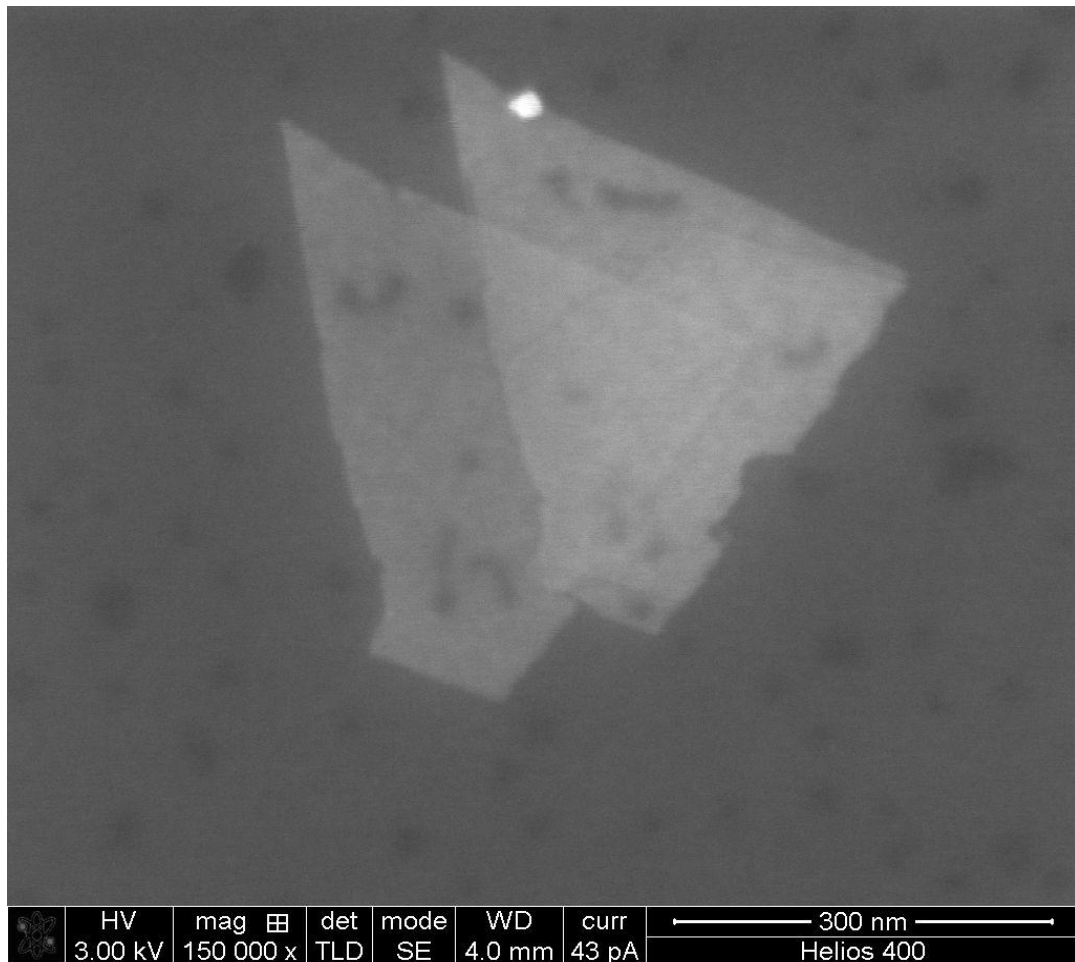


Figure 7: SEM image of FG.

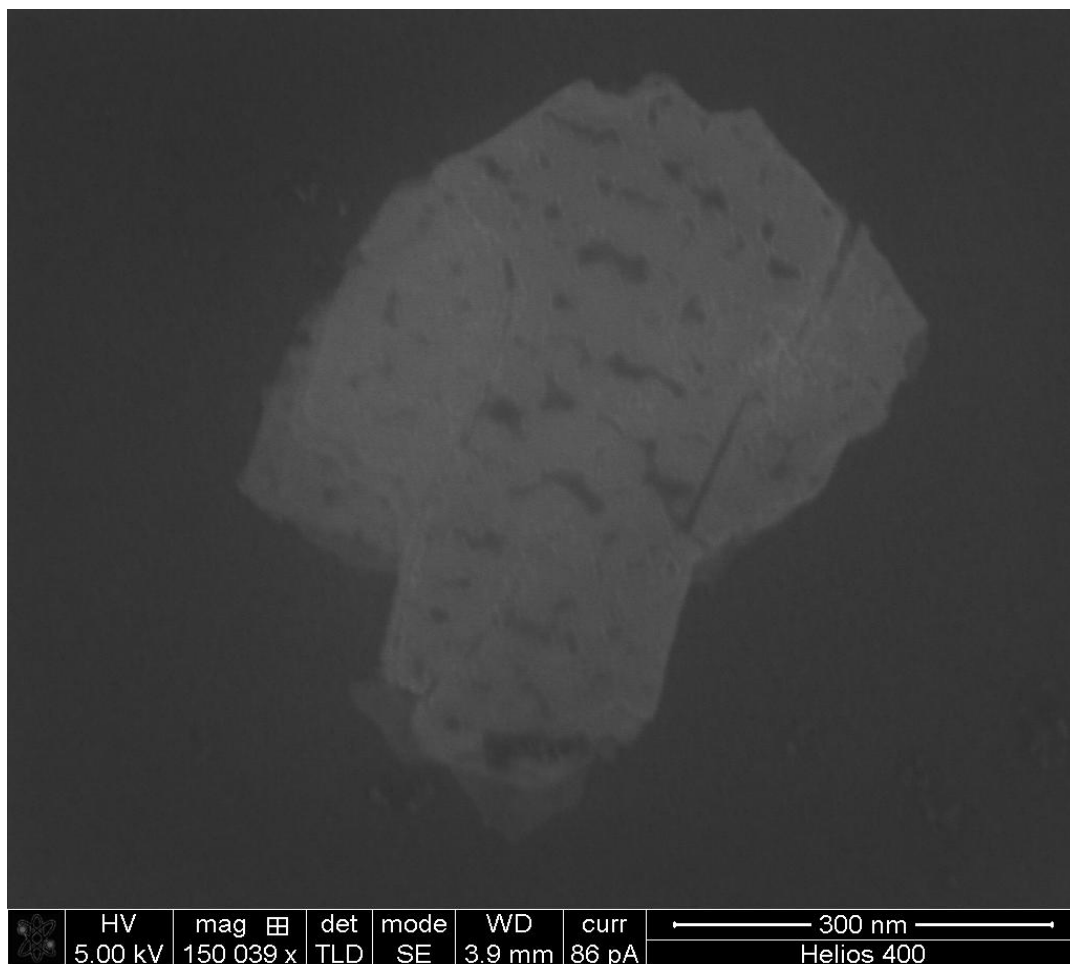


Figure 8: SEM image of FG.

The SEM images reveal FG to be thin, plate-like, stacked sheets. There is a high degree of variation in the shapes of the plates and the sheets appear to fracture along similar lines. SEM images also shows the lateral dimensions of FG sheets to be in the hundreds of nanometers range.

3.1.2 AFM of FG

A sample of FG was spin coated on mica and tested with AFM. The result of this testing, shown in Figure 9, demonstrates the mean height (Rz) of FG plates is approximately 4.2 angstroms. This is similar to thickness of single sheets of graphene

which have been reported to be approximately 4 angstroms.⁸⁹ Preparation for these samples included dispersion in water followed by spin coating on a mica substrate. This indicates that, although there are certainly few layer FG (FLFG) sheets present as demonstrated by SEM results, some single sheets of FG can be isolated from aqueous dispersions without the need for harsh conditions (e.g. ultrasonication, etc.) or surfactants.

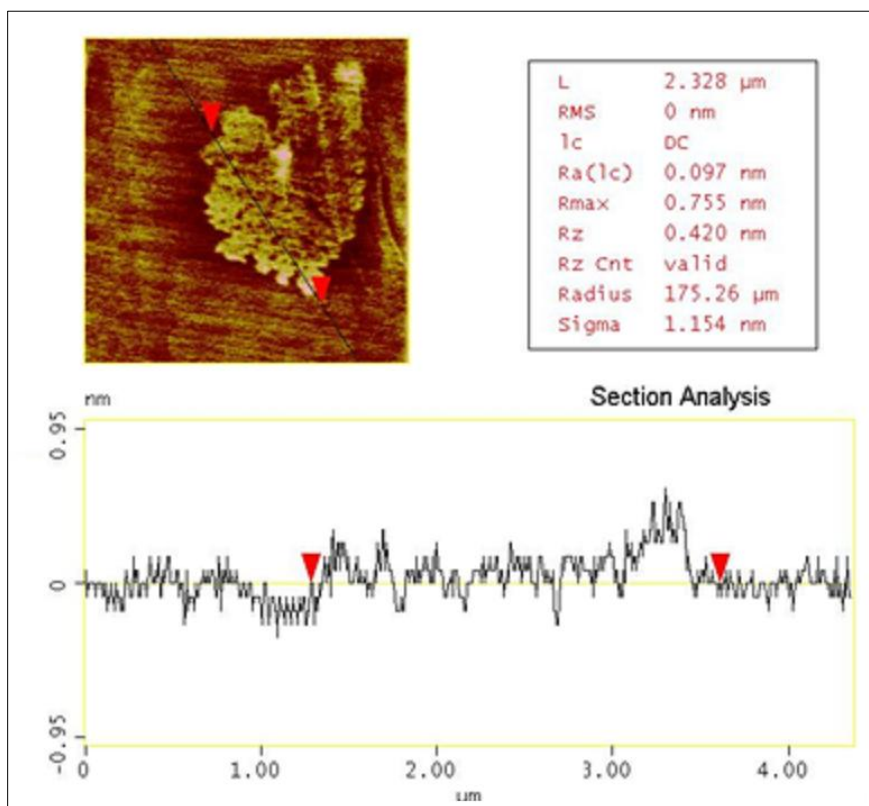


Figure 9: AFM of FG sheet.

3.1.3 FT-IR of FG and HA

FT-IR analysis was done on a sample of FG and HA for comparison. The results are shown in Figure 10. The C=O stretch at 1700 cm^{-1} is present in the HA sample and absent in the FG sample indicating that HA has carbonyl functionalities whereas FG does

not. This indicates that the carbonyl containing functionalities present in HA have been reduced (via the method given in Reference 175) to hydroxyl in FG. Other peaks show little change between HA and FG with regard to other functionalities and a broad hydroxyl peak is present in both samples.

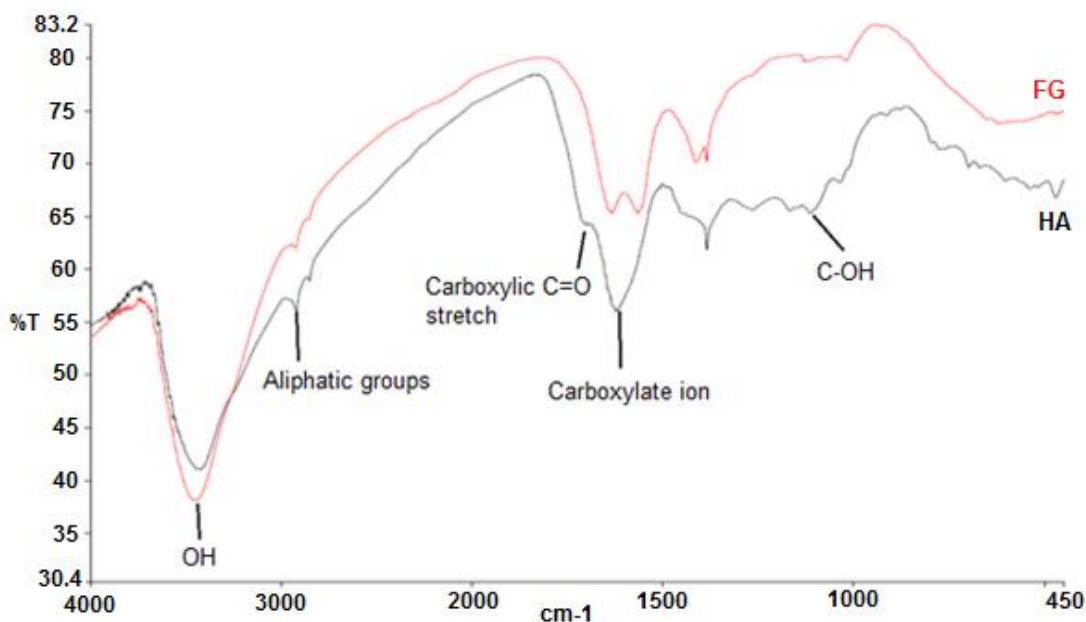


Figure 10: FT-IR of FG and HA.

3.1.4 Raman of FG and HA

Raman Spectroscopy was performed on FG and HA for comparison. The Raman spectrum for HA is shown in Figure 11 and the Raman spectrum from FG is shown in Figure 12.

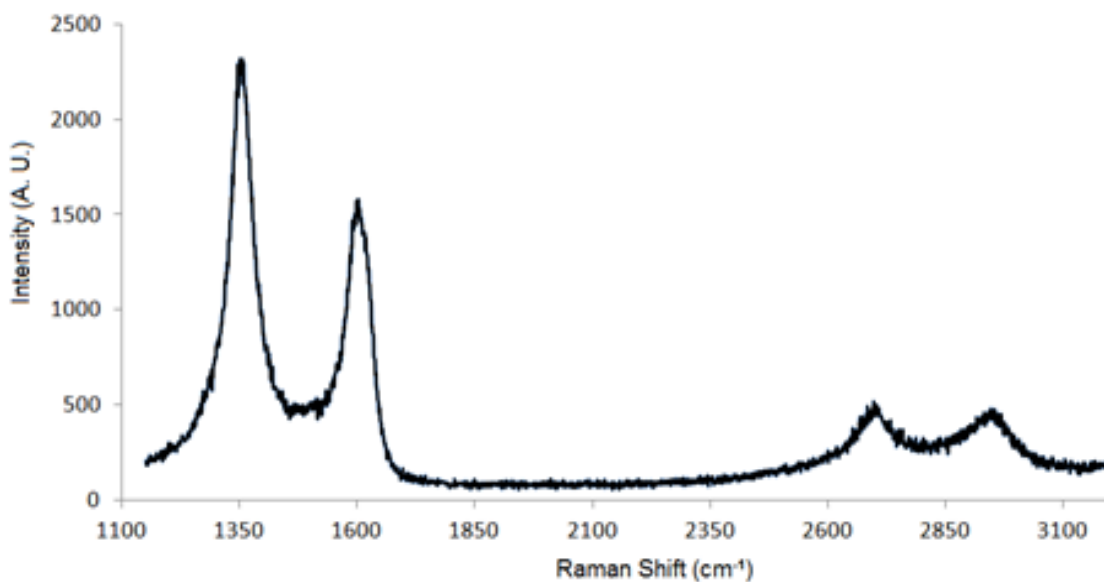


Figure 11: Raman spectrum of HA.

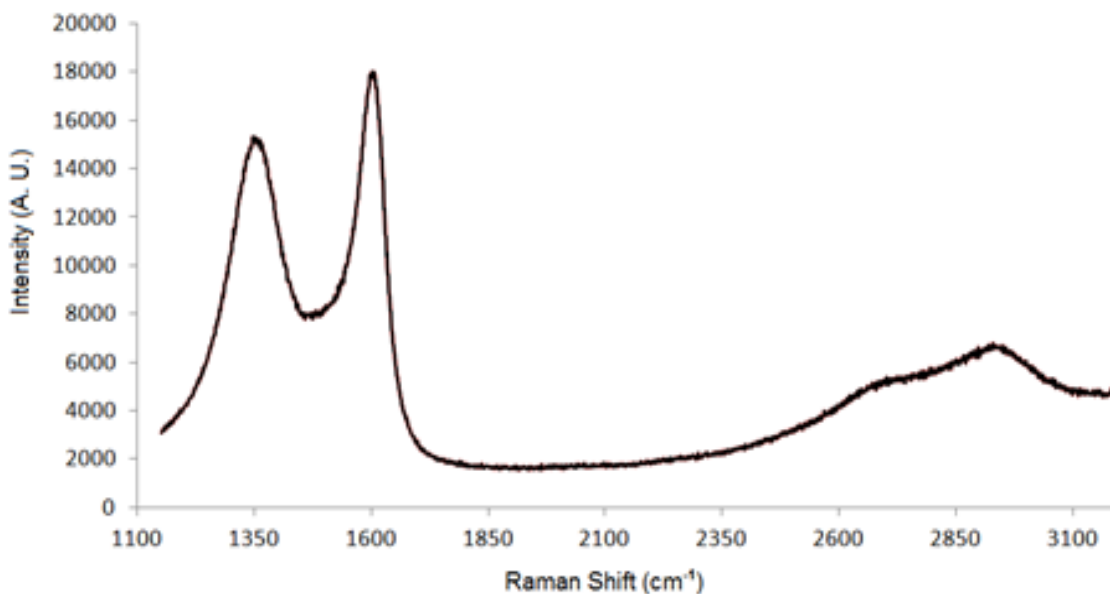


Figure 12: Raman spectrum of FG.

Raman spectroscopy of pristine graphite shows one peak at 1600 cm^{-1} which is known as the G peak and one peak at 2700 cm^{-1} known as the 2D peak. The former arises from the E_{2g} vibrational mode of sp^2 hybridized carbon rings and the latter from an out of plane

vibrational mode.¹⁷⁶ Another peak is sometimes observed in bulk graphite, FLG, SLG, graphene oxide (GO), and reduced graphene oxide (rGO) at approximately 1350 cm^{-1} known as the D peak. This peak is forbidden in pristine systems of π -bonded carbon rings but appears at the edges of sheets and where there are small, isolated regions of hybridized carbon rings such as those in GO and rGO. Thus, the D peak is an indirect, and relative, measure of sp^3 hybridized carbons¹¹² and disorder in graphene systems.¹⁷⁷ Oxidation of graphite to GO shows a decrease in relative intensity of the G peak and an increase in the relative intensity of the D peak because there is an increase in disorder in the carbon ring systems¹⁷⁷ and the size of the in-plane sp^2 hybridized domains is reduced¹²² as the graphene sheets are oxidized. One might expect the reduction of GO to rGO to lead to an increase in the relative intensity of the G peak and a reduction in relative intensity of the D peak, or a decrease in the $I_{\text{D}}/I_{\text{G}}$ ratio, as the aromaticity of the system is restored and there are examples of this.^{149,155,178} However, there are ample examples of reduction of GO to rGO increasing the $I_{\text{D}}/I_{\text{G}}$ ratio.¹⁷⁹⁻¹⁸¹ It is proposed that this latter case is due to the formation of an increased number of graphitic domains that are smaller in size.¹²² Our results correspond with the former case and we see a reduction in the relative intensity of the D peak and an increase in the relative intensity of the G peak. Since HA was subjected to reducing conditions (catalytic reduction under a pressurized hydrogen atmosphere as described in Reference 175) it was concluded that this is due to a restoration of aromaticity in the carbon ring systems.

3.1.5 XPS of FG and HA

XPS was used to probe the changes to the chemical structure of FG with XPS results of HA used for comparison. XPS for the C1s region for FA and HA are shown in Figure 13 and the O1s region are shown in Figure 14.

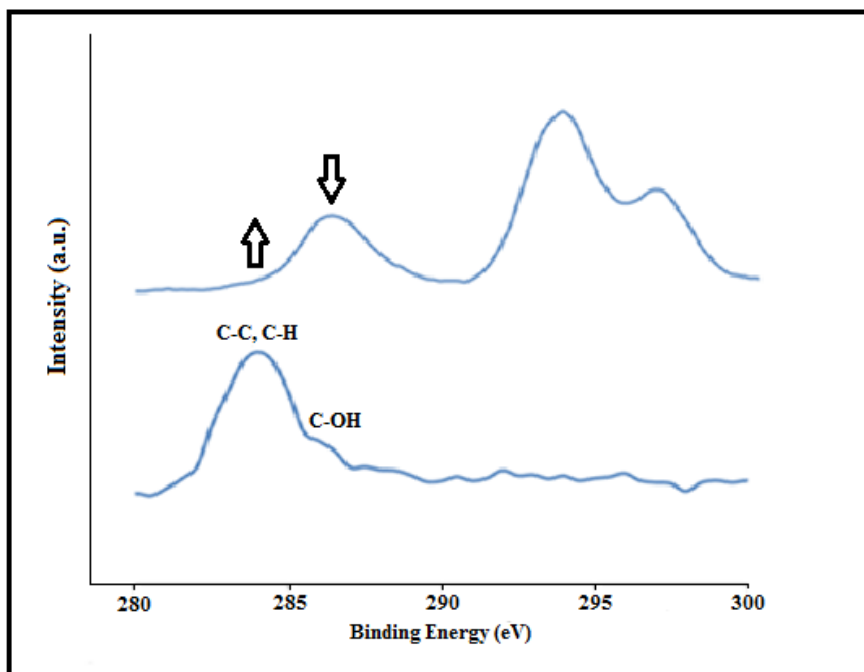


Figure 13: XPS of the C1s region for HA (top) and FG (bottom) offset for clarity.

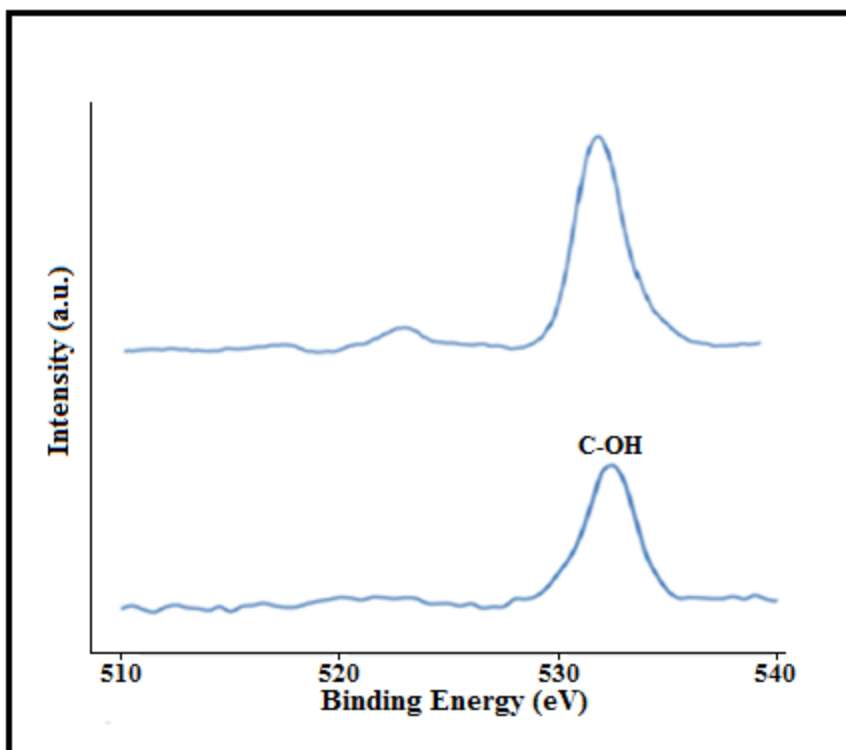


Figure 14: XPS of the O1s region for HA (top) and FG (bottom) offset for clarity.

The lower binding energy peak in the C1s spectrum (~284 eV) can be assigned to C-H and C-C bonds while the higher energy peak (~286 eV) can be assigned to C-OH bonds.¹⁵⁵ The XPS spectrum shows a clear relative increase in the former and relative decrease in the latter after reduction of HA to FG. This indicates C-C and/or C-H bonds are being formed as C-OH bonds are being reduced. The O1s region of the XPS shows a peak ~532.5 eV which has been assigned to C-OH bonds.¹⁵⁵ This region of the XPS for HA and FG shows that while there is a decrease in relative intensity of the C-OH peak after the reduction of HA to FG, a significant peak remains indicating the presence of C-OH in both samples.

3.2 Characterization of Polymers and Nanocomposites

3.2.1 DMA of MAfPP and HA-MAfPP Nanocomposites

DMA analysis was performed on samples of MAfPP with HA loadings of 0.0% (wt/wt) (neat), 1.0% (wt/wt), and 2.0% (wt/wt). Figure 15 shows the DMA result for samples of each loading. Detailed results for each sample tested may be found in Appendix Section B.

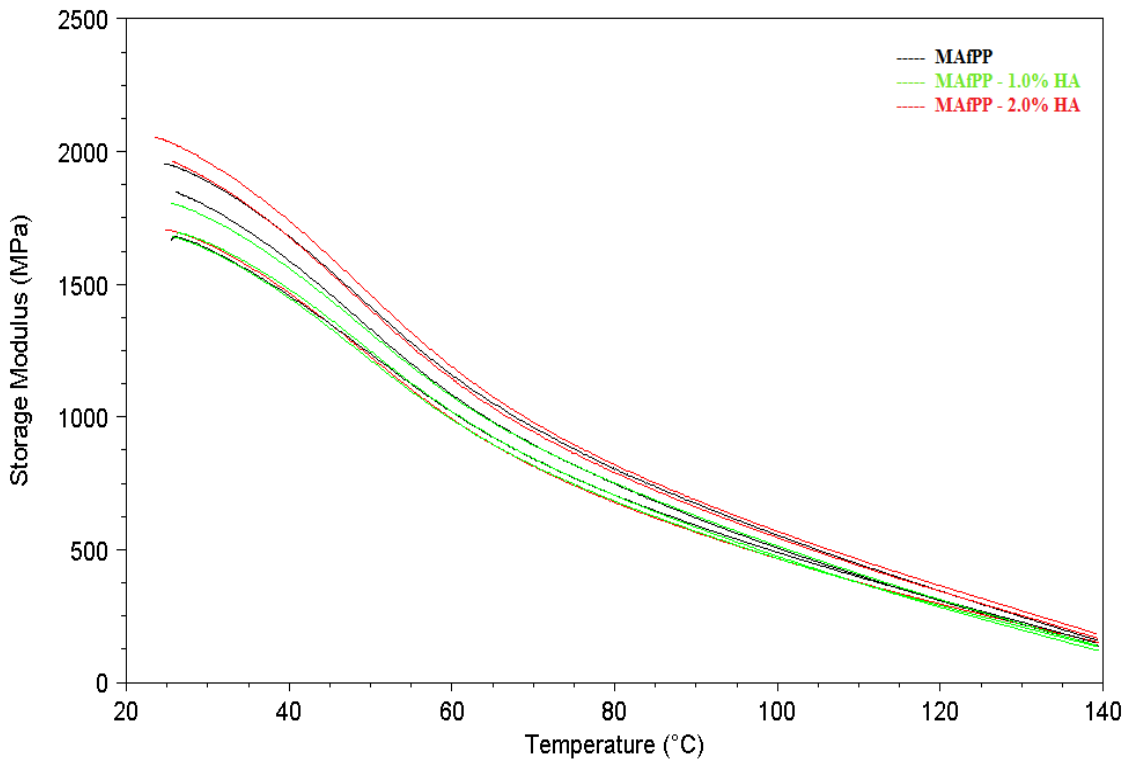


Figure 15: DMA of MAfPP and HA-MAfPP samples.

An analysis of the storage modulus of each of these samples at 30° C was performed in order to determine if any significant mechanical reinforcement could be discerned. Details of the analysis may be found in Appendix Section B. The results are displayed in Figure 16 showing the average of the samples as well as error associated with each.

These data show no significant mechanical reinforcement between the neat MAfPP, 1% HA-MAfPP, and 2% HA-MAfPP samples.

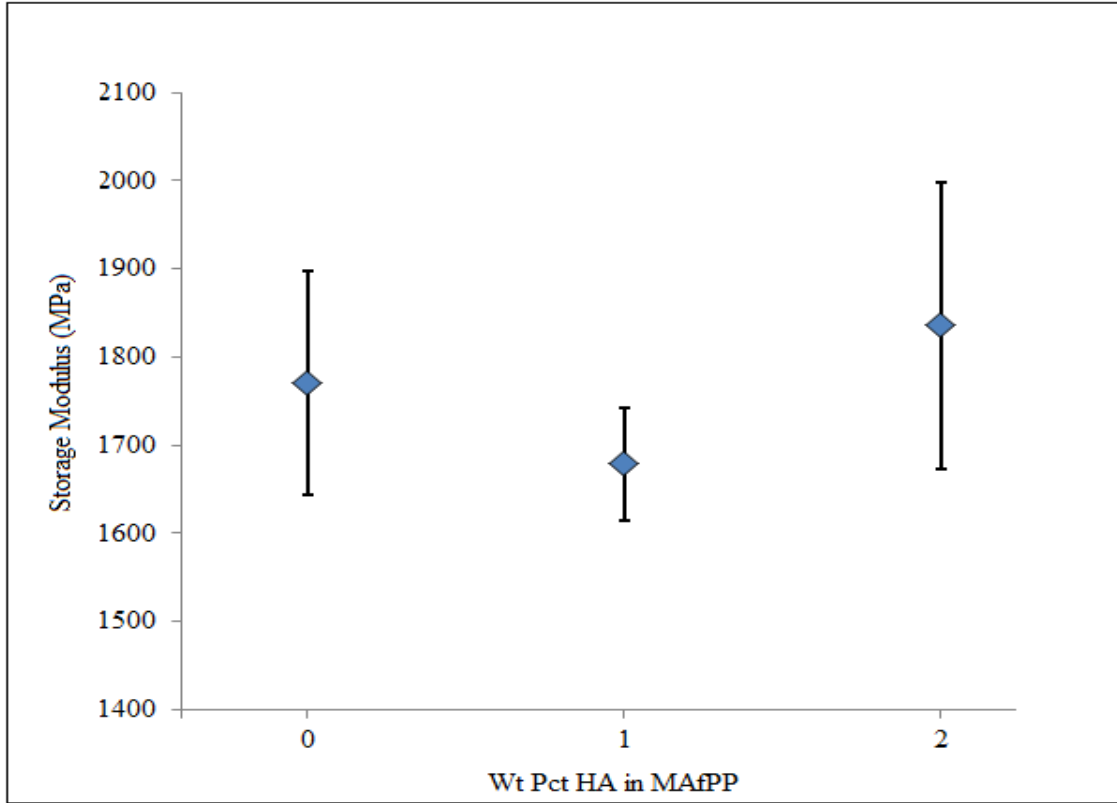


Figure 16: Average storage modulus of HA-MAfPP samples at 30° C.

3.2.2 DMA of PS and HA-PS Nanocomposites

DMA analysis was performed on samples of PS with HA loadings of 0.0% (wt/wt) (neat), 1.0% (wt/wt), and 2.0% (wt/wt). Figure 17 shows the DMA result for samples of each loading. Detailed results for each sample tested may be found in Appendix Section C.

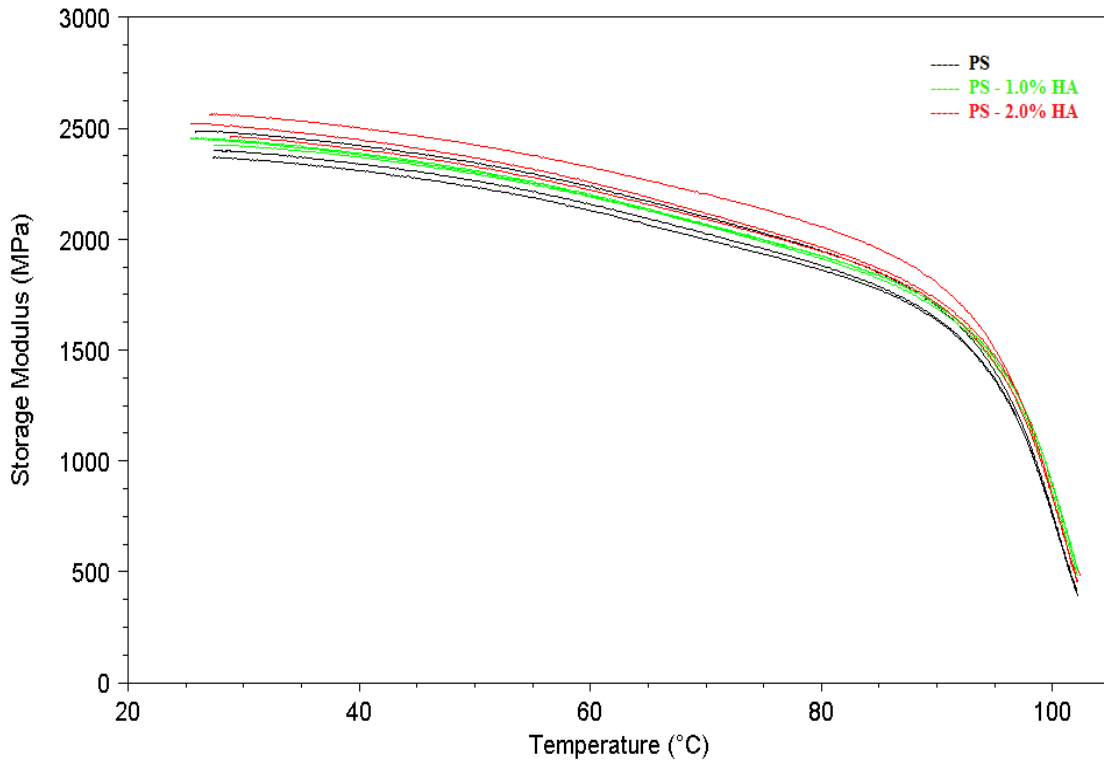


Figure 17: DMA of PS and HA-PS samples.

As with the previous case, an analysis of the storage modulus of each of these samples at 30° C was performed in order to determine if any significant mechanical reinforcement could be discerned. Details of the analysis may be found in Appendix Section C. The results are displayed in Figure 18 showing the average of the samples as well as error associated with each. These data show modest mechanical reinforcement in the 2% HA-PS samples (an average of ~104%) but no significant mechanical reinforcement in the 1% HA-PS samples compared to the neat samples.

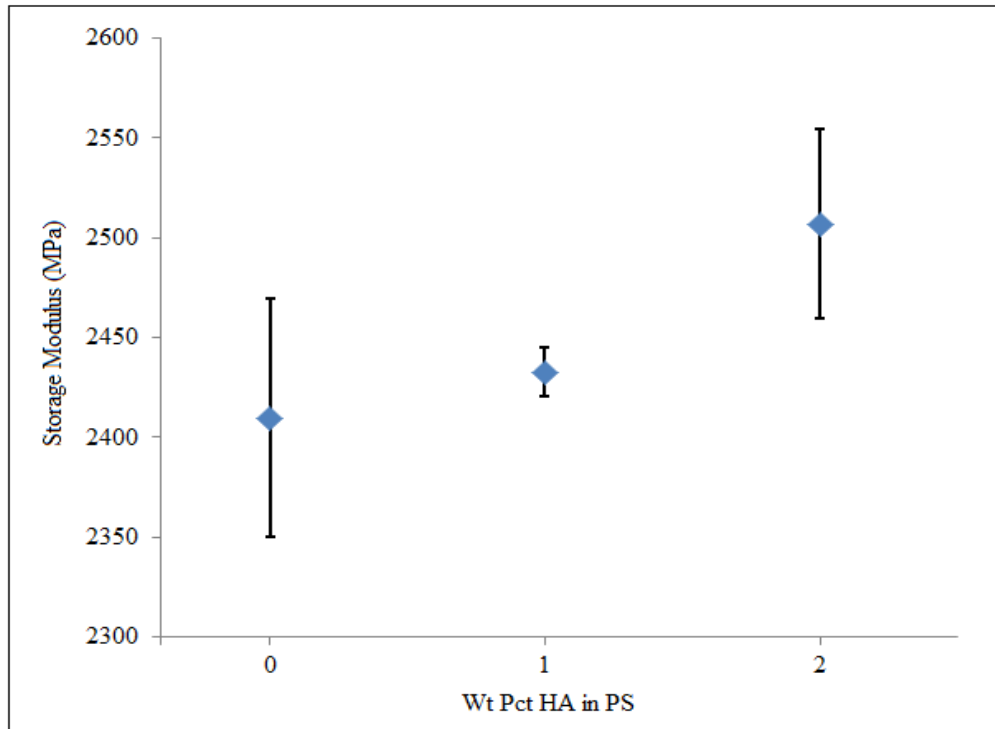


Figure 18: Average storage modulus of HA-PS samples at 30° C.

3.2.3 DMA of PU and FG-PU Nanocomposites

DMA analysis was performed on samples of PU with FG loadings of 0.0% (wt/wt) (neat), 0.1% (wt/wt), 0.5% (wt/wt), 1.0% (wt/wt), and 2.0% (wt/wt). Figure 19 shows the DMA result for representative samples of each loading. Detailed results for each sample tested may be found in Appendix Section D.

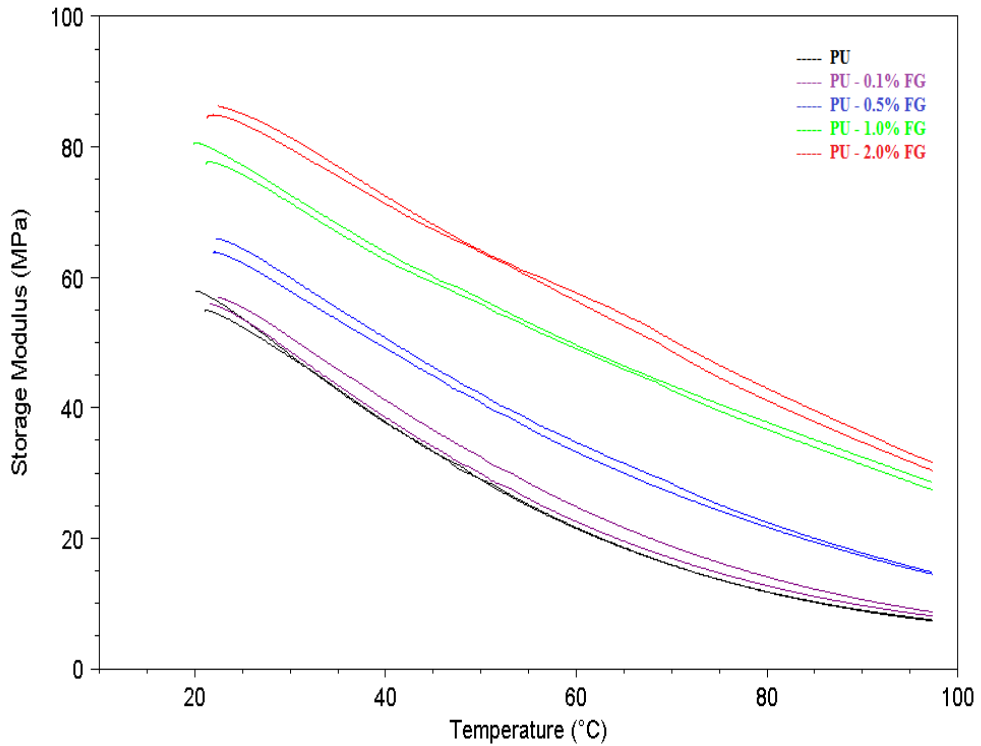


Figure 19: DMA of PU and FG-PU samples.

As with the previous two cases, an analysis of the storage modulus of each of these samples at 30° C was performed in order to determine if any significant mechanical reinforcement could be discerned. Details of the analysis may be found in Appendix Section D. The results are displayed in Figure 20 showing the average of the samples as well as error associated with each. These data show little mechanical reinforcement in the 0.1% FG-PU samples, an average increase of ~121% in the 0.5% FG-PU samples, an average increase of ~150% in the 1.0% FG-PU samples, and an average increase of ~168% in the 2.0% FG-PU samples compared to the neat samples.

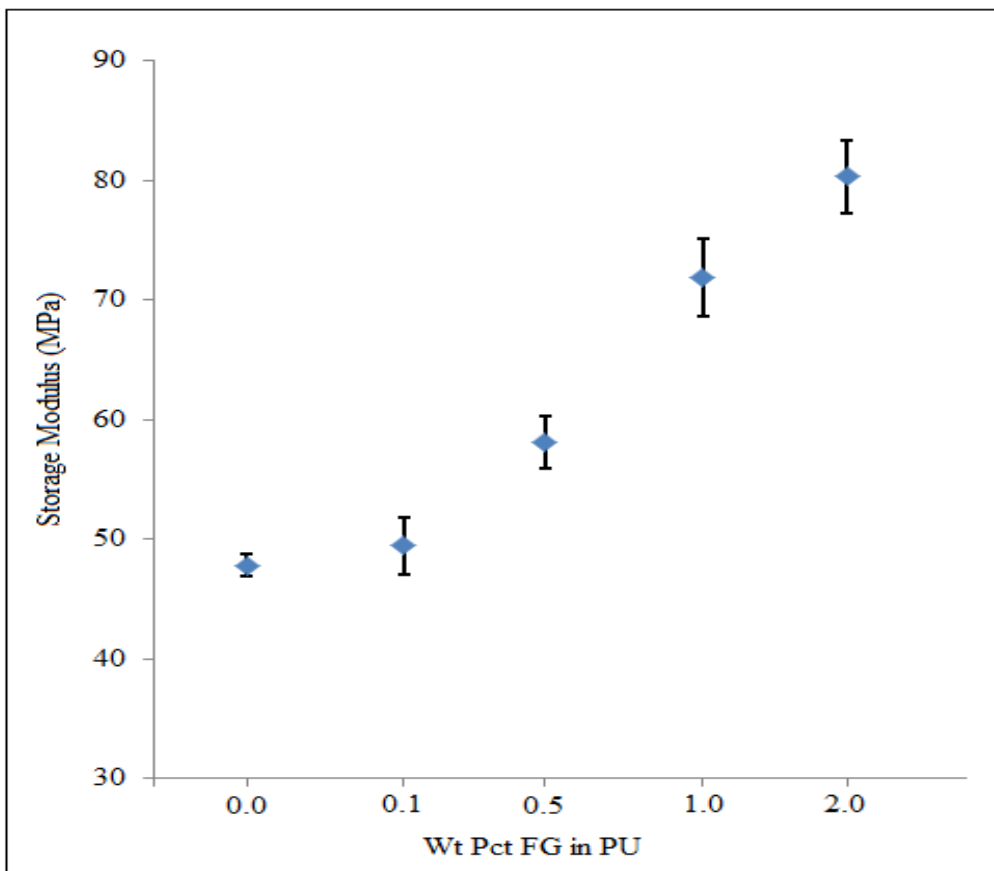


Figure 20: Average storage modulus of FG-PU samples at 30° C.

Table 2 shows recently reported values of the storage modulus increase in comparable materials. The results from this work are shown in the bottom two lines. This Table shows that the experimental values for the level of mechanical reinforcement in FG-PU nanocomposites exceeds that of the other nanocomposites including those at higher loadings. It is interesting to note that a decline in percent reinforcement is seen between 1.0% and 2.0% loadings of the PP-graphene nanocomposites which is often seen in systems lacking adequate dispersion.¹⁸² The FG-PU nanocomposites show an increase in percent reinforcement at 1.0% and 2.0% loadings which, coupled with the XRD results

in Section 3.2.5, reinforces the conclusion that adequate dispersion was achieved in the FG-PU materials.

Table 2: Mechanical reinforcement of polymer-graphene nanocomposites.

Polymer	Dispersed Phase	Processing	Dispersed Phase Conc.	Temp.	Storage Modulus Increase	Reference
PMMA	rGO	solvent/melt	1.0%	~30° C	~113%	183
PMMA	rGO	solvent/melt	4.0%	~30° C	~134%	183
PU	GO	in situ polymerization	4.4%	-100° C	~119%	184
PP	graphene	melt	1.0%	25° C	136%	185
PP	graphene	melt	2.0%	25° C	128%	185
PU	FG	solvent	1.0%	30° C	150%	Experimental
PU	FG	solvent	2.0%	30° C	168%	Experimental

There are significant independent variables that affect reinforcement in polymer nanocomposite materials (e.g. aspect ratio, modulus, orientation), however, the level of reinforcement seen in these samples can be compared to the amount of reinforcement provided by other dispersed phase materials such as montmorillonite nanoclays. In order to get the same level of reinforcement as shown in the 1.0% FG-PU samples (~150%) using montmorillonite nanoclays one would need a loading level of approximately 4%.¹⁸² The theoretical value of the modulus is 160 MPa using the Halpin-Tsai equation of disk shaped fillers for nanocomposite reinforcement with 1% (wt/wt) graphene as the randomly oriented filler (See Appendix Section E for variables used).¹⁸⁶⁻¹⁸⁸ The experimental modulus at 1.0% loading shown in these results (71.87 MPa) is 45% of this theoretical value. Further studies would be beneficial in elucidating all the factors that are at work in FG-PU systems, but these comparisons highlight the significance of the results presented here.

3.2.4 XRD of HA

The XRD of HA is shown in Figure 21. The HA powder sample showed no strong, sharp peaks.

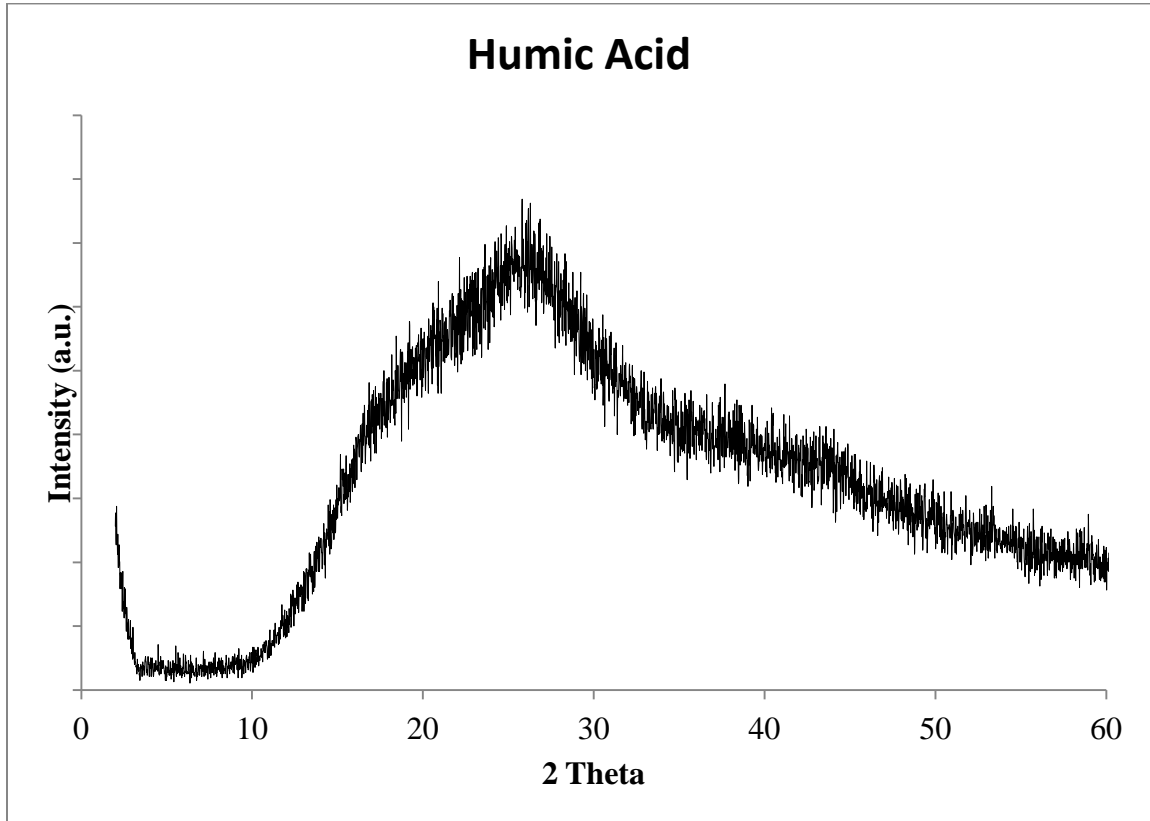


Figure 21: XRD of HA powder.

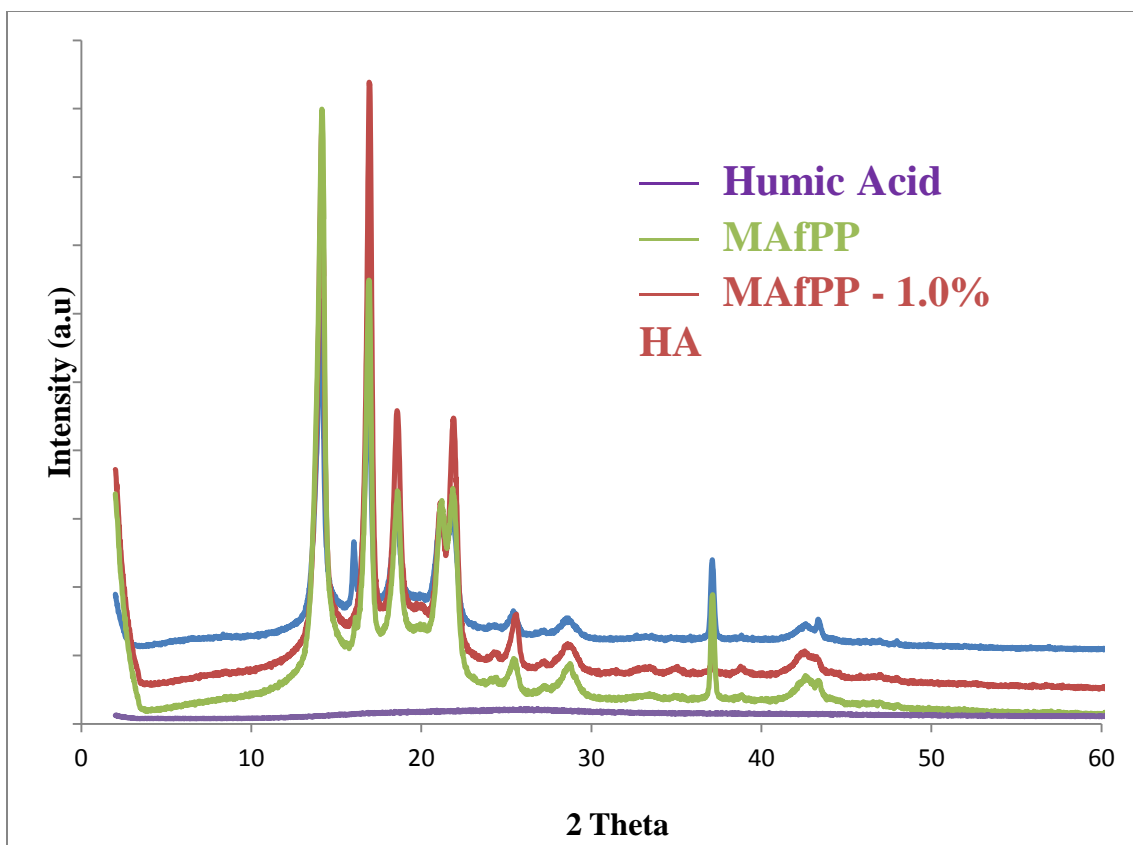


Figure 22: XRD of HA, MAfPP, 1.0% HA-MAfPP, and 2.0%HA-MAfPP. Scans are offset for clarity.

The XRD of HA compared to those of MAfPP, 1.0% HA-MAfPP, and 2.0% HA-MAfPP is shown in Figure 22. The relative lack of intensity of any peak in HA compared to those in MAfPP make it of limited use with regard to probing the level of exfoliation of HA in HA-MAfPP nanocomposites. The XRD of HA compared to those of PS, 1.0% HA-PS, and 2.0% HA-PS are shown in Figure 23. In the comparison of PS, HA-PS, and HA materials the HA sample lacked any significant peaks making it of limited use with regard to probing the level of exfoliation of HA in HA-PS nanocomposites. Nevertheless, the MAfPP, HA-MAfPP, PS, and HA-PS XRD scans are individually presented in Appendix Section F.

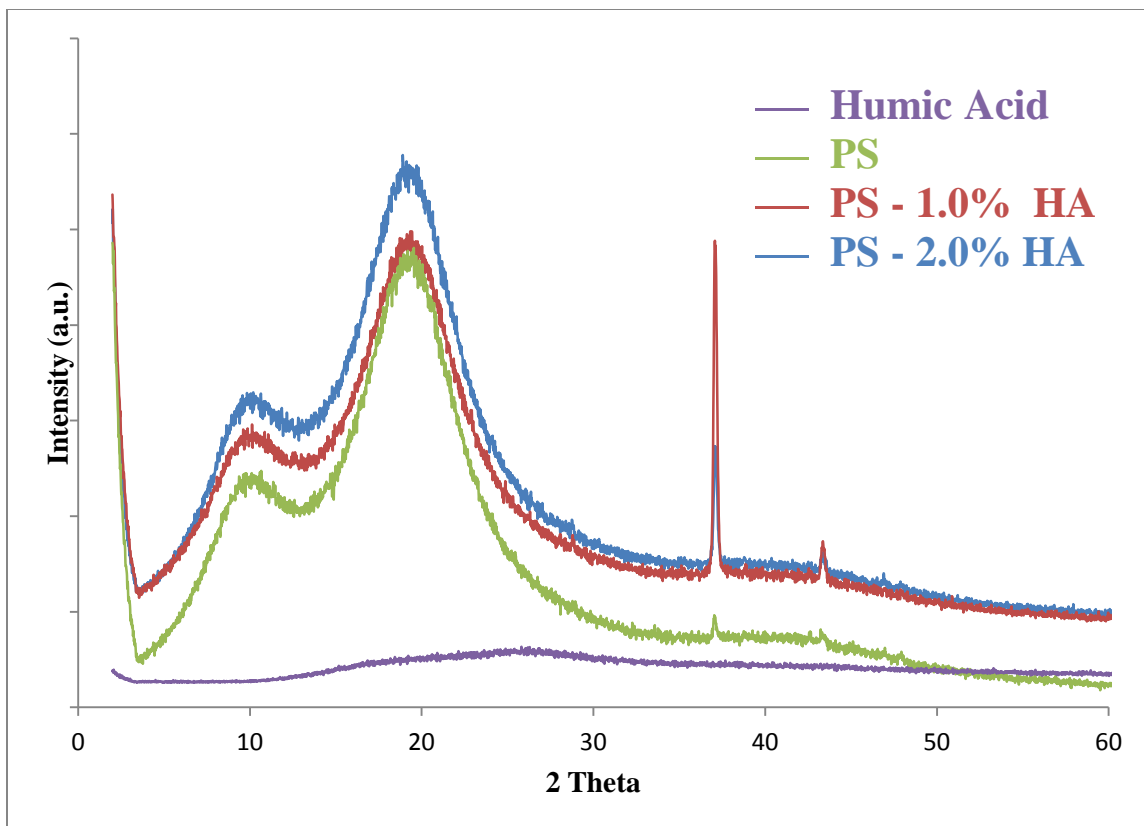


Figure 23: XRD of HA, PS, 1.0% HA-PS, and 2.0%HA-PS. Scans are offset for clarity.

3.2.5 XRD of FG and PU

XRD was performed on FG powder and the results are shown in Figure 24. The strong, sharp peaks in this scan indicate crystallinity in the FG powder. The presence of these peaks provided the opportunity to use XRD as a means of probing exfoliation of FG in FG-PU materials. The XRD of FG is compared with those of neat PU, 0.1% FG-PU, 0.5% FG-PU, 1.0% FG-PU, and 2.0% FG-PU samples in Figure 25. These data show no peaks in the FG-PU samples other than those in the neat PU sample. This is evidence that there is no significant crystallinity associated with FG in the FG-PU nanocomposite material and that no stacking of FG sheets or intercalation of FG sheets has occurred and

some level of exfoliation has been achieved. Individual XRD scans of PU and FG-PU samples are shown in Appendix Section G.

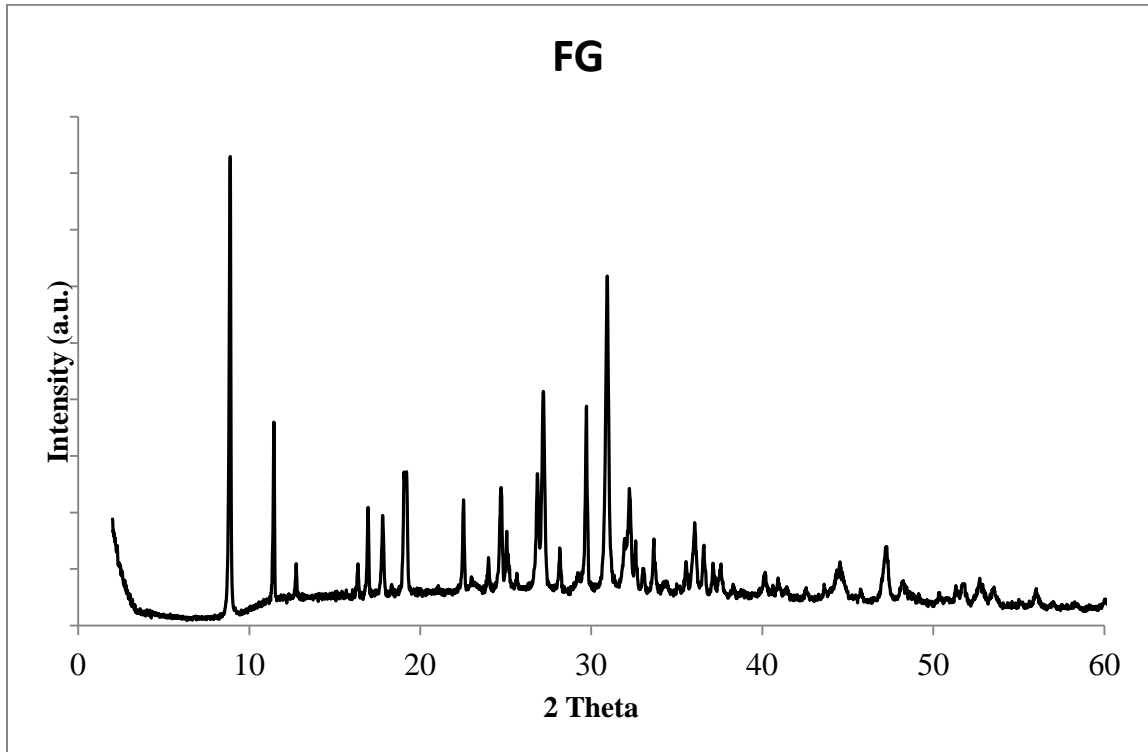


Figure 24: XRD of FG powder.

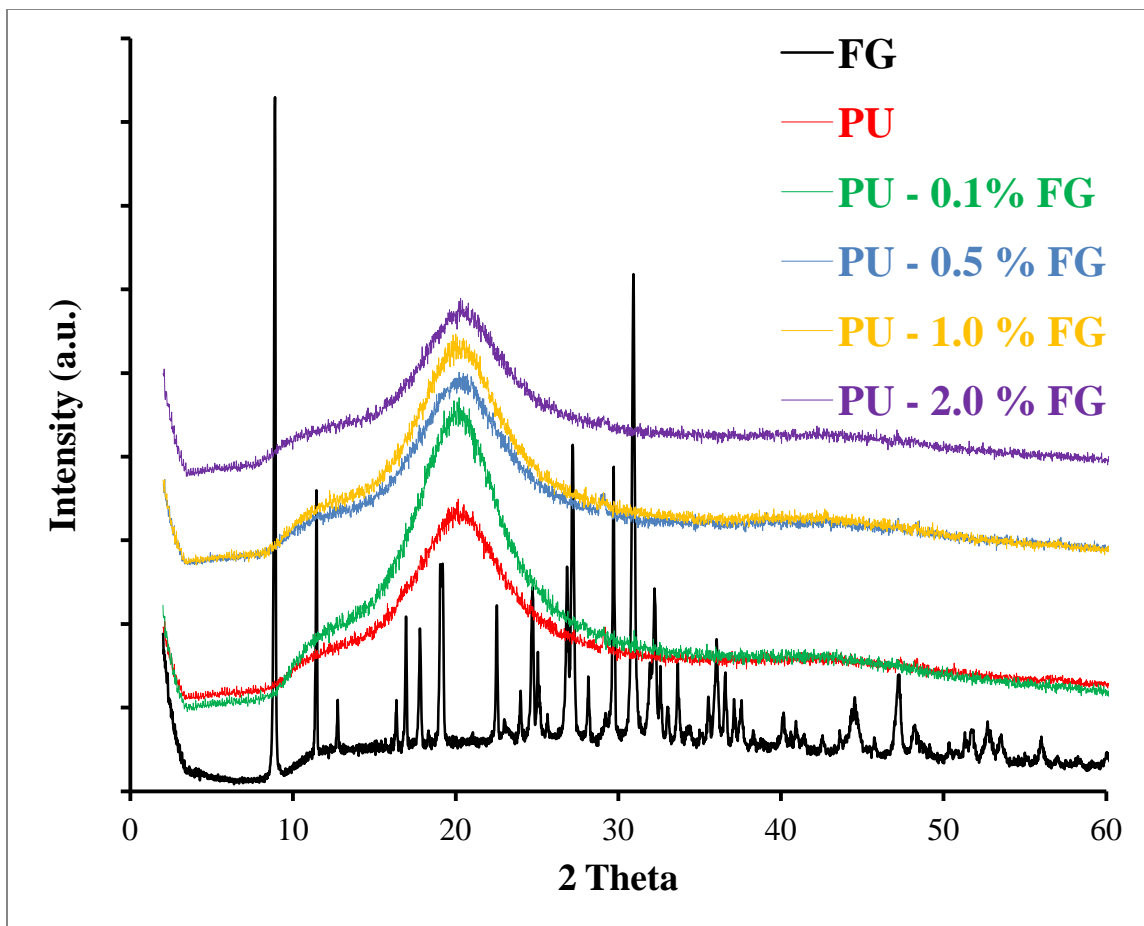


Figure 25: XRD of FG and FG-PU samples offset for clarity.

CHAPTER 4: CONCLUSIONS

4.1 Summary

FG derived from HA is atomically thin with a plate-like morphology. Reduction of HA leads to FG without carboxylate containing functionalities but it does have hydroxyl functionalities present. Raman indicates the reduction of HA also leads to larger domains of conjugated carbon ring systems in the resulting FG and XPS supports this conclusion. These properties present the possibility of very high aspect ratio at lateral dimensions in the hundreds of nanometers which could lead to a very high level of interfacial interaction in polymer nanocomposite materials. This makes FG an interesting target for inclusion in such materials. In the nanocomposite materials tested HA did not show significant mechanical reinforcement whereas FG showed an improvement in modulus of as much as 168%. The 1% loading of FG in PU showed a level of mechanical reinforcement comparable to that of 4% loading of nanoclay and approximately 45% of the mechanical reinforcement predicted by the Halpin-Tsai equation for a disk shaped graphene sheet dispersed phase. In addition, XRD data show that there is no crystalline structure in FG-PU nanocomposites indicating no stacking of FG sheets or intercalation of FG sheets has occurred and some level of exfoliation has been achieved.

The process to make FG is similar to that used to make rGO. The methods for making rGO require the oxidation of graphite followed by a reduction of the resulting GO. FG uses a different starting material, humic acid, which is reduced in a manner similar to the reduction techniques performed on rGO with no prior oxidation necessary. Thus, FG provides a new, shorter synthetic route to graphene-like material than current

methods used to make rGO. FG displays superior mechanical reinforcement of the storage modulus in polymer nanocomposites than that shown by rGO in comparable polymer nanocomposite materials. Therefore, FG provides an interesting alternative for commercial applications for which rGO is currently being considered, developed, and used.

4.2 Future Work

Further characterization of FG would be helpful in elucidating the atomic structure of the sheets, possibly via high resolution transmission electron microscopy. It would also be useful to know the modulus of individual FG sheets either via molecular dynamics¹⁸⁹ or direct measurement⁷ as has been done with graphene. Other properties of FG that should be examined include electrical conductivity, thermal conductivity, barrier properties, etc. alone and in polymer nanocomposites.

It would be informative to compare the mechanical reinforcement of HA and FG using the same loadings in the same matrix. Although there are challenges, the PU used in this study might work as one such material if a technique were developed that provided fine control of film growth conditions (e.g. pH, temperature, humidity, etc.). However, some other matrix (e.g. PU, PVOH, etc.) could also be used provided that both HA and FG interacted well with the matrix and sufficient dispersion of both materials was achieved.

Another valuable research opportunity exists with the variation of the functionalization of humic acid. The size, polarity, and morphology of the sheets may be changed with the addition of a variety of functional groups. This would allow for the tuning of material for compatibility with a selected polymer. In addition, the material

could be copolymerized with a variety of polymers to include nanosheets in the polymer backbone.

Commercialization of FG should also be assessed. This assessment should include a comparison of the cost and availability of HA, the starting material for FG, to those of graphite, the starting material of rGO. A study of the suitability of FG in applications for which rGO is currently being considered and used should be initiated. These analyses would be useful for targeting potential commercial applications of FG and could be used to produce a more detailed analysis of its commercial viability.

APPENDIX SECTION

Section A. Abbreviations and Definitions

Table 3: Abbreviations and Definitions.

Abbreviation	Definition
AFM	Atomic Force Microscopy/Microscope
CVD	Chemical Vapor Deposition
diH ₂ O	Deionized Water
DLG	Double Layer Graphene
DMA	Dynamic Mechanical Analysis
DMF	N,N-Dimethylformamide
eGO	Exfoliated Graphene Oxide
EPD	Electrophoretic Deposition
FG	Functionalized Graphene
FLFG	Few Layer Functionalized Graphene
FLG	Few Layer Graphene
FT-IR	Fourier Transform Infrared Spectroscopy/Spectrometer
GIC	Graphite Intercalation Compound
GO	Graphite Oxide
HA	Humic Acid
ILC	Ionic Liquid Crystal
MAfPP	Maleic Anhydride functionalized Polypropylene (Exxelor™ PO 1020 in this study)
NMP	N-Methyl Pyrrolidone
PAH	Polycyclic Aromatic Hydrocarbon
PECVD	Plasma Enhance Chemical Vapor Deposition
PS	Polystyrene
PU	Polyurethane (Bahydrol™ 124 in this study)
PVOH	Polyvinyl Alcohol
rGO	Reduced Graphene Oxide
SC	Super Critical
SEM	Scanning Electron Microscopy/Microscope
SiC	Silicon Carbide
SLG	Single Layer Graphene
TEM	Transmission Electron Microscopy/Microscope
THF	Tetrahydrofuran
UV	Ultraviolet
XPS	X-ray Photoelectron Spectroscopy/Spectrometer
XRD	X-ray Diffraction/Diffractometer

Section B. DMA Results for MAfPP and HA-MAfPP Nanocomposites

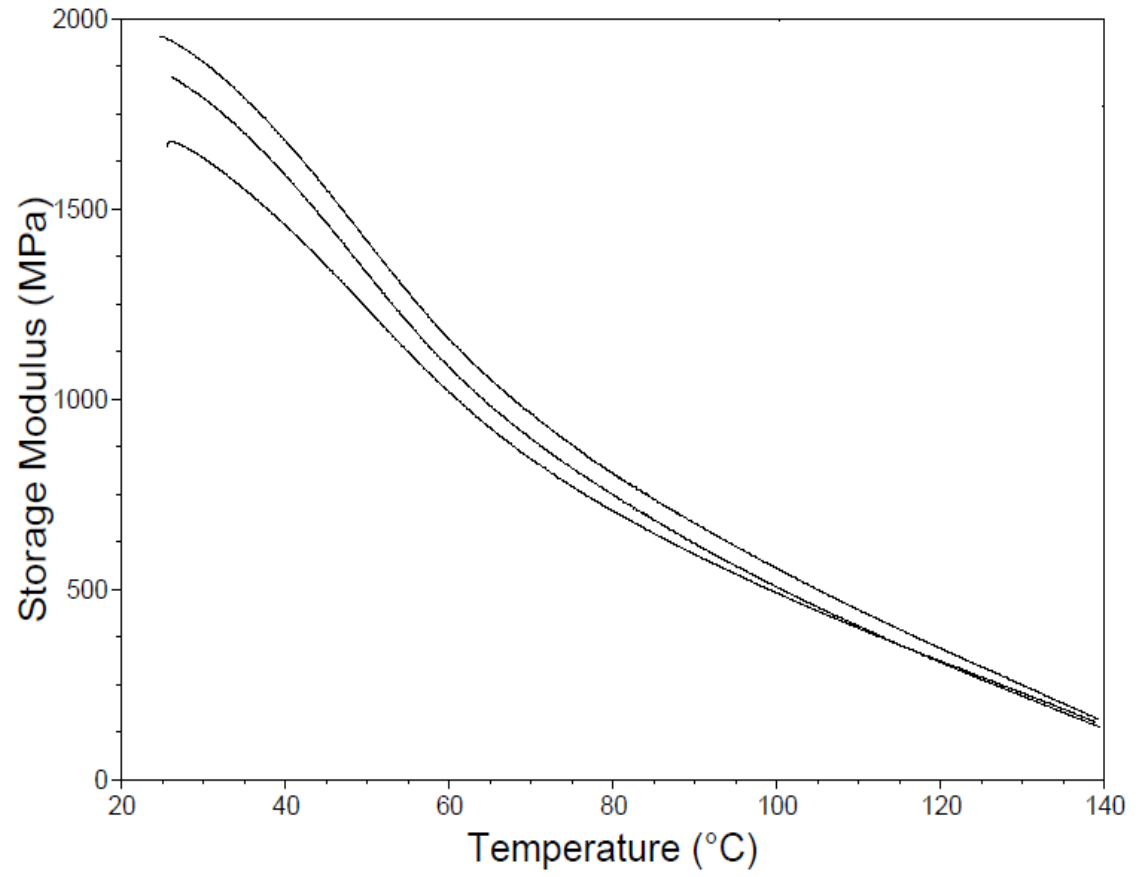


Figure 26: DMA of neat MAfPP samples.

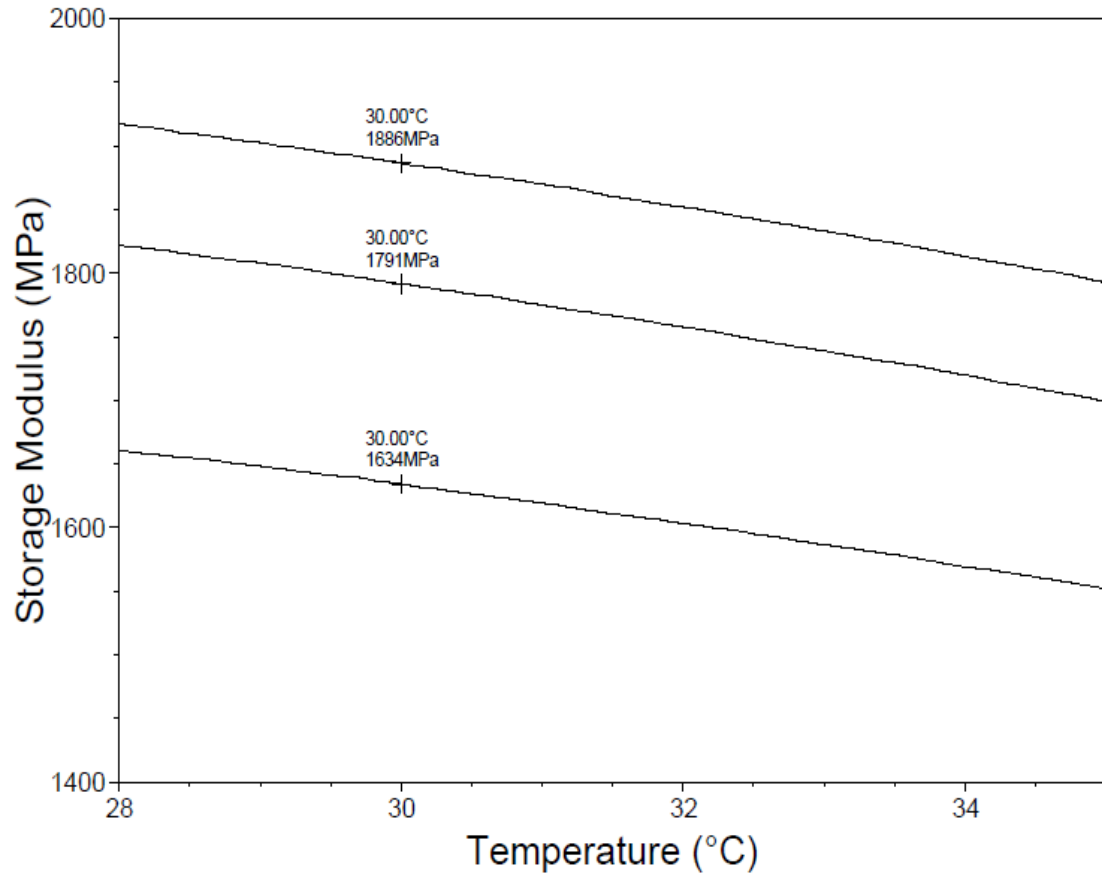


Figure 27: DMA results for neat MAfPP showing storage modulus at 30° C.

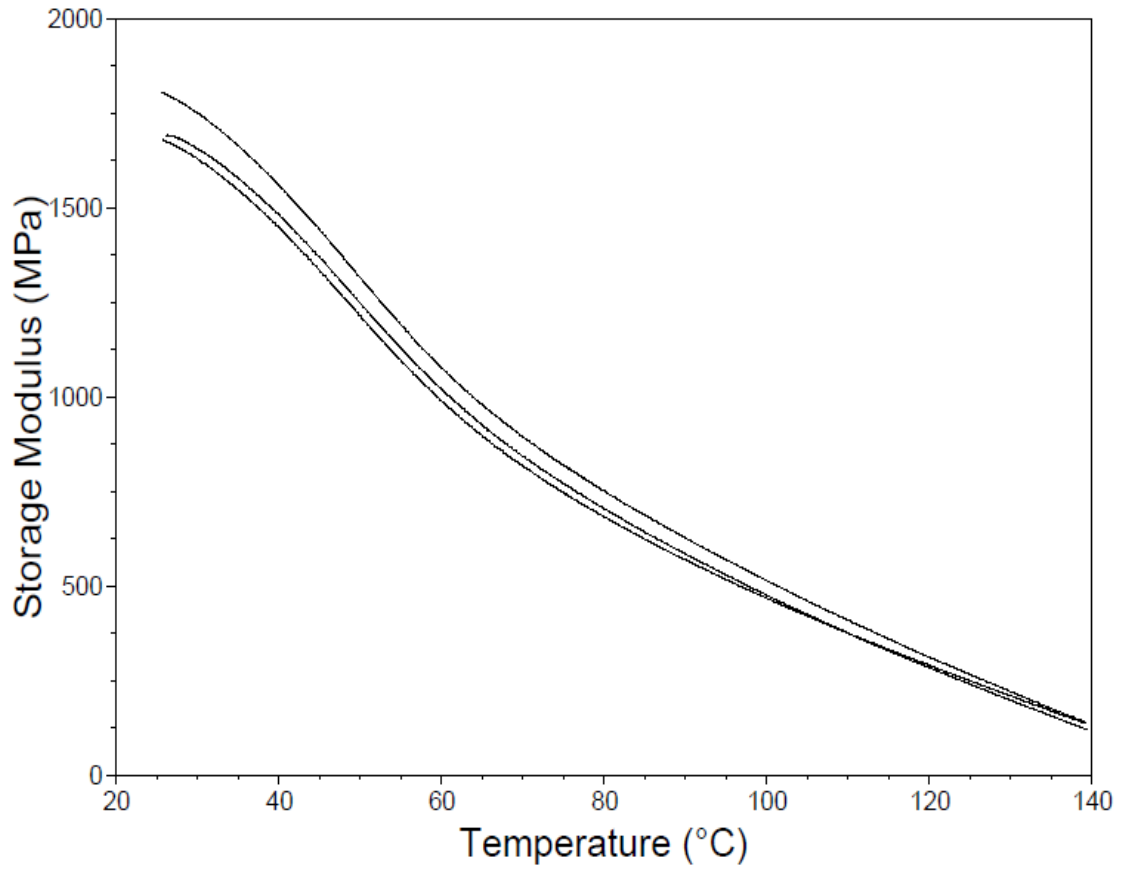


Figure 28: DMA of MAfPP - 1.0% HA samples.

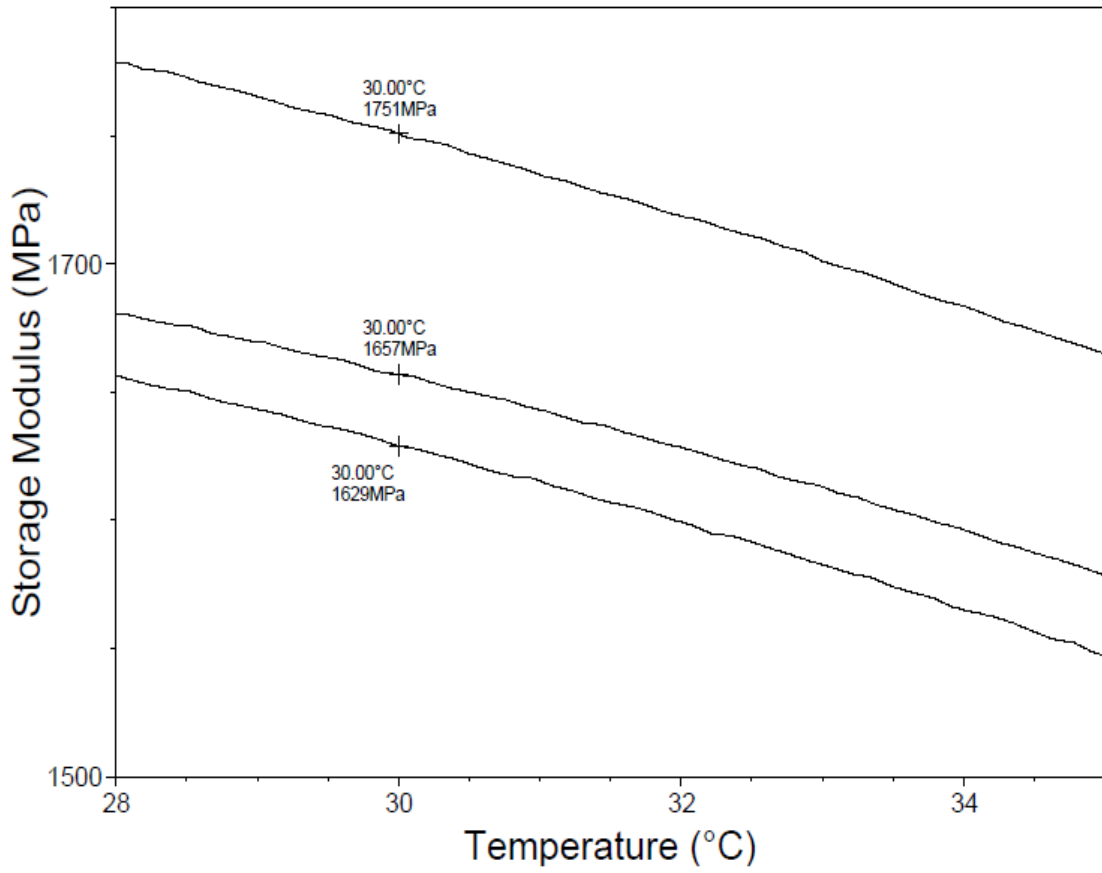


Figure 29: DMA results for MAfPP - 1.0% HA showing storage modulus at 30° C.

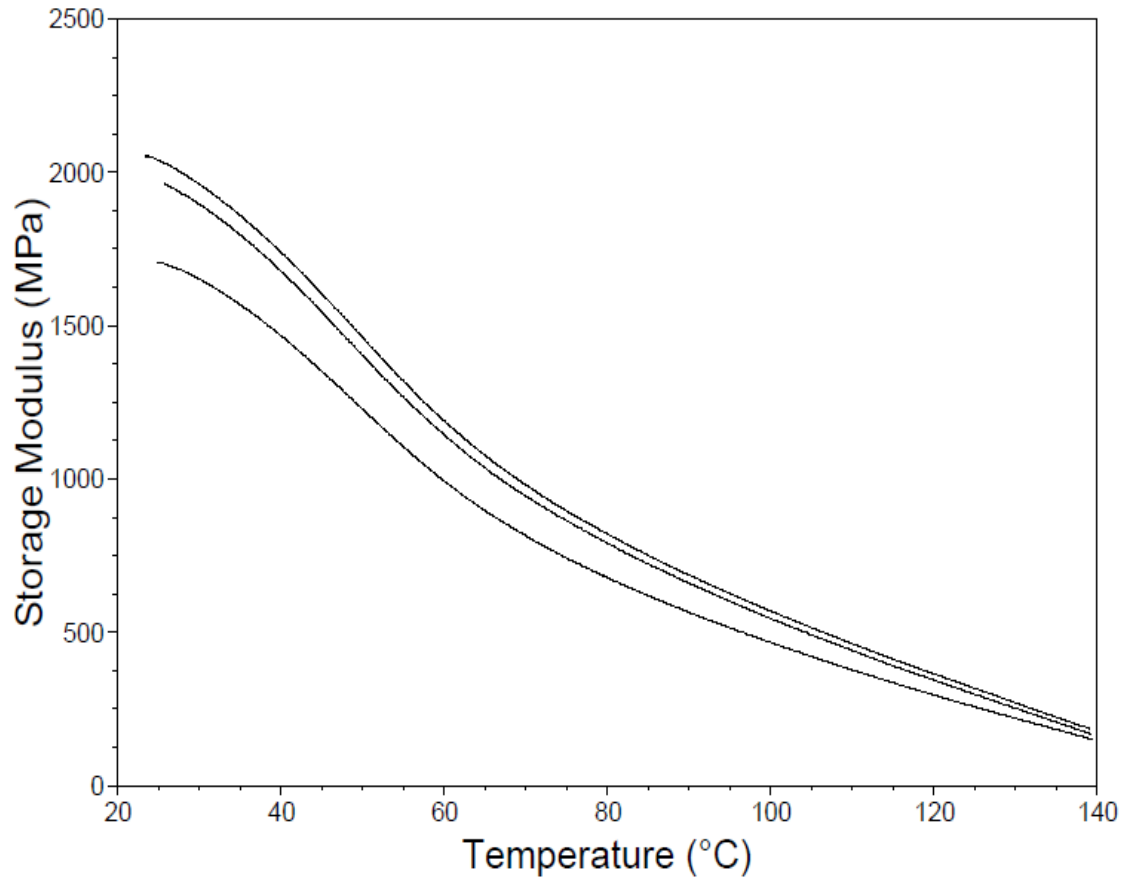


Figure 30: DMA of MAfPP - 2.0% HA samples.

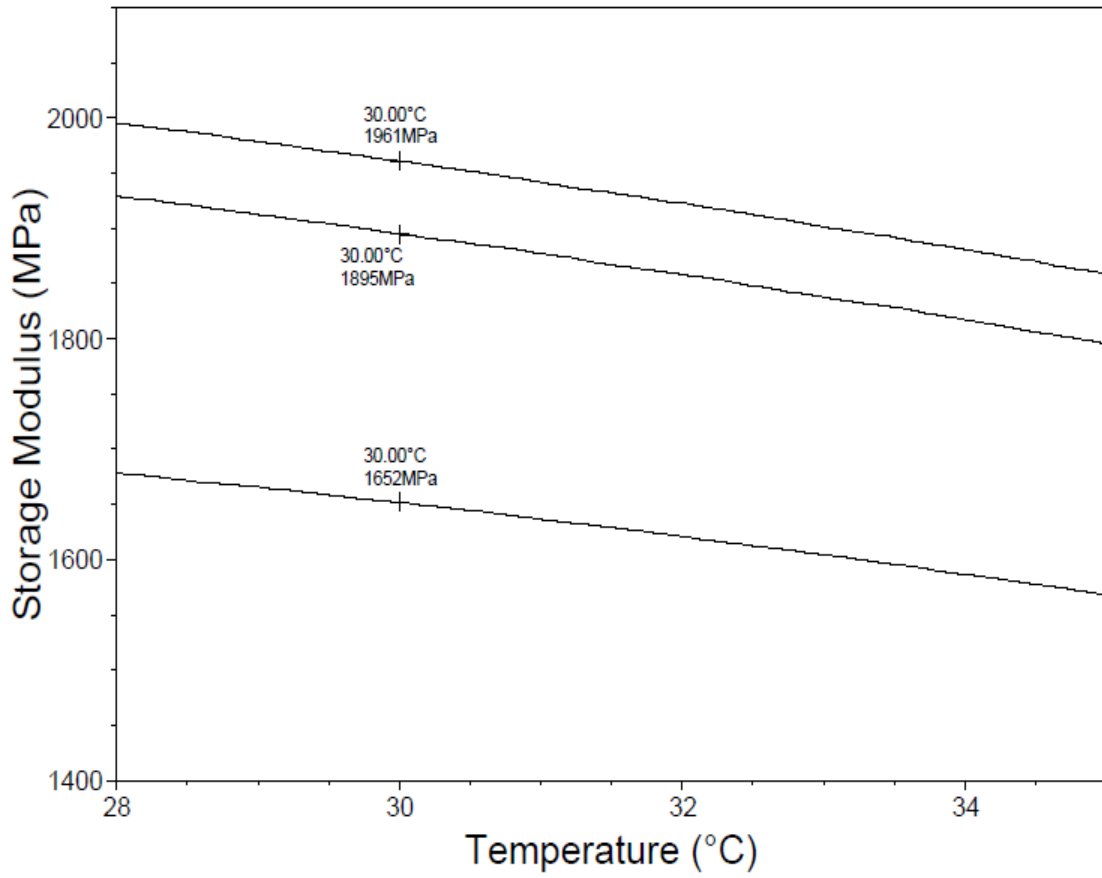


Figure 31: DMA results for MAfPP - 2.0% HA showing storage modulus at 30° C.

Table 4: Calculations of average storage modulus and standard deviation in MAfPP and HA-MAfPP samples.

	MAfPP Storage Modulus (Mpa)	MAfPP - 1.0% HA Storage Modulus (Mpa)	MAfPP - 2.0% HA Storage Modulus (Mpa)
Sample 1	1886	1751	1961
Sample 2	1791	1657	1895
Sample 3	1634	1629	1652
Average	1770	1679	1836
Std Dev	127.3	63.91	162.7

Section C. DMA Results for PS and HA-PS Nanocomposites

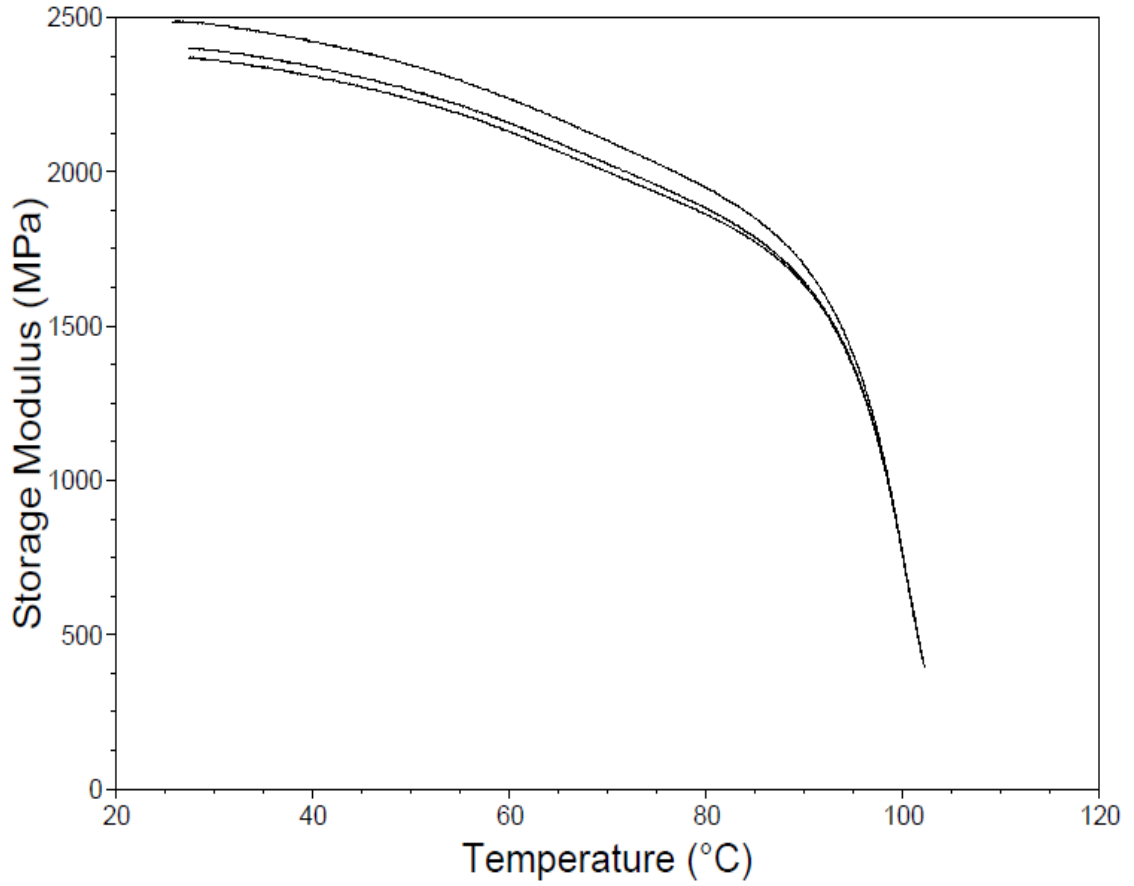


Figure 32: DMA of neat PS samples.

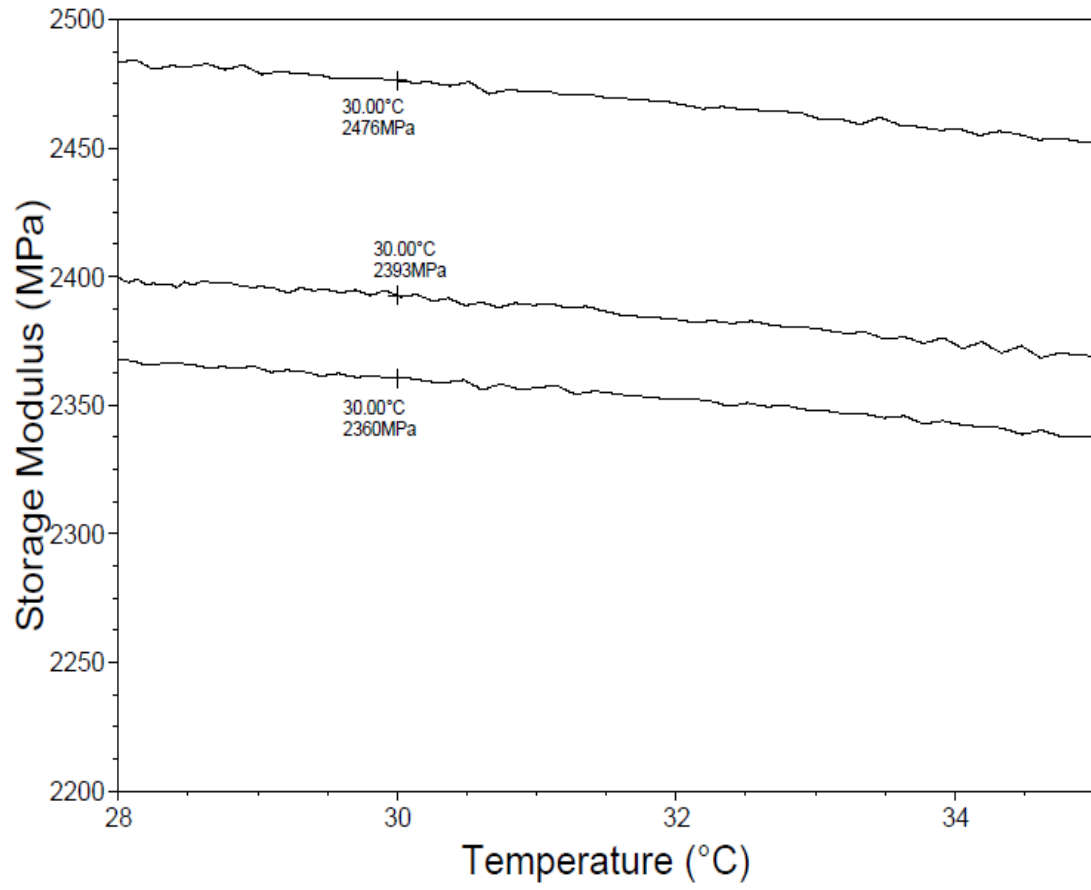


Figure 33: DMA results for neat PS showing storage modulus at 30° C.

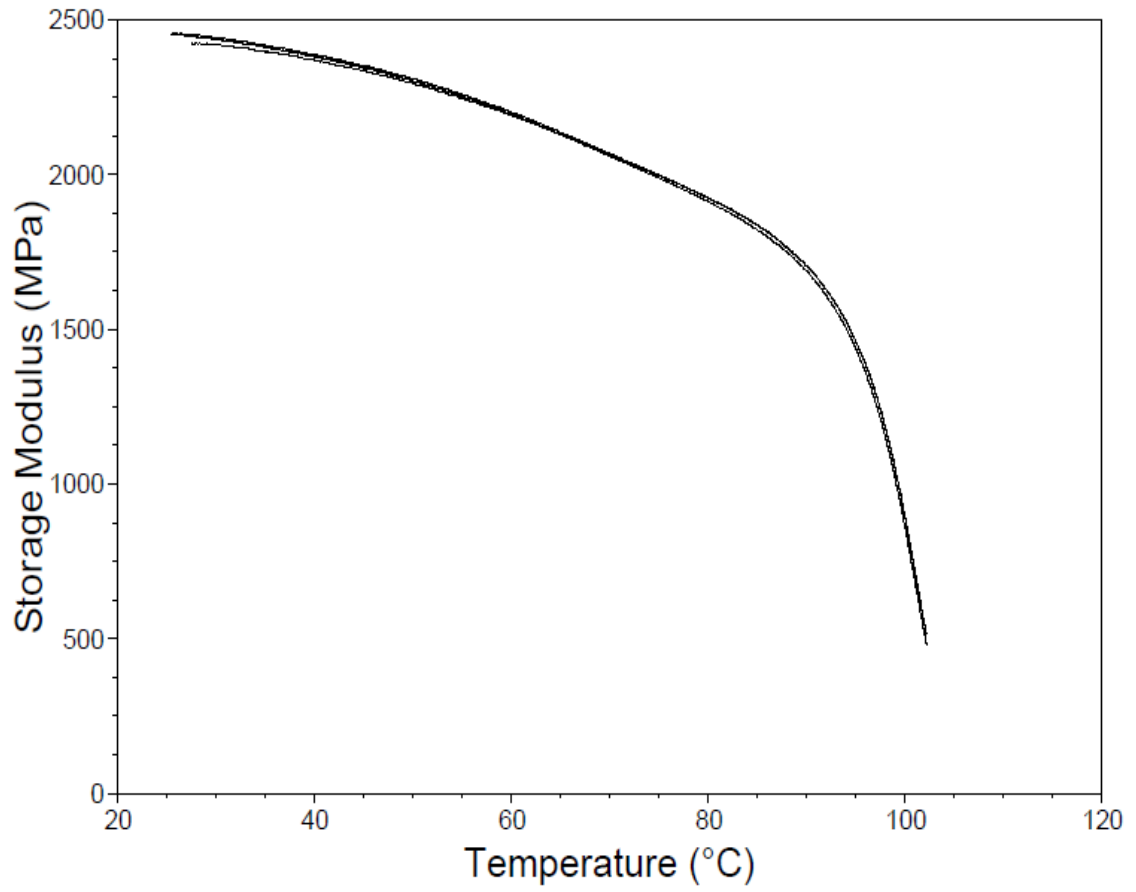


Figure 34: DMA of PS - 1.0% HA samples.

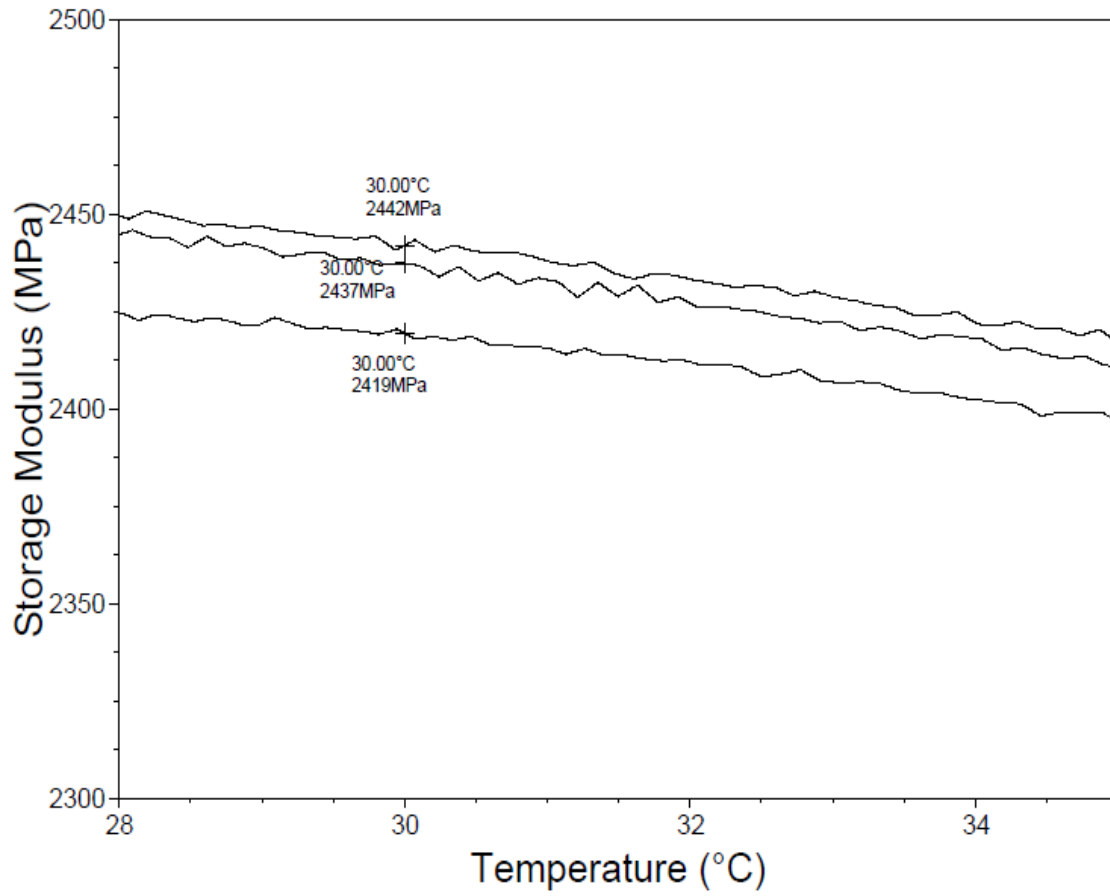


Figure 35: DMA results for PS - 1.0% HA showing storage modulus at 30° C.

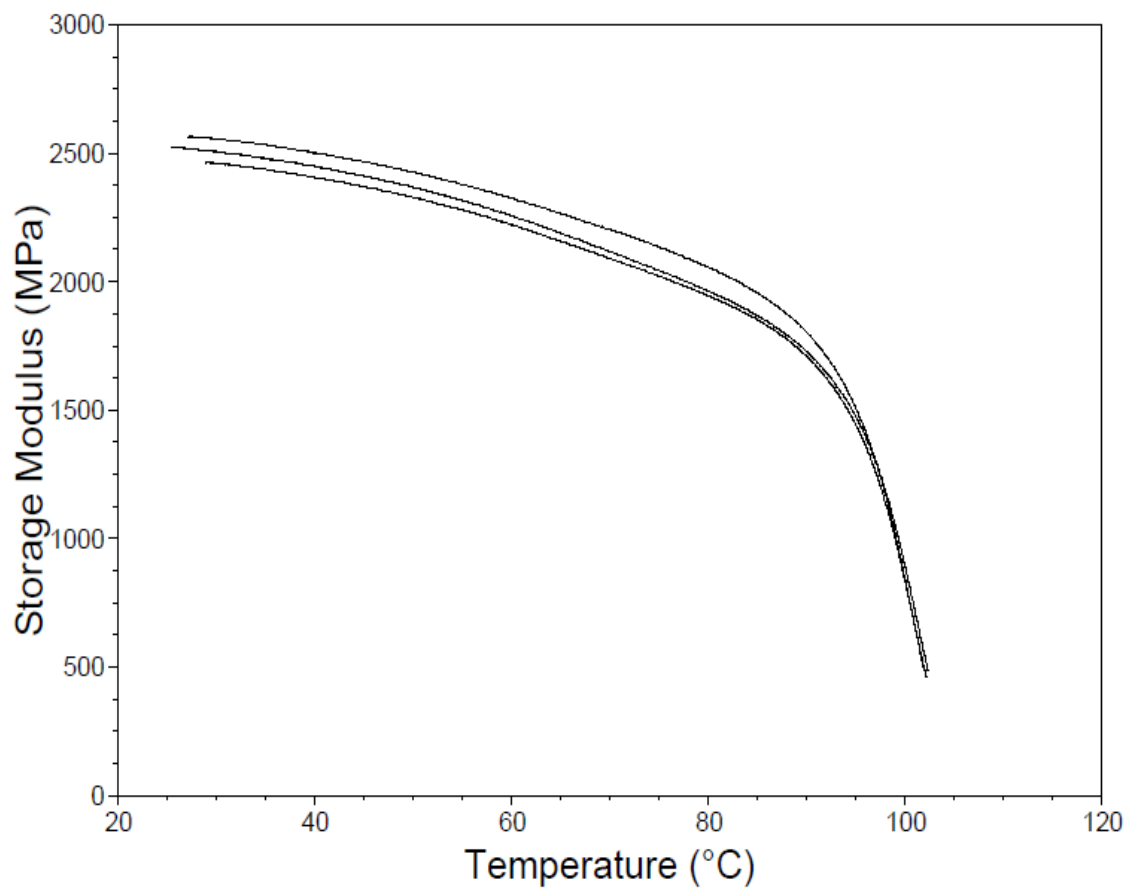


Figure 36: DMA of PS - 2.0% HA samples.

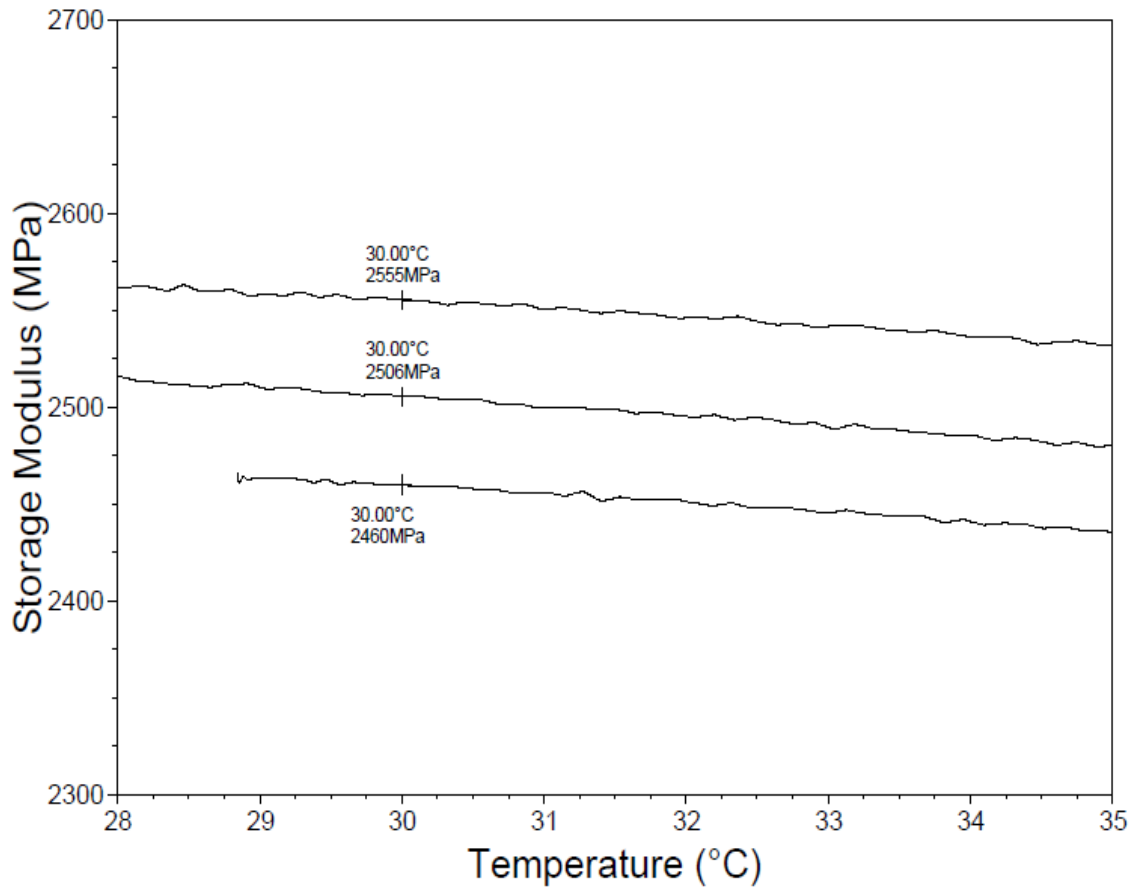


Figure 37: DMA results for PS - 2.0% HA showing storage modulus at 30° C.

Table 5: Calculations of average storage modulus and standard deviation in PS and HA-PS samples.

	PS Storage Modulus (Mpa)	PS - 1.0% HA Storage Modulus (Mpa)	PS- 2.0% HA Storage Modulus (Mpa)
Sample 1	2476	2442	2555
Sample 2	2393	2437	2506
Sample 3	2360	2419	2460
Average	2410	2433	2507
Std Dev	59.77	12.10	47.51

Section D. DMA Results for PU and FG-PU Nanocomposites

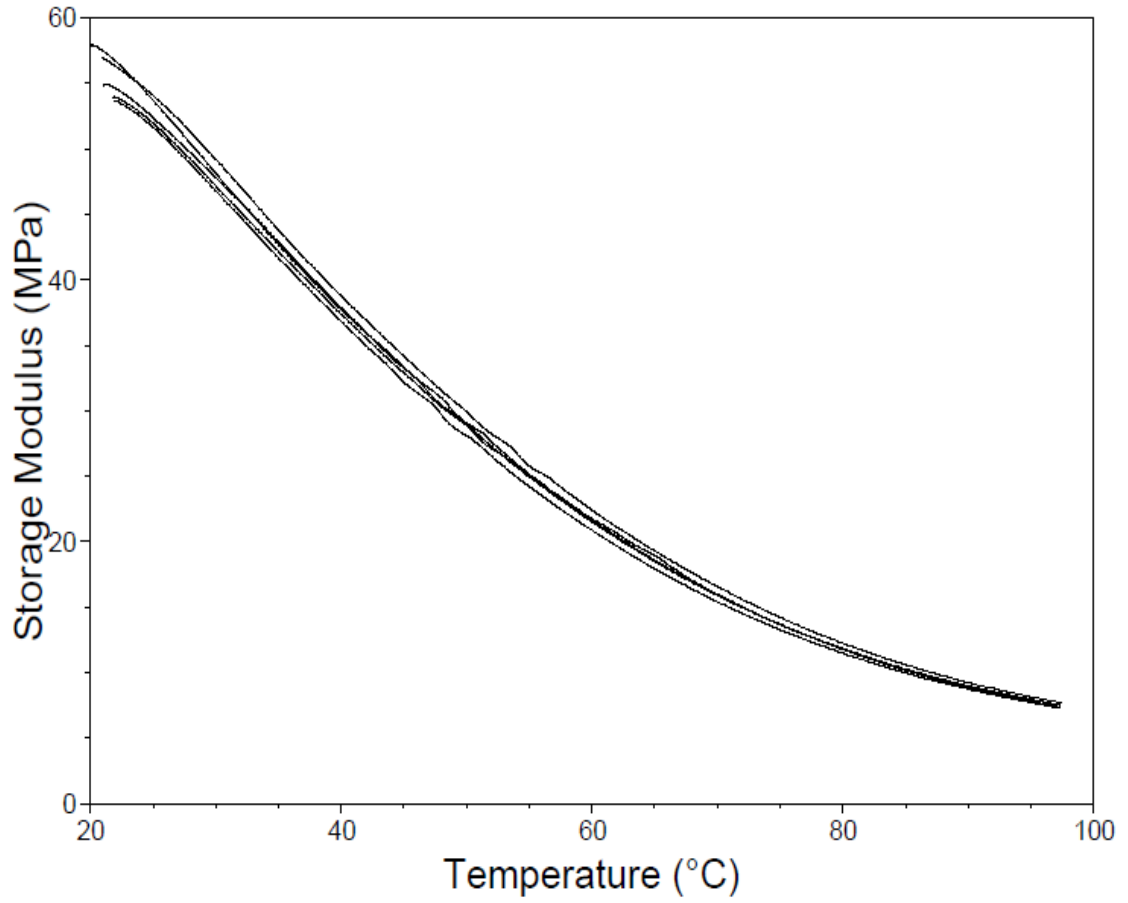


Figure 38: DMA of neat PU samples.

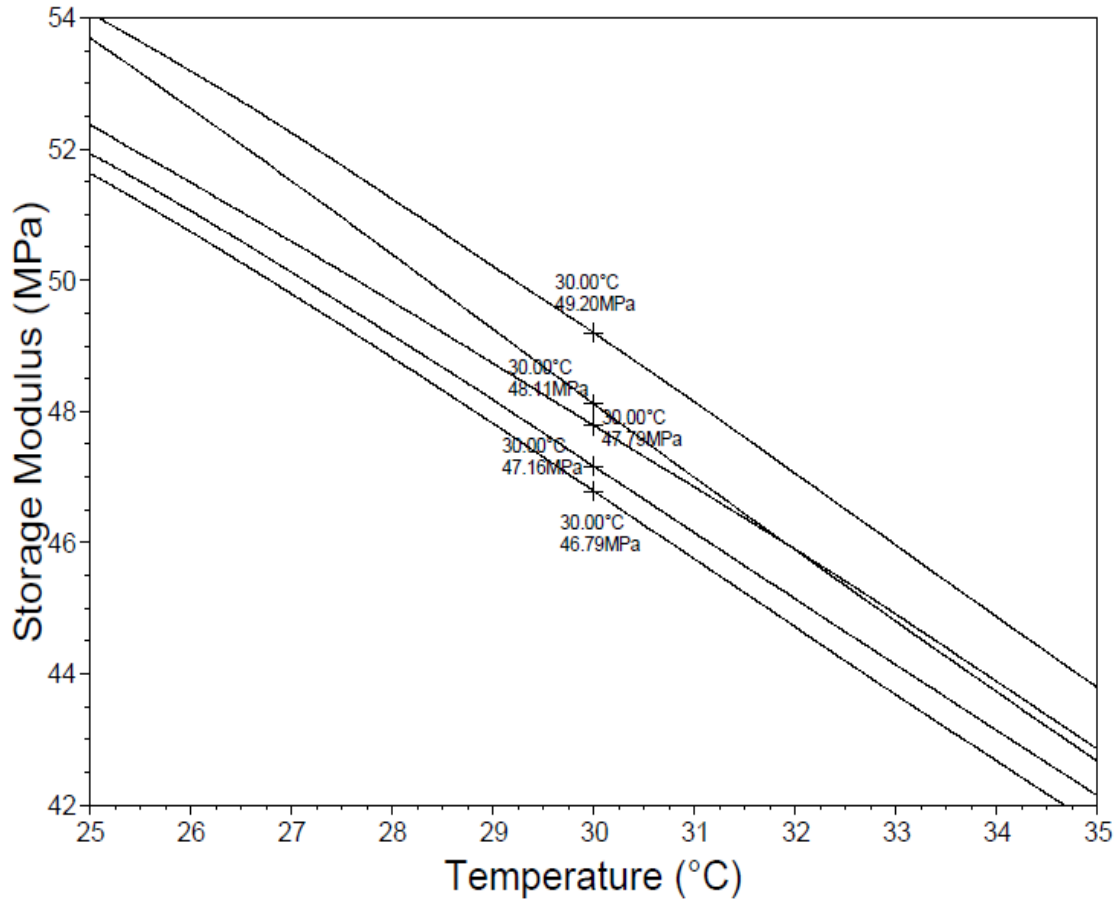


Figure 39: DMA results for neat PU showing storage modulus at 30° C.

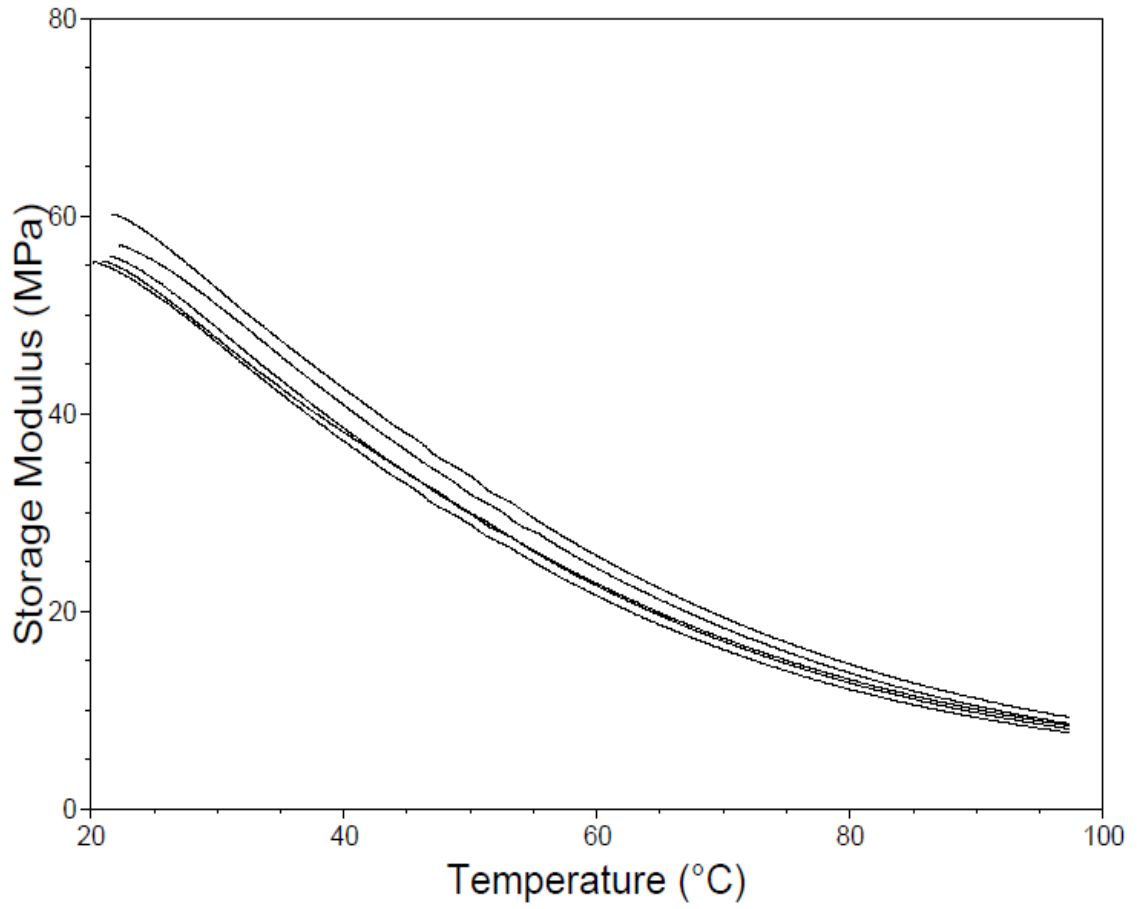


Figure 40: DMA of PU - 0.1% FG samples.

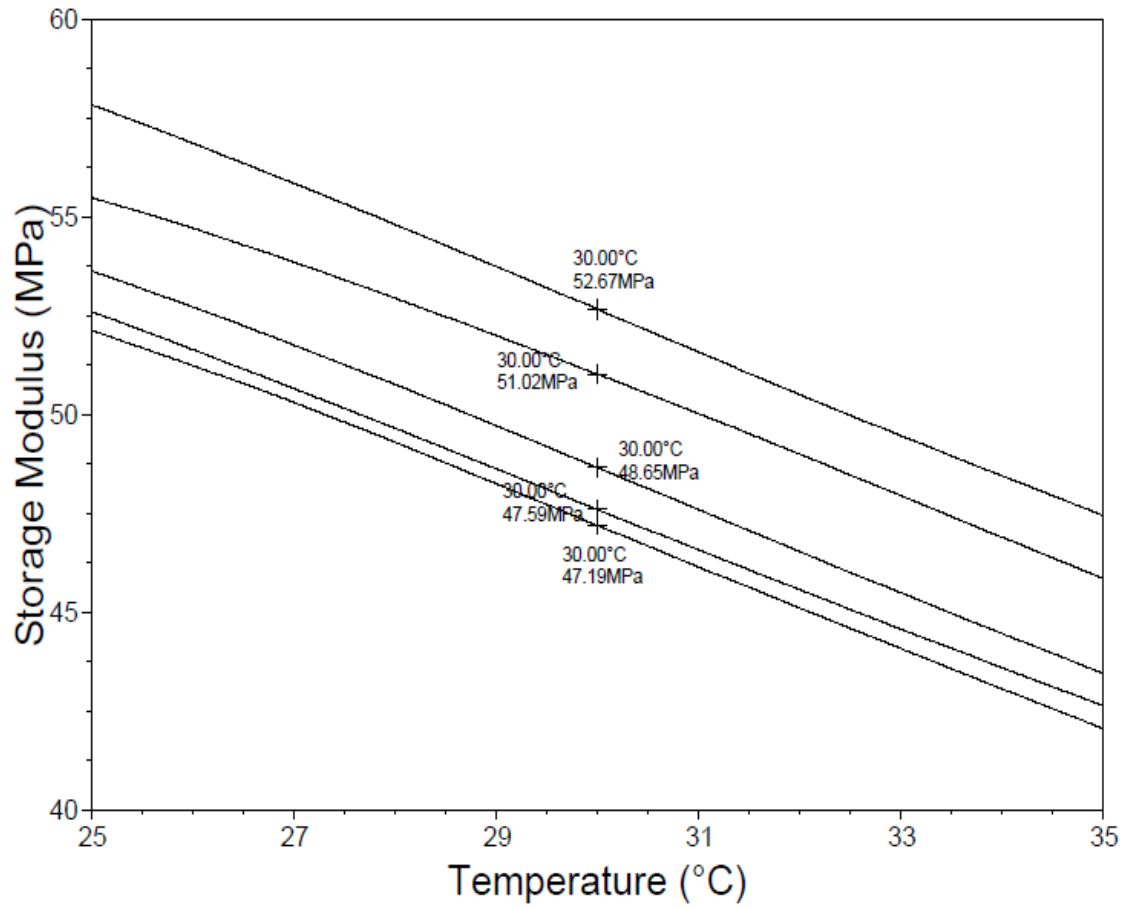


Figure 41: DMA results for PU - 0.1% FG showing storage modulus at 30° C.

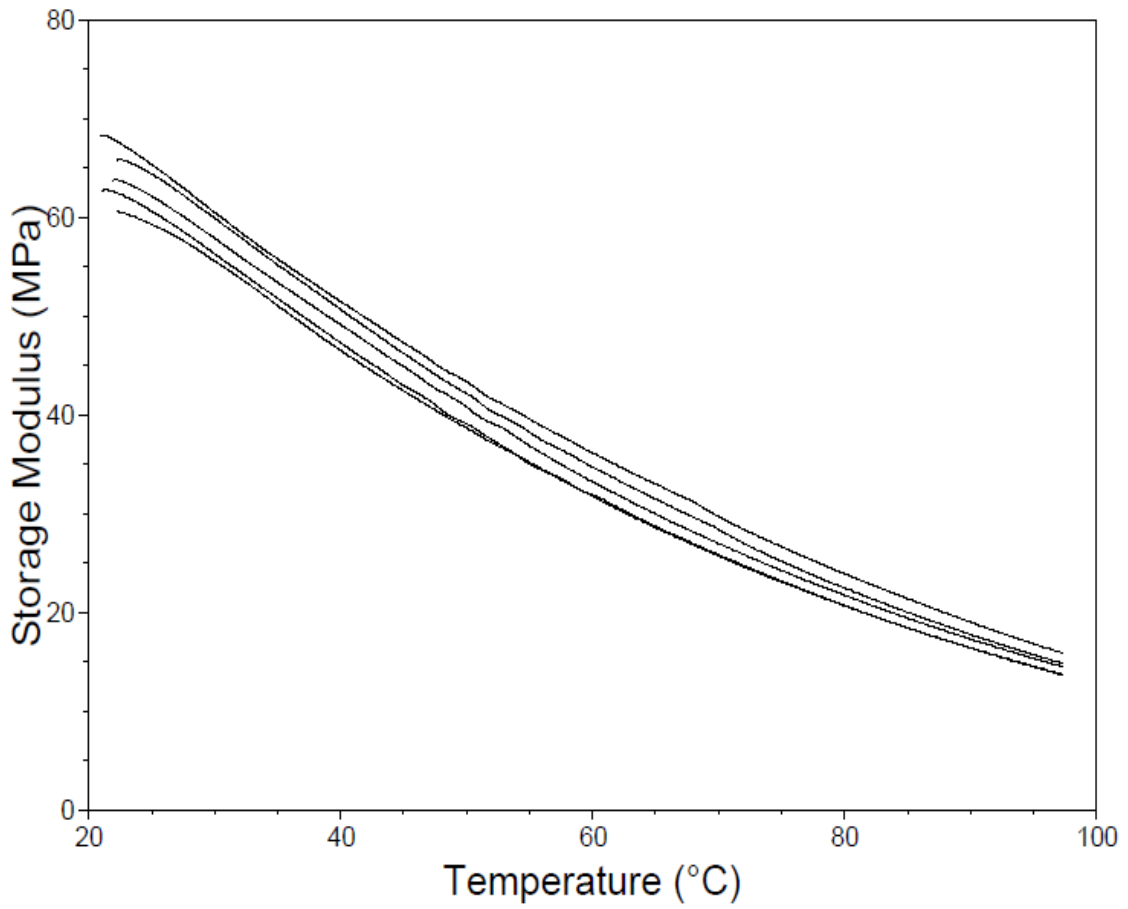


Figure 42: DMA of PU - 0.5% FG samples.

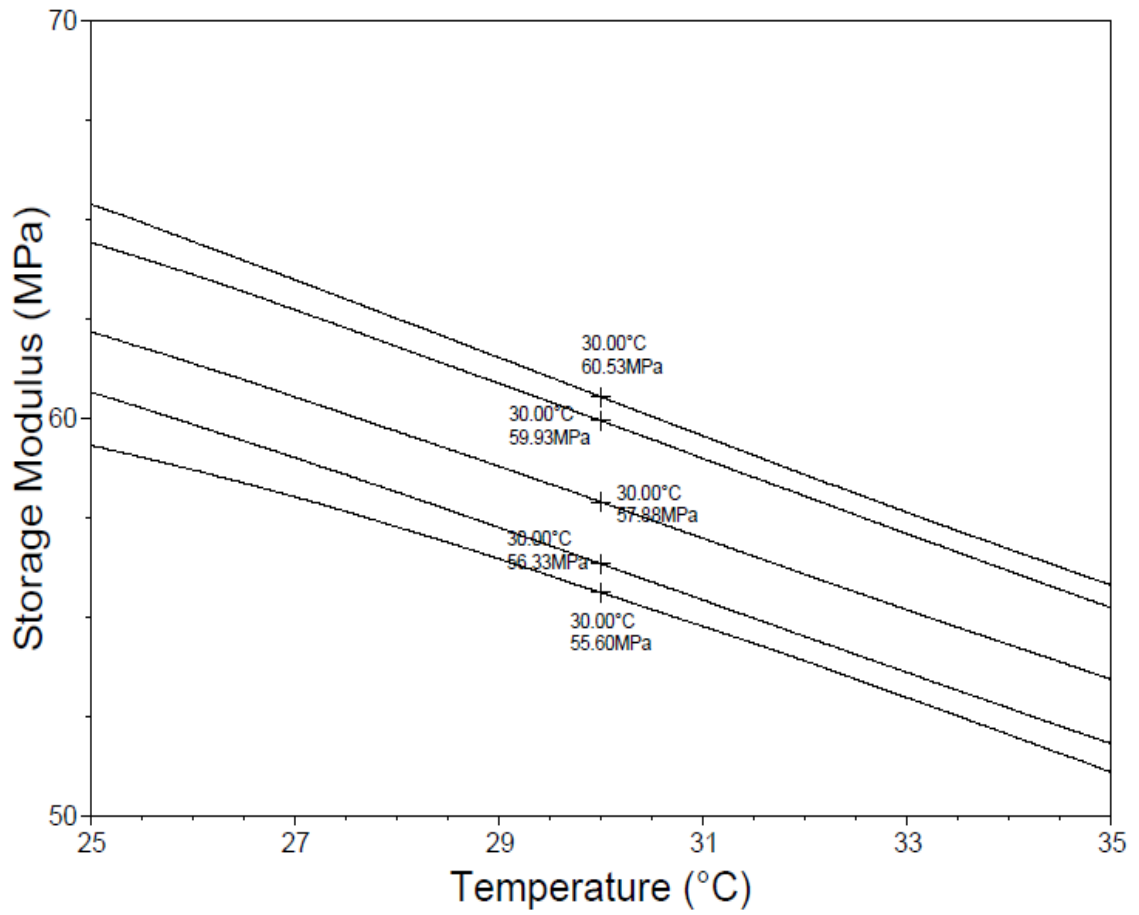


Figure 43: DMA results for PU - 0.5% FG showing storage modulus at 30° C.

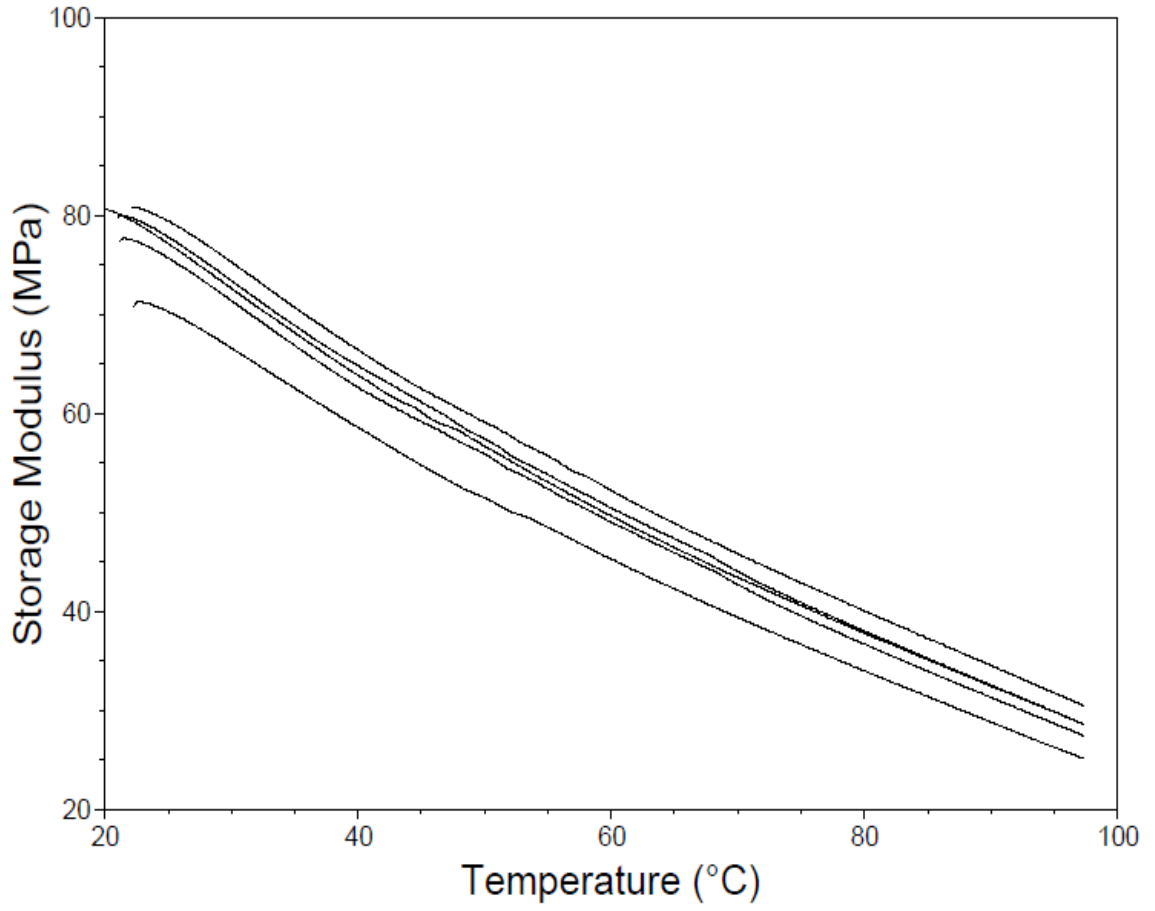


Figure 44: DMA of PU - 1.0% FG samples.

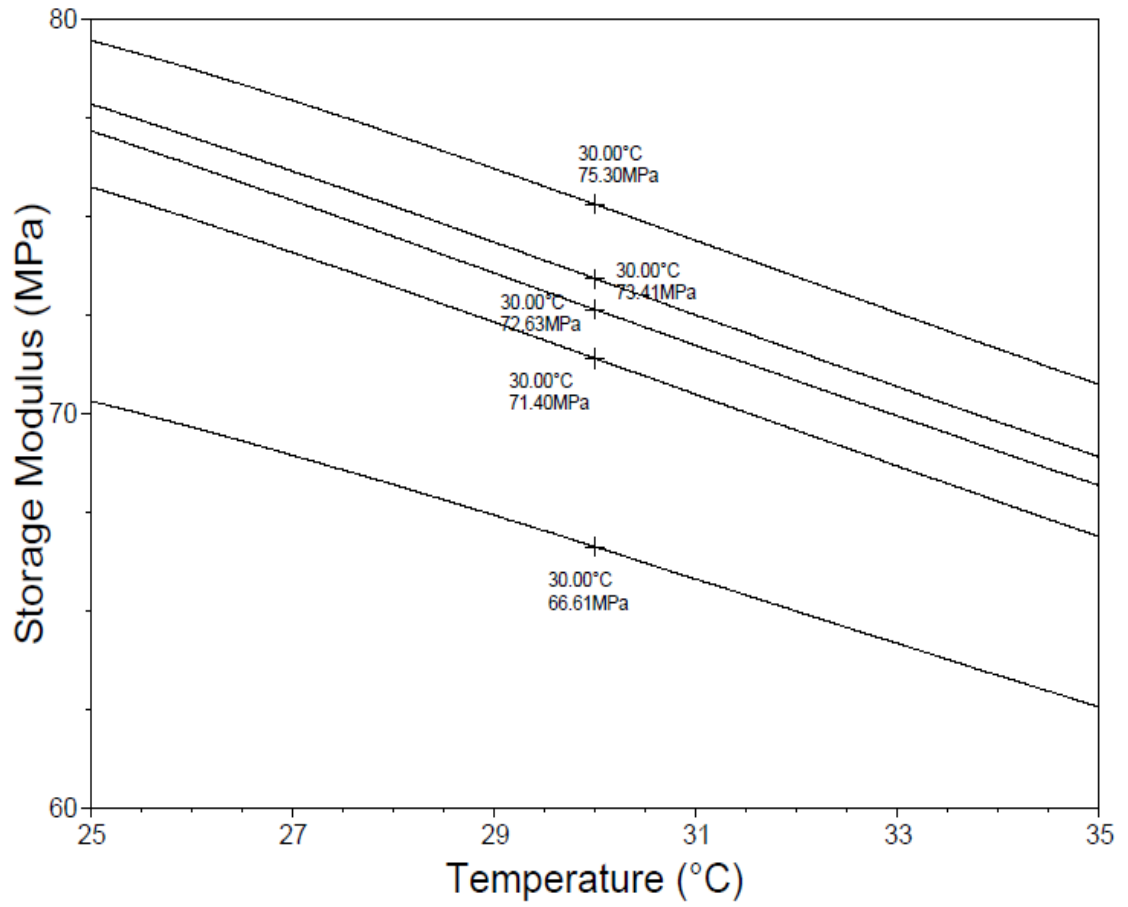


Figure 45: DMA results for PU - 1.0% FG showing storage modulus at 30° C.

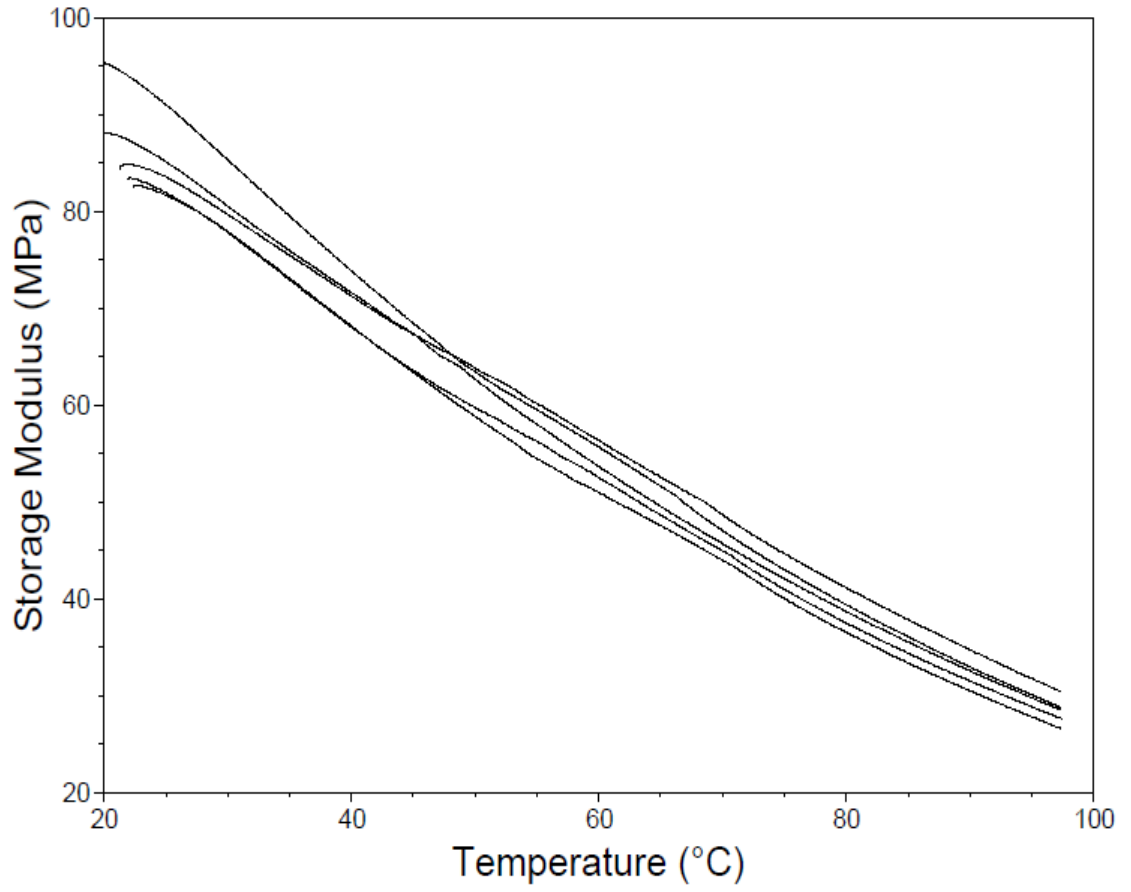


Figure 46: DMA of PU - 2.0% FG samples.

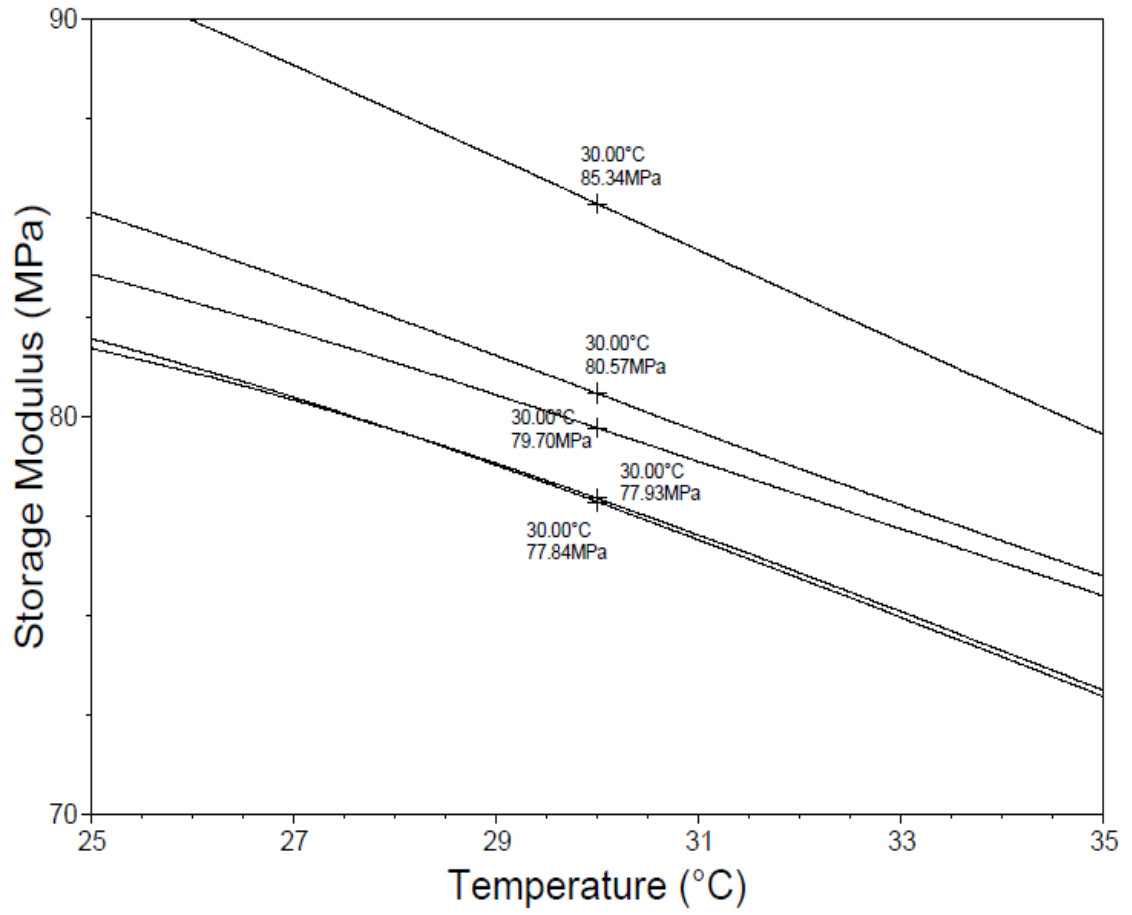


Figure 47: DMA results for PU - 2.0% FG showing storage modulus at 30° C.

Table 6: Calculations of average storage modulus and standard deviation in PU and FG-PU samples.

	PU Storage Modulus (Mpa)	PU - 0.1% FG Storage Modulus (Mpa)	PU - 0.5% FG Storage Modulus (Mpa)	PU - 1.0% FG Storage Modulus (Mpa)	PU - 2.0% FG Storage Modulus (Mpa)
Sample 1	49.20	52.67	60.53	75.30	85.34
Sample 2	48.11	51.02	59.93	73.41	80.57
Sample 3	47.79	48.65	57.88	72.63	79.70
Sample 4	47.16	47.59	56.33	71.40	77.93
Sample 5	46.79	47.19	55.60	66.61	77.84
Average	47.81	49.42	58.05	71.87	80.28
Std Dev	0.9335	2.347	2.161	3.264	3.062

Section E. Variables Used in Halpin-Tsai Equation

Table 7: Variables used in Halpin-Tsai Equation with references.

Variable	Value	Reference
Polyurethane Modulus	47.81 Mpa	Experimental
Polyurethane Density	1.06 g/cm ³	[¹⁹⁰]
Graphene Modulus	1000 Gpa	[⁷]
Graphite Density	2.16	[¹⁹¹]
FG Aspect Ratio	500	[¹⁷⁵]

Section F. Individual XRD Scans of MAfPP and PS Samples

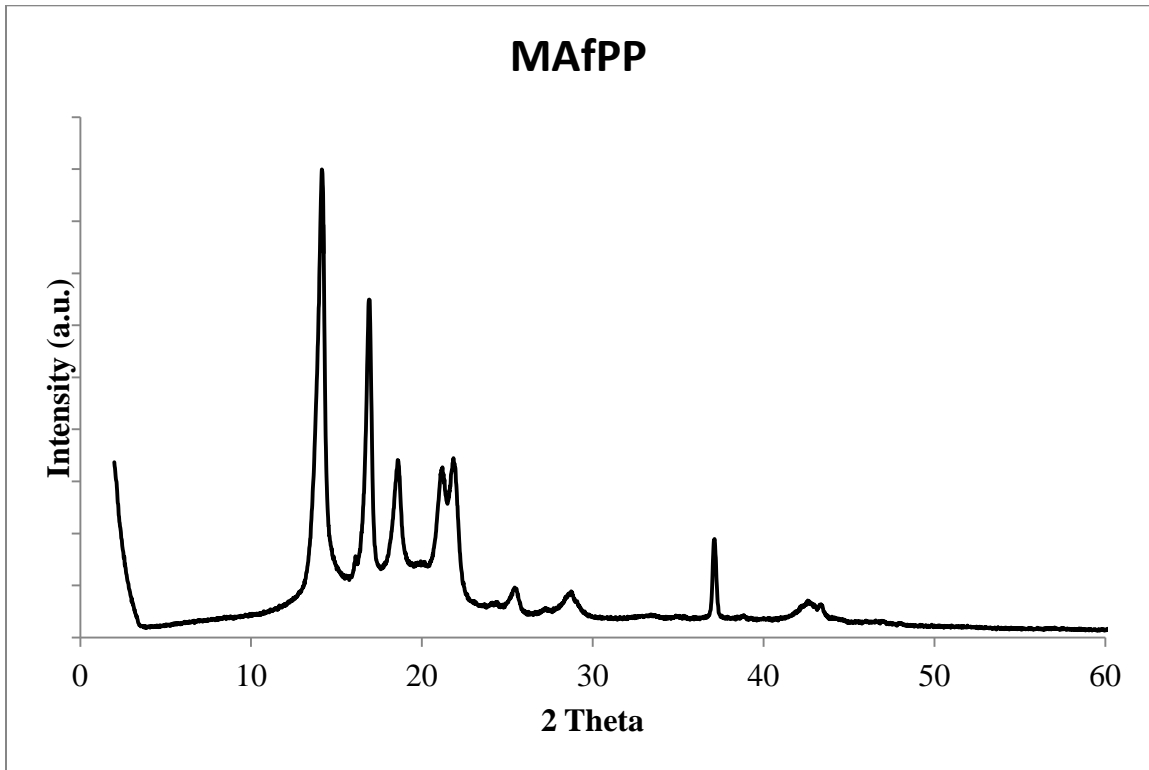


Figure 48: XRD of neat MAfPP.

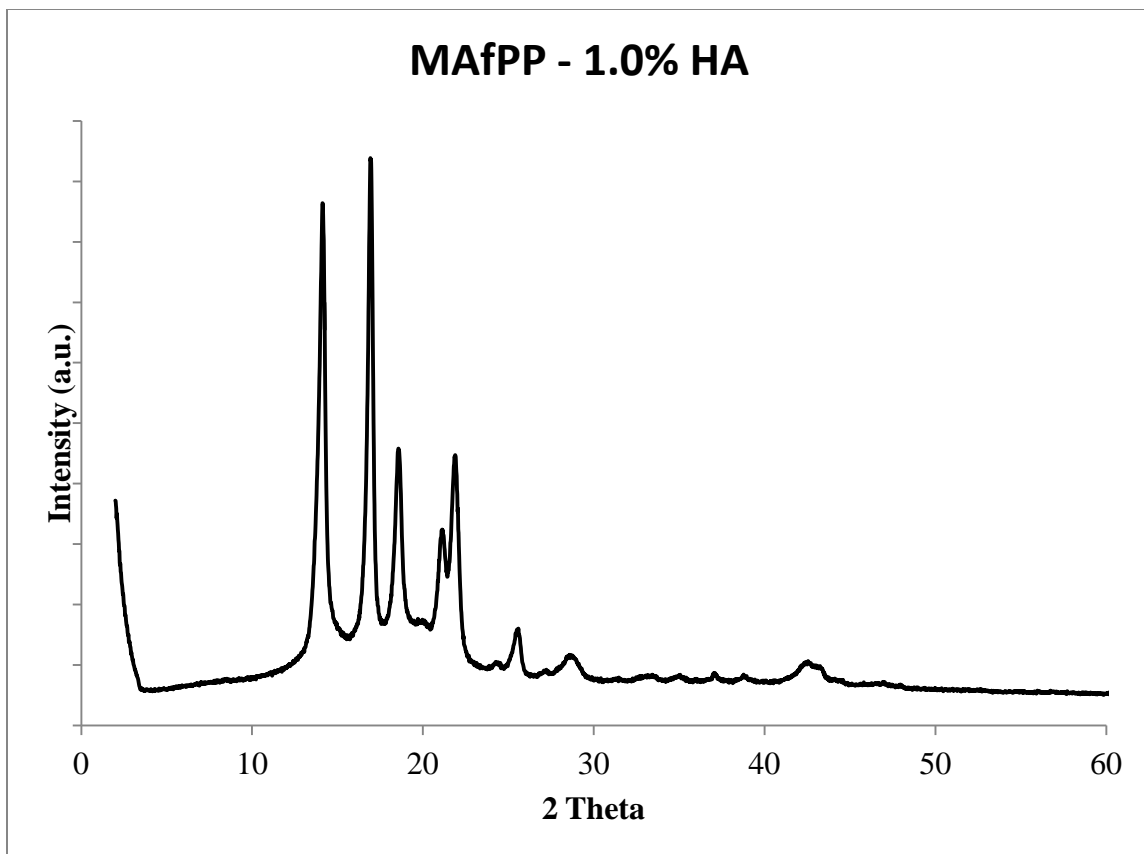


Figure 49: XRD of MAfPP - 1.0% HA sample.

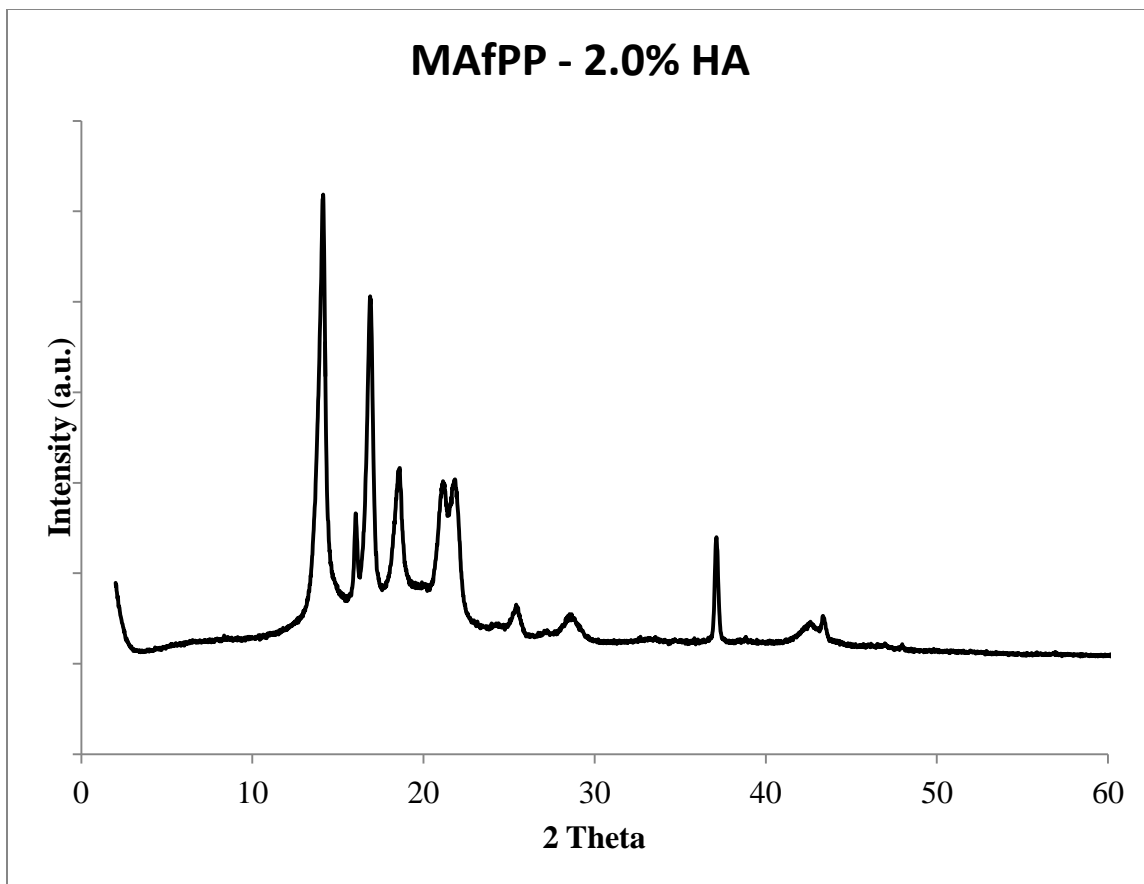


Figure 50: XRD of MAfPP - 2.0% HA sample.

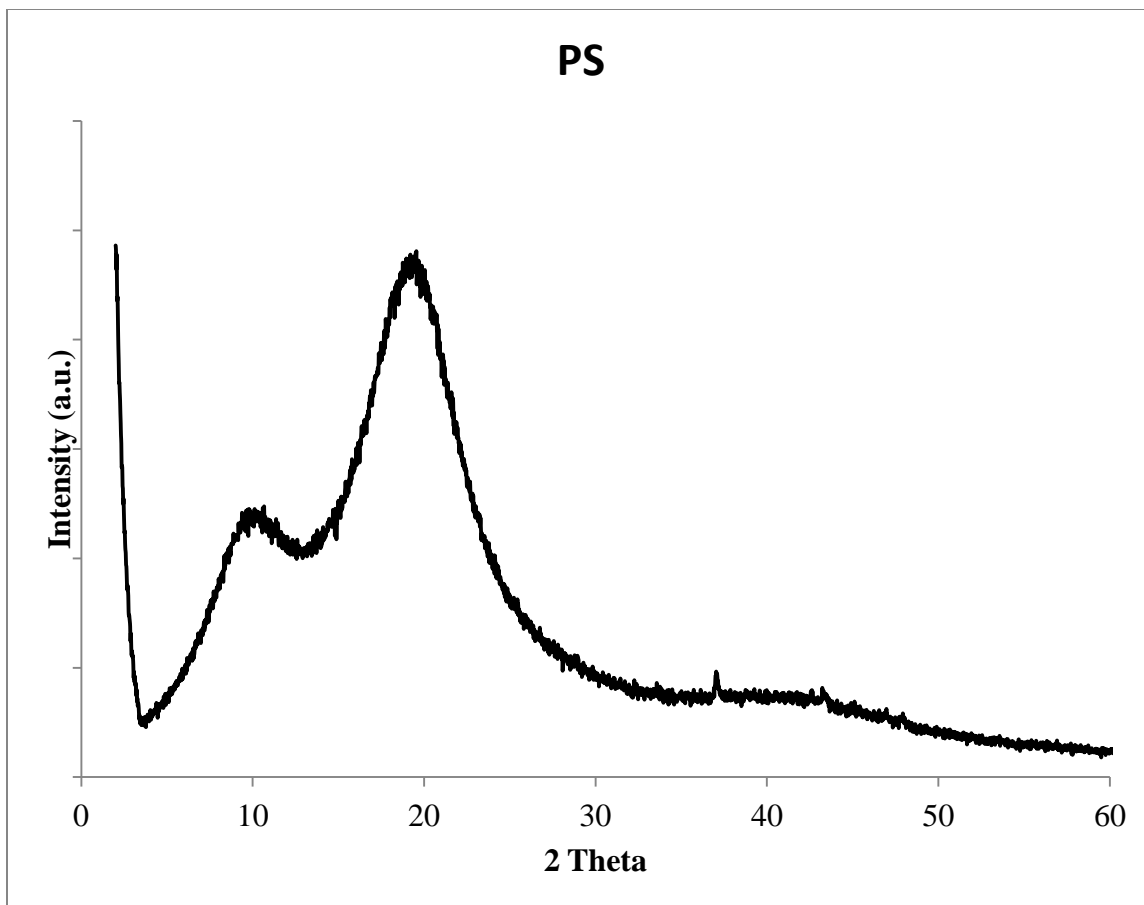


Figure 51: XRD of neat PS sample.

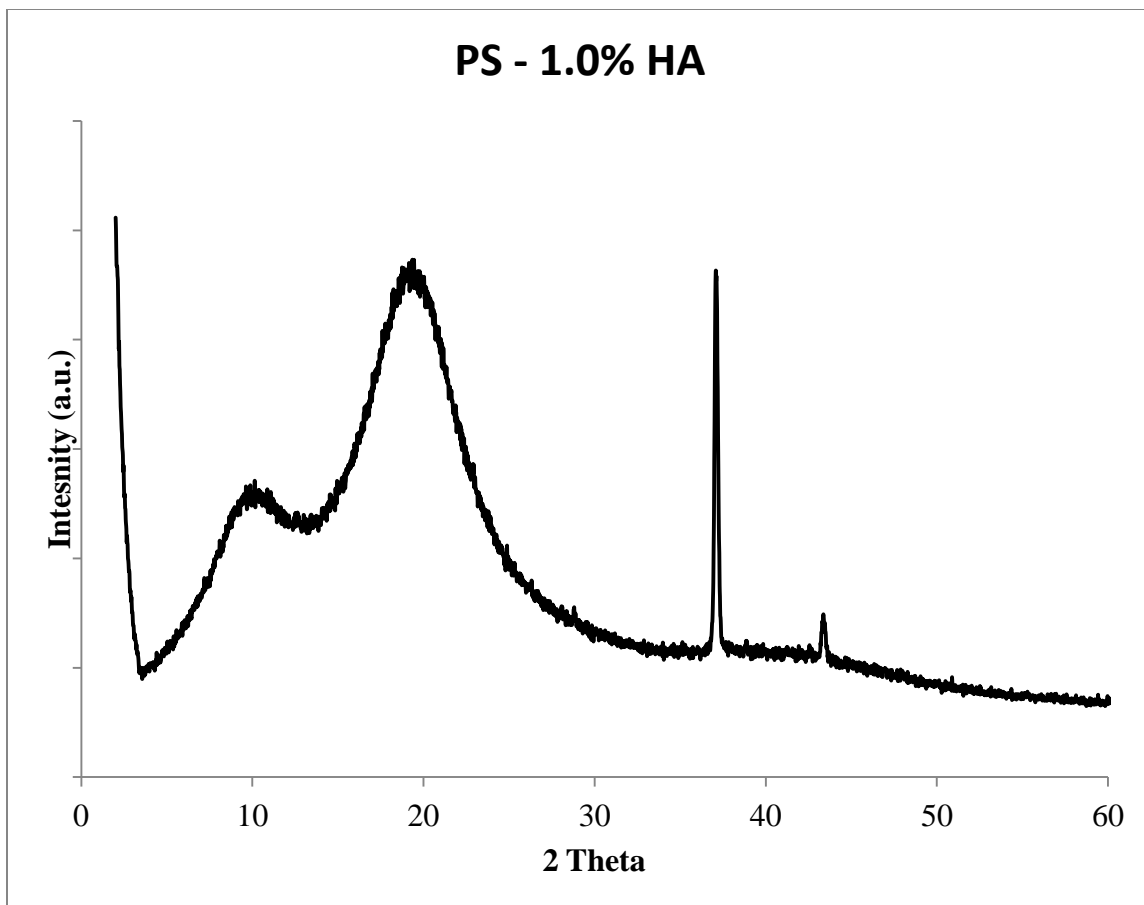


Figure 52: XRD of PS - 1.0% HA sample.

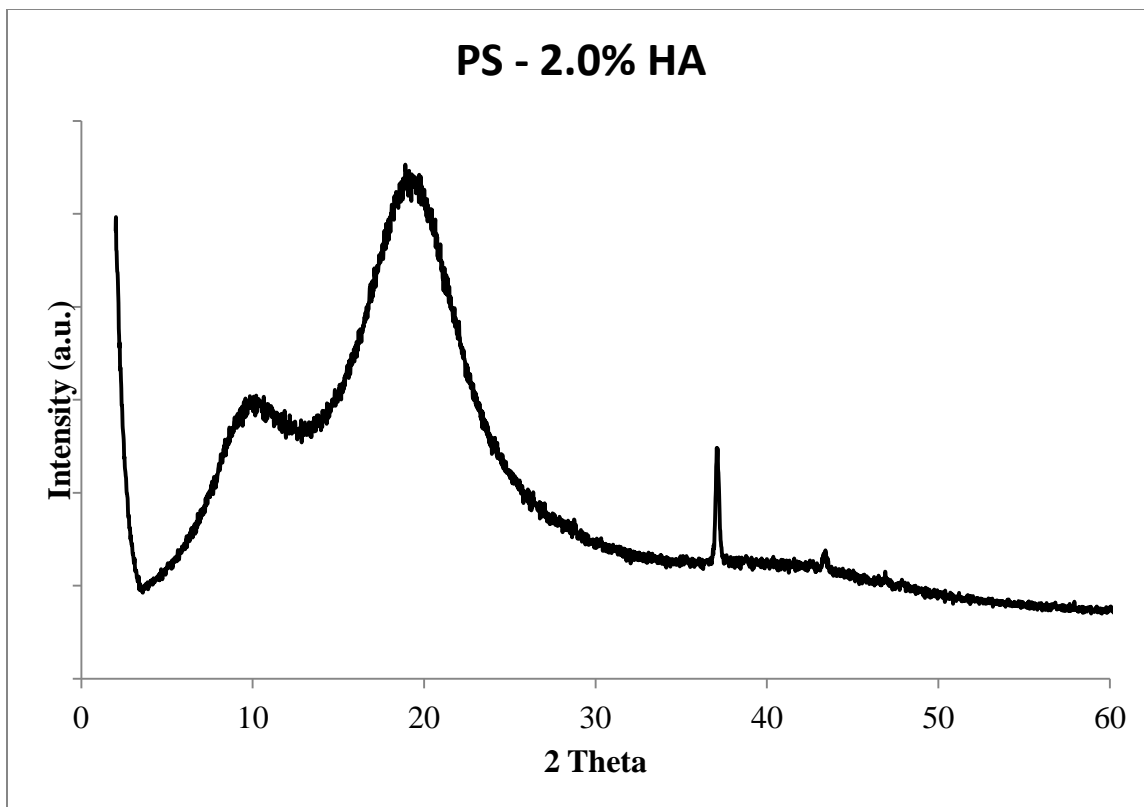


Figure 53: XRD of PS - 2.0% HA sample.

Section G. Individual XRD Scans of PU and FG-PU Samples

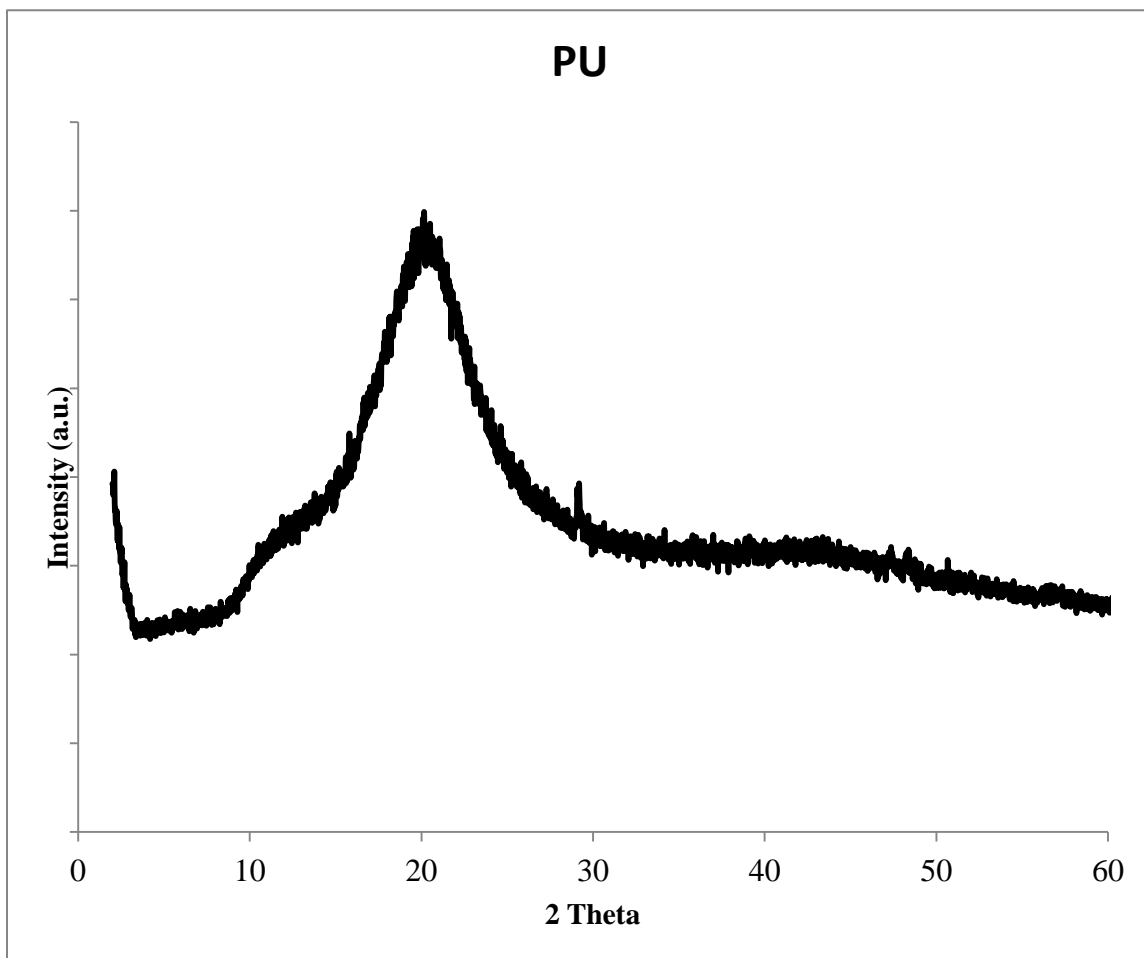


Figure 54: XRD of neat PU sample.

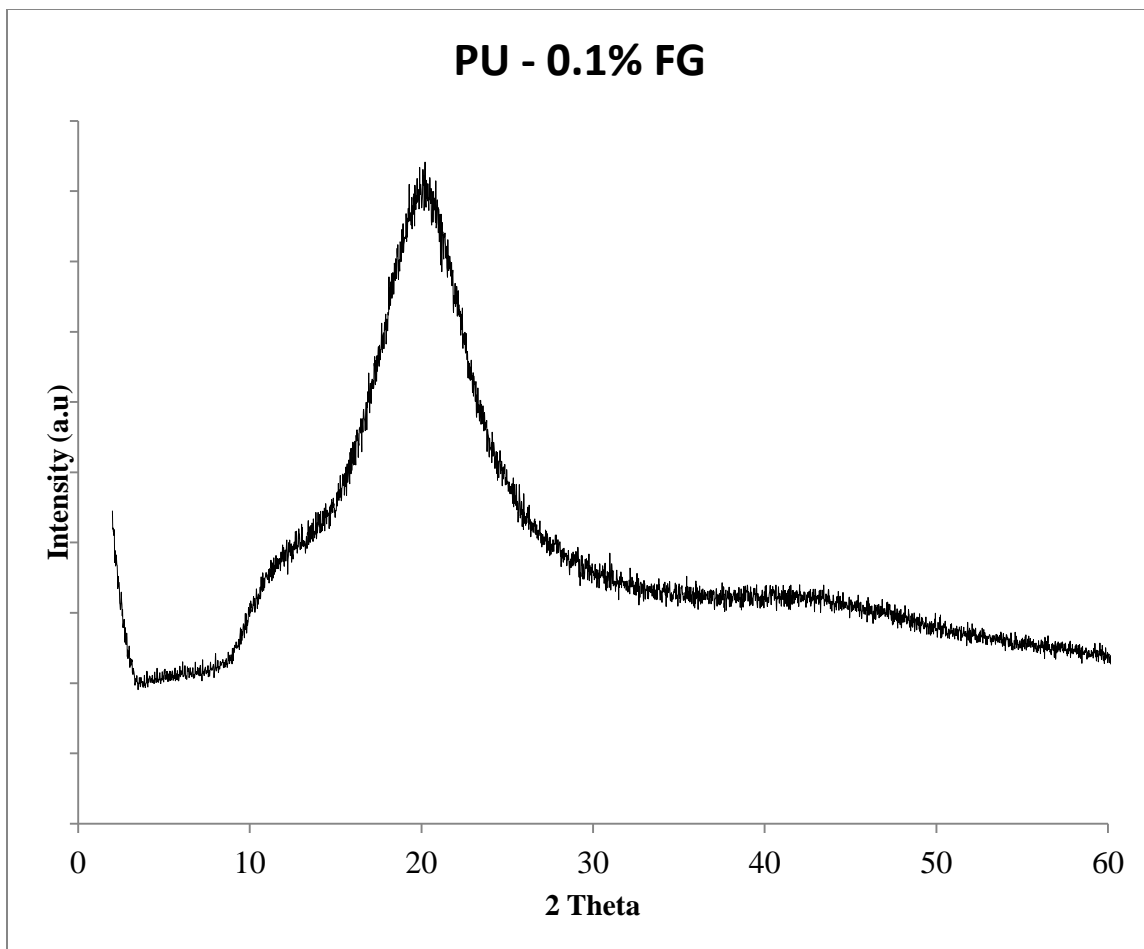


Figure 55: XRD of PU - 0.1% FG sample.

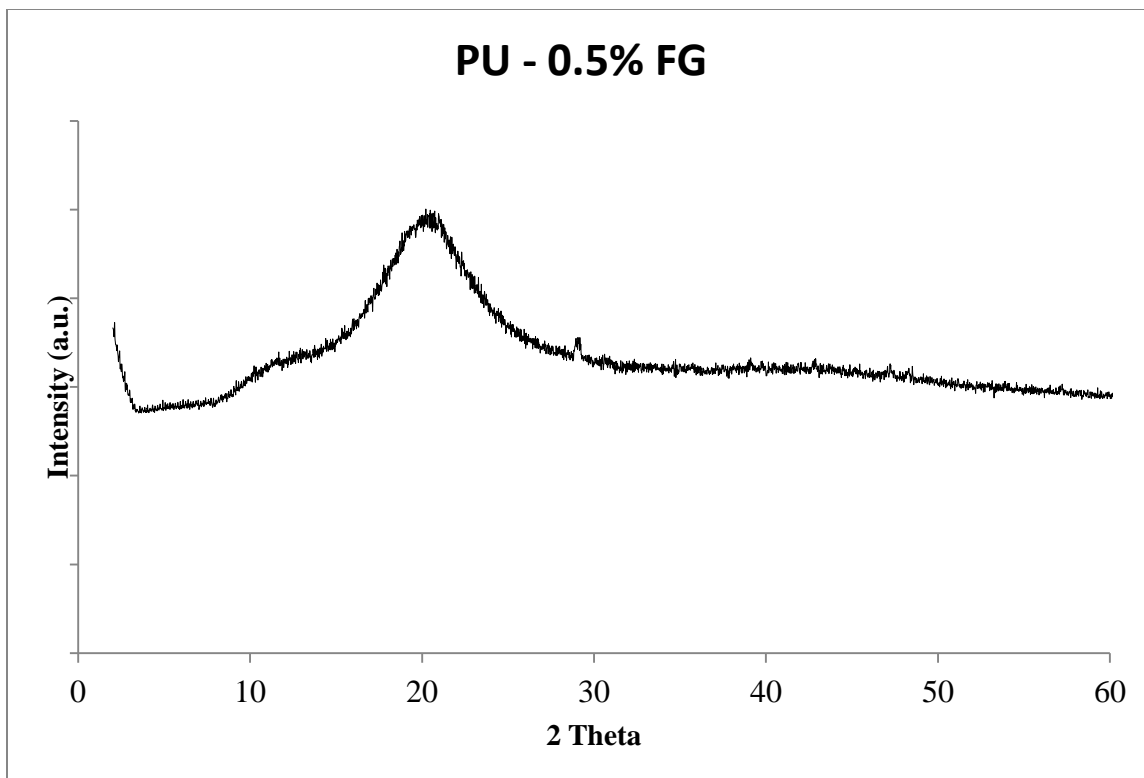


Figure 56: XRD of PU - 0.5% FG sample.

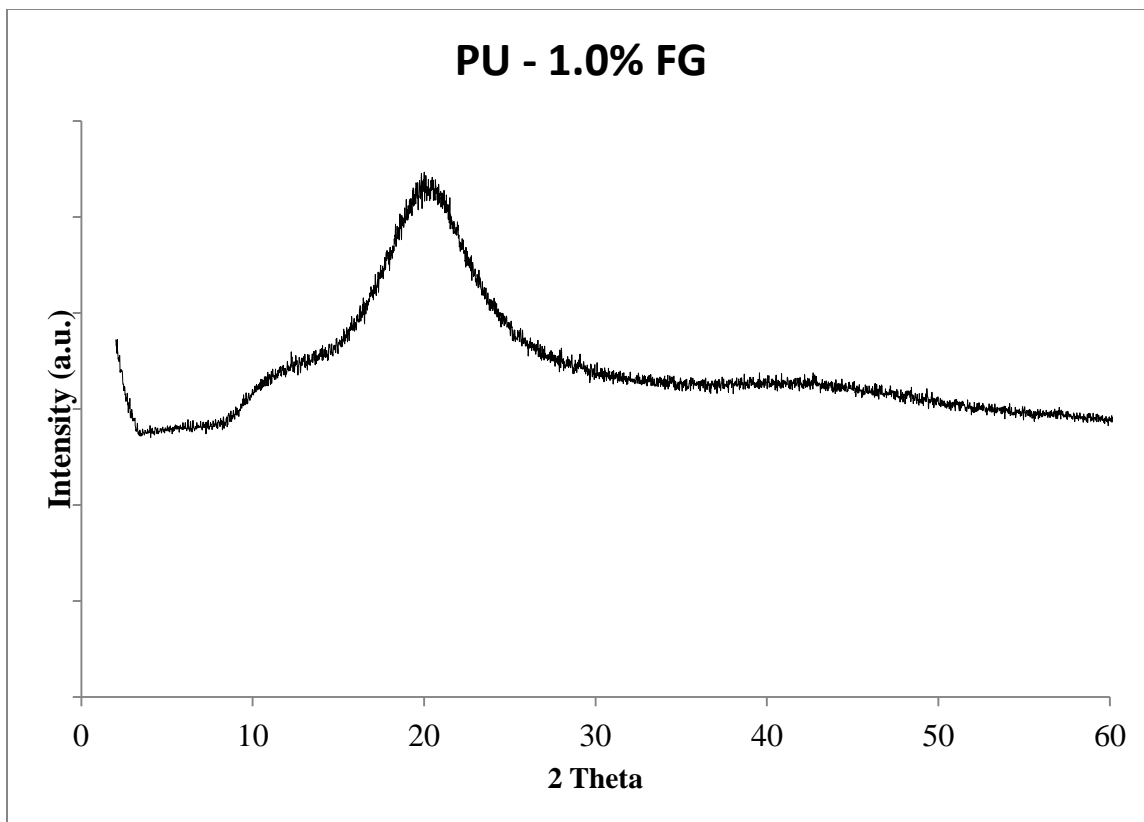


Figure 57: XRD of PU - 1.0% FG sample.

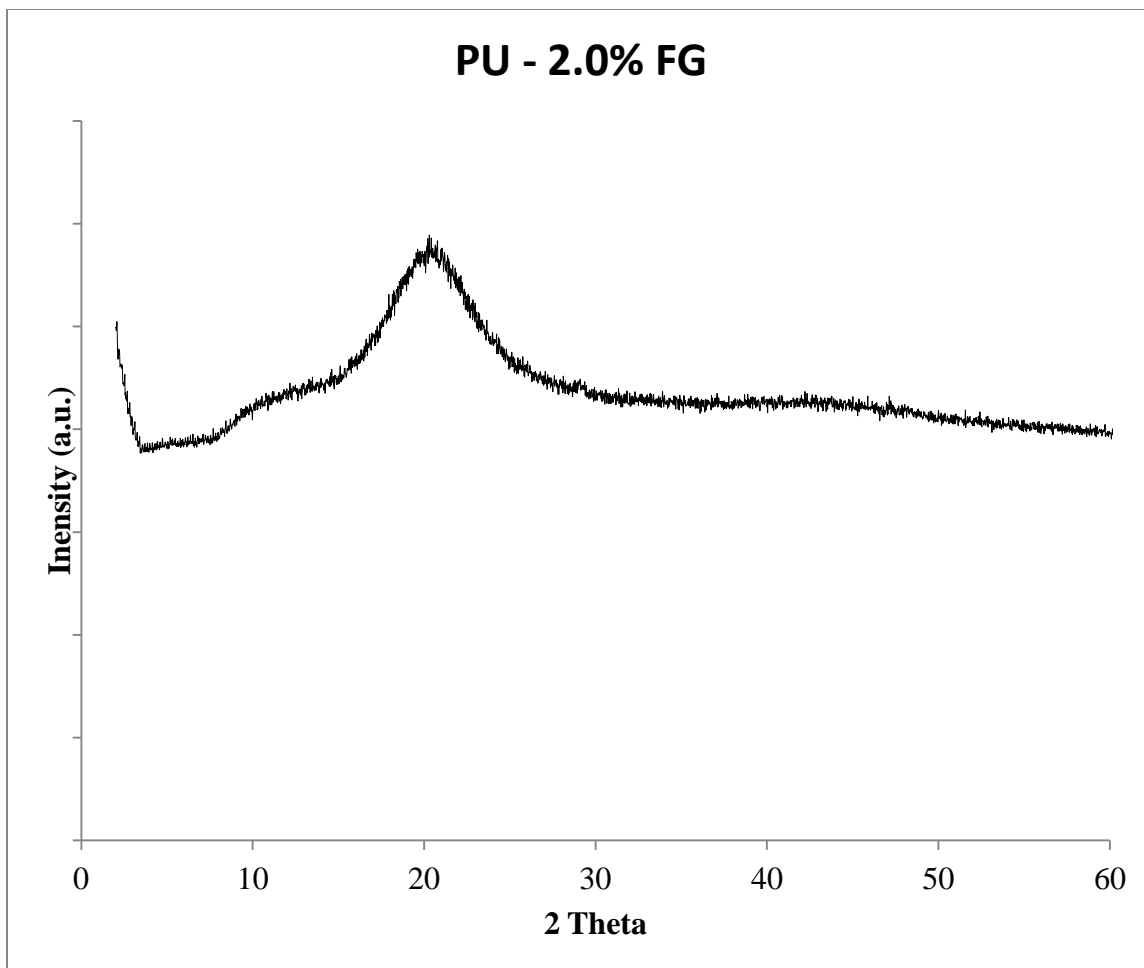


Figure 58: XRD of PU - 2.0% FG sample.

REFERENCES

- (1) Thomas, S.; Joseph, K.; Molhotra, S. K. *Polymer Composites, Volume 1: Macro- and Microcomposites*; Wiley-VCH: Hoboken, NJ, 2012.
- (2) Shaw, A.; Sriramula, S.; Gosling, P. D.; Chryssanthopoulos, M. K. *Compos. Part B Eng.* **2010**, *41* (6), 446–453.
- (3) Menard, K. P. *Dynamic Mechanical Analysis: A Practical Introduction*, 2nd ed.; CRC Press: Boca Raton, FL, 2008.
- (4) Fu, S.-Y.; Feng, X.-Q.; Lauke, B.; Mai, Y.-W. *Compos. Part B Eng.* **2008**, *39* (6), 933–961.
- (5) AZoM.com. E-Glass Fibre <http://www.azom.com/article.aspx?ArticleID=764> (accessed Jun 29, 2015).
- (6) East Coast Fibreglass Supplies Ltd. <http://www.ecfibreglasssupplies.co.uk/t-GlassReinforcedPlastics.aspx>.
- (7) Lee, C.; Wei, X.; Kysar, J. W.; Hone, J. *Science* **2008**, *321* (5887), 385–388.
- (8) The Engineering Toolbox http://www.engineeringtoolbox.com/young-modulus-d_417.html.
- (9) Encyclopaedia Britannica. Nanoparticle <http://www.britannica.com/science/nanoparticle> (accessed Jul 2, 2015).
- (10) Novoselov, K. S.; Fal'ko, V. I.; Colombo, L.; Gellert, P. R.; Schwab, M. G.; Kim, K. *Nature* **2012**, *490* (7419), 192–200.
- (11) Beall, G. W.; Duraia, E.-S. M.; Yu, Q.; Liu, Z. *Phys. E Low-dimensional Syst. Nanostructures* **2014**, *56*, 331–336.
- (12) Badami, D. V. *Nature* **1962**, *193*, 569–570.
- (13) Berger, C.; Song, Z.; Li, T.; Li, X.; Ogbazghi, A. Y.; Feng, R.; Dai, Z.; Marchenkov, A. N.; Conrad, E. H.; First, P. N.; Heer, W. A. De. *J. Phys. Chem. B* **2004**, *108*, 19912–19916.
- (14) Berger, C.; Song, Z.; Li, X.; Wu, X.; Brown, N.; Naud, C.; Mayou, D.; Li, T.; Hass, J.; Marchenkov, A. N.; Conrad, E. H.; First, P. N.; de Heer, W. a. *Science* **2006**, *312* (5777), 1191–1196.
- (15) Emtsev, K. V.; Speck, F.; Seyller, T.; Ley, L. *Phys. Rev. B* **2008**, *77* (15), 155303.

- (16) Hannon, J. B.; Copel, M.; Tromp, R. M. *Phys. Rev. Lett.* **2011**, *107* (16), 166101.
- (17) Borovikov, V.; Zangwill, A. *Phys. Rev. B* **2009**, *80* (12), 121406.
- (18) Hannon, J. B.; Tromp, R. M. *Phys. Rev. B* **2008**, *77* (24), 241404.
- (19) Luxmi, N. S.; Feenstra, R. M.; Fisher, P. J. *J. Vac. Sci. Technol. B Microelectron. Nanom. Struct.* **2010**, *28* (4), C5C1.
- (20) Huang, Q.; Chen, X.; Liu, J.; Wang, W. W.; Wang, G.; Yang, R.; Liu, Y.; Guo, L. *Chem. Commun. (Camb)*. **2010**, *46* (27), 4917–4919.
- (21) Aristov, V. Y.; Urbanik, G.; Kummer, K.; Vyalikh, D. V.; Molodtsova, O. V.; Preobrajenski, A. B.; Zakharov, A. a; Hess, C.; Hänke, T.; Büchner, B.; Vobornik, I.; Fujii, J.; Panaccione, G.; Ossipyan, Y. a; Knupfer, M. *Nano Lett.* **2010**, *10* (3), 992–995.
- (22) Ouerghi, a.; Marangolo, M.; Belkhou, R.; El Moussaoui, S.; Silly, M. G.; Eddrief, M.; Largeau, L.; Portail, M.; Fain, B.; Sirotti, F. *Phys. Rev. B* **2010**, *82* (12), 125445.
- (23) Ouerghi, a.; Balan, a.; Castelli, C.; Picher, M.; Belkhou, R.; Eddrief, M.; Silly, M. G.; Marangolo, M.; Shukla, a.; Sirotti, F. *Appl. Phys. Lett.* **2012**, *101* (2), 021603.
- (24) Hass, J.; Varchon, F.; Millán-Otoya, J.; Sprinkle, M.; Sharma, N.; de Heer, W.; Berger, C.; First, P.; Magaud, L.; Conrad, E. *Phys. Rev. Lett.* **2008**, *100* (12), 125504.
- (25) Virojanadara, C.; Syväjarvi, M.; Yakimova, R.; Johansson, L.; Zakharov, a.; Balasubramanian, T. *Phys. Rev. B* **2008**, *78* (24), 245403.
- (26) Juang, Z.-Y.; Wu, C.-Y.; Lo, C.-W.; Chen, W.-Y.; Huang, C.-F.; Hwang, J.-C.; Chen, F.-R.; Leou, K.-C.; Tsai, C.-H. *Carbon N. Y.* **2009**, *47* (8), 2026–2031.
- (27) Yoneda, T.; Shibuya, M.; Mitsuhashi, K.; Visikovskiy, A.; Hoshino, Y.; Kido, Y. *Surf. Sci.* **2010**, *604* (17-18), 1509–1515.
- (28) Woodworth, A. A.; Stinespring, C. D. *Carbon N. Y.* **2010**, *48* (7), 1999–2003.
- (29) Edwards, R. S.; Coleman, K. S. *Nanoscale* **2013**, *5* (1), 38–51.
- (30) Avouris, P.; Dimitrakopoulos, C. *Mater. Today* **2012**, *15* (3), 86–97.
- (31) Chen, L.; Hernandez, Y.; Feng, X.; Müllen, K. *Angew. Chem. Int. Ed. Engl.* **2012**, *51* (31), 7640–7654.

- (32) Yu, Q.; Lian, J.; Siriponglert, S.; Li, H.; Chen, Y. P.; Pei, S.-S. *Appl. Phys. Lett.* **2008**, *93* (11), 113103.
- (33) An, H.; Lee, W.-J.; Jung, J. *Curr. Appl. Phys.* **2011**, *11* (4), S81–S85.
- (34) Kondo, D.; Yagi, K.; Sato, M.; Nihei, M.; Awano, Y.; Sato, S.; Yokoyama, N. *Chem. Phys. Lett.* **2011**, *514* (4-6), 294–300.
- (35) Sutter, E.; Albrecht, P.; Sutter, P. *Appl. Phys. Lett.* **2009**, *95* (13), 133109.
- (36) Wang, S. M.; Pei, Y. H.; Wang, X.; Wang, H.; Meng, Q. N.; Tian, H. W.; Zheng, X. L.; Zheng, W. T.; Liu, Y. C. *J. Phys. D. Appl. Phys.* **2010**, *43* (45), 455402.
- (37) Ramon, M. E.; Gupta, A.; Corbet, C.; Ferrer, D. A.; Movva, H. C. P.; Ram, M. E.; Carpenter, G.; Colombo, L.; Bourianoff, G.; Doczy, M.; Akinwande, D.; Tutuc, E.; Banerjee, S. K. **2011**, 7198–7204.
- (38) Ago, H.; Ito, Y.; Mizuta, N.; Yoshida, K.; Hu, B.; Orofeo, C. M.; Tsuji, M.; Ikeda, K.; Mizuno, S. *ACS Nano* **2010**, *4* (12), 7407–7414.
- (39) Rut'kov, E. V.; Kuz'michev, a. V.; Gall', N. R. *Phys. Solid State* **2011**, *53* (5), 1092–1098.
- (40) Roth, S.; Osterwalder, J.; Greber, T. *Surf. Sci.* **2011**, *605* (9-10), L17–L19.
- (41) Müller, F.; Grandthyll, S.; Zeitz, C.; Jacobs, K.; Hüfner, S.; Gsell, S.; Schreck, M. *Phys. Rev. B* **2011**, *84* (7), 075472.
- (42) Vo-Van, C.; Kimouche, A.; Reserbat-Plantey, A.; Fruchart, O.; Bayle-Guillemaud, P.; Bendiab, N.; Coraux, J. *Appl. Phys. Lett.* **2011**, *98* (18), 181903.
- (43) Kim, K. S.; Zhao, Y.; Jang, H.; Lee, S. Y.; Kim, J. M.; Kim, K. S.; Ahn, J.-H.; Kim, P.; Choi, J.-Y.; Hong, B. H. *Nature* **2009**, *457* (7230), 706–710.
- (44) Reina, A.; Jia, X.; Ho, J.; Nezich, D.; Son, H. *Nano Lett.* **2009**, *9*, 30–35.
- (45) Reina, A.; Thiele, S.; Jia, X.; Bhaviripudi, S.; Dresselhaus, M. S.; Schaefer, J. a.; Kong, J. *Nano Res.* **2010**, *2* (6), 509–516.
- (46) Chae, S. J.; Güneş, F.; Kim, K. K.; Kim, E. S.; Han, G. H.; Kim, S. M.; Shin, H.-J.; Yoon, S.-M.; Choi, J.-Y.; Park, M. H.; Yang, C. W.; Pribat, D.; Lee, Y. H. *Adv. Mater.* **2009**, *21* (22), 2328–2333.
- (47) Kwon, S.-Y.; Ciobanu, C. V.; Petrova, V.; Shenoy, V. B.; Bareño, J.; Gambin, V.; Petrov, I.; Kodambaka, S. *Nano Lett.* **2009**, *9* (12), 3985–3990.

- (48) Murata, Y.; Nie, S.; Ebnonnasir, a.; Starodub, E.; Kappes, B. B.; McCarty, K. F.; Ciobanu, C. V.; Kodambaka, S. *Phys. Rev. B* **2012**, *85* (20), 205443.
- (49) Gao, T.; Xie, S.; Gao, Y.; Liu, M.; Chen, Y.; Zhang, Y.; Liu, Z. *ACS Nano* **2011**, *5* (11), 9194–9201.
- (50) Mattevi, C.; Kim, H.; Chhowalla, M. *J. Mater. Chem.* **2011**, *21* (10), 3324.
- (51) Li, X.; Cai, W.; An, J.; Kim, S.; Nah, J.; Yang, D.; Piner, R.; Velamakanni, A.; Jung, I.; Tutuc, E.; Banerjee, S. K.; Colombo, L.; Ruoff, R. S. *Science* **2009**, *324* (5932), 1312–1314.
- (52) Liu, W.; Li, H.; Xu, C.; Khatami, Y.; Banerjee, K. *Carbon N. Y.* **2011**, *49* (13), 4122–4130.
- (53) Li, X.; Magnuson, C. W.; Venugopal, A.; An, J.; Suk, J. W.; Han, B.; Borysiak, M.; Cai, W.; Velamakanni, A.; Zhu, Y.; Fu, L.; Vogel, E. M.; Voelkl, E.; Colombo, L.; Ruoff, R. S. *Nano Lett.* **2010**, *10* (11), 4328–4334.
- (54) Li, X.; Magnuson, C.; Venugopal, A.; Tromp, R. M.; Hannon, J. B.; Vogle, E. M.; Colombo, L.; Ruoff, R. S. *J. Am. Chem. Soc.* **2011**, 3–6.
- (55) Lee, Y.; Bae, S.; Jang, H.; Jang, S.; Zhu, S.-E.; Sim, S. H.; Song, Y. II; Hong, B. H.; Ahn, J.-H. *Nano Lett.* **2010**, *10* (2), 490–493.
- (56) Luo, Z.; Lu, Y.; Singer, D. W.; Berck, M. E.; Somers, L. A.; Goldsmith, B. R.; Johnson, A. T. C. **2011**, 1441–1447.
- (57) Oznuher, T.; Pince, E.; Polat, E. O.; Balci, O.; Salihoglu, O.; Kocabas, C. *Appl. Phys. Lett.* **2011**, *98* (18), 183101.
- (58) Liu, N.; Fu, L.; Dai, B.; Yan, K.; Liu, X.; Zhao, R.; Zhang, Y.; Liu, Z. *Nano Lett.* **2011**, *11* (1), 297–303.
- (59) Liu, X.; Fu, L.; Liu, N.; Gao, T.; Zhang, Y.; Liao, L.; Liu, Z. *J. Phys. ...* **2011**, 11976–11982.
- (60) Chen, S.; Brown, L.; Levendorf, M.; Cai, W.; Ju, S.-Y.; Edgeworth, J.; Li, X.; Magnuson, C. W.; Velamakanni, A.; Piner, R. D.; Kang, J.; Park, J.; Ruoff, R. S. *ACS Nano* **2011**, *5* (2), 1321–1327.
- (61) Chen, S.; Cai, W.; Piner, R. D.; Suk, J. W.; Wu, Y.; Ren, Y.; Kang, J.; Ruoff, R. S. *Nano Lett.* **2011**, *11* (9), 3519–3525.
- (62) Weatherup, R. S.; Bayer, B. C.; Blume, R.; Ducati, C.; Baetz, C.; Schlögl, R.; Hofmann, S. *Nano Lett.* **2011**, *11* (10), 4154–4160.

- (63) Dai, B.; Fu, L.; Zou, Z.; Wang, M.; Xu, H.; Wang, S.; Liu, Z. *Nat. Commun.* **2011**, 2 (May), 522.
- (64) John, R.; Ashokreddy, a; Vijayan, C.; Pradeep, T. *Nanotechnology* **2011**, 22 (16), 165701.
- (65) Gullapalli, H.; Reddy, A. L. M.; Kilpatrick, S.; Dubey, M.; Ajayan, P. M. *Small* **2011**, 7, 1697–1700.
- (66) Chen, W.; Chen, H.; Lan, H.; Cui, P.; Schulze, T. P.; Zhu, W.; Zhang, Z. *Phys. Rev. Lett.* **2012**, 109 (26), 265507.
- (67) Liang, X.; Sperling, B. a; Calizo, I.; Cheng, G.; Hacker, C. A.; Zhang, Q.; Obeng, Y.; Yan, K.; Peng, H.; Li, Q.; Zhu, X.; Yuan, H.; Walker, A. R. H.; Liu, Z.; Peng, L.-M.; Richter, C. a. *ACS Nano* **2011**, 5 (11), 9144–9153.
- (68) Liu, N.; Pan, Z.; Fu, L.; Zhang, C.; Dai, B.; Liu, Z. *Nano Res.* **2011**, 4 (10), 996–1004.
- (69) Qi, J. L.; Zheng, W. T.; Zheng, X. H.; Wang, X.; Tian, H. W. *Appl. Surf. Sci.* **2011**, 257 (15), 6531–6534.
- (70) Terasawa, T.; Saiki, K. *Carbon N. Y.* **2012**, 50 (3), 869–874.
- (71) Yuan, G. D.; Zhang, W. J.; Yang, Y.; Tang, Y. B.; Li, Y. Q.; Wang, J. X.; Meng, X. M.; He, Z. B.; Wu, C. M. L.; Bello, I.; Lee, C. S.; Lee, S. T. *Chem. Phys. Lett.* **2009**, 467 (4-6), 361–364.
- (72) Kim, J.; Ishihara, M.; Koga, Y.; Tsugawa, K.; Hasegawa, M.; Iijima, S. *Appl. Phys. Lett.* **2011**, 98 (9), 091502.
- (73) Zhu, M.; Wang, J.; Holloway, B. C.; Outlaw, R. a.; Zhao, X.; Hou, K.; Shutthanandan, V.; Manos, D. M. *Carbon N. Y.* **2007**, 45 (11), 2229–2234.
- (74) Nandamuri, G.; Roumimov, S.; Solanki, R. *Appl. Phys. Lett.* **2010**, 96 (15), 154101.
- (75) Herron, C. R.; Coleman, K. S.; Edwards, R. S.; Mendis, B. G. *J. Mater. Chem.* **2011**, 21 (10), 3378.
- (76) Dato, A.; Frenklach, M. *New J. Phys.* **2010**, 12 (12), 125013.
- (77) Dato, A.; Radmilovic, V.; Lee, Z.; Phillips, J.; Frenklach, M. *Nano Lett.* **2008**, 8 (7), 2012–2016.
- (78) Berresheim, A. J.; Muller, M.; Mullen, K. *Chem. Rev.* **1999**, 99, 1747–1785.

- (79) Dotz, F.; Brand, J. D.; Ito, S.; Gherghel, L.; Mullen, K. *J. Am. Chem. Soc.* **2000**, *122*, 7707–7717.
- (80) Müller, M.; Kübel, C.; Müllen, K. *Chem. - A Eur. J.* **1998**, *4* (11), 2099–2109.
- (81) Tyutyulkov, N.; Madjarova, G.; Dietz, F.; Mullen, K. *J. Phys. ...* **1998**, *102*, 10183–10189.
- (82) Watson, M. D.; Fechtenko, A.; Mullen, K. *Chem. Rev.* **2001**, *101*, 1267–1300.
- (83) Gutman, I.; Tomović, Ž.; Müllen, K.; Rabe, J. P. *Chem. Phys. Lett.* **2004**, *397* (4-6), 412–416.
- (84) Simpson, C. D.; Brand, J. D.; Berresheim, A. J.; Przybilla, L.; Räder, H. J.; Müllen, K. *Chemistry* **2002**, *8* (6), 1424–1429.
- (85) Nuckolls, C.; Katz, T. J.; Castellanos, L. *J. Am. Chem. Soc.* **1996**, *118*, 3767–3768.
- (86) Kastler, M.; Schmidt, J.; Pisula, W.; Sebastiani, D.; Mullen, K. *J. Am. Chem. Soc.* **2006**, *128*, 9526–9534.
- (87) Draper, S. M.; Gregg, D. J.; Madathil, R. *J. Am. Chem. Soc.* **2002**, *124*, 3486–3487.
- (88) Allen, M. J.; Tung, V. C.; Kaner, R. B. *Chem. Rev.* **2010**, *110*, 132–145.
- (89) Novoselov, K. S.; Geim, A. K.; Morozov, S. V.; Jiang, D.; Zhang, Y.; Dubonos, S. V.; Grigorieva, I. V.; Firsov, A. A. *Science (80-.)*. **2004**, *306* (5696), 666–669.
- (90) Hernandez, Y.; Nicolosi, V.; Lotya, M.; Blighe, F. M.; Sun, Z.; De, S.; McGovern, I. T.; Holland, B.; Byrne, M.; Gun'Ko, Y. K.; Boland, J. J.; Niraj, P.; Duesberg, G.; Krishnamurthy, S.; Goodhue, R.; Hutchison, J.; Scardaci, V.; Ferrari, A. C.; Coleman, J. N. *Nat. Nanotechnol.* **2008**, *3* (9), 563–568.
- (91) Hernandez, Y.; Lotya, M.; Rickard, D.; Bergin, S. D.; Coleman, J. N. *Langmuir* **2010**, *26* (5), 3208–3213.
- (92) Aylesworth, J. W. Expanded Graphite. 1191383, 1916.
- (93) Chung, D. D. L. *J. Mater. Sci.* **1987**, *22*, 4190–4198.
- (94) Safavi, A.; Mahyari, F. A.; Tohidi, M. *Mater. Res. Bull.* **2013**, *48* (9), 3399–3404.
- (95) Fu, W.; Kiggans, J.; Overbury, S. H.; Schwartz, V.; Liang, C. *Chem. Commun. (Camb)*. **2011**, *47* (18), 5265–5267.

- (96) Pu, N.-W.; Wang, C.-A.; Sung, Y.; Liu, Y.-M.; Ger, M.-D. *Mater. Lett.* **2009**, *63* (23), 1987–1989.
- (97) Nomine, M.; Bonnetain, L. *J. Chim. Phys.* **1969**, *66*, 1731.
- (98) Beguin, F.; Setton, R.; Hamwi, A.; Touzain, P. *Mater. Sci. Eng.* **1979**, *40*, 167–173.
- (99) Vallés, C.; Drummond, C.; Saadaoui, H.; Furtado, C. A.; He, M.; Roubeau, O.; Ortolani, L.; Monthieux, M.; Pénicaud, A. *J. Am. Chem. Soc.* **2008**, *130*, 15802–15804.
- (100) Enoki, T.; Suzuki, M.; Endo, M. *Graphite Intercalation Compounds and Applications*; Oxford University Press, Inc.: Oxford, 2003.
- (101) Wang, G.; Wang, B.; Park, J.; Wang, Y.; Sun, B.; Yao, J. *Carbon N. Y.* **2009**, *47* (14), 3242–3246.
- (102) Englert, J. M.; Rohrl, J.; Schmidt, C. D.; Graupner, R.; Hundhausen, M.; Hauke, F.; Hirsch, A. *Adv. Mater.* **2009**, *21* (42), 4265–4269.
- (103) Brownson, D. a. C.; Metters, J. P.; Kampouris, D. K.; Banks, C. E. *Electroanalysis* **2011**, *23* (4), 894–899.
- (104) Su, C.-Y.; Lu, A.-Y.; Xu, Y.; Chen, F.-R.; Khlobystov, A. N.; Li, L.-J. *ACS Nano* **2011**, *5* (3), 2332–2339.
- (105) Wang, J.; Manga, K. K.; Bao, Q.; Loh, K. P. *J. Am. Chem. Soc.* **2011**, *133*, 8888–8891.
- (106) Huang, H.; Xia, Y.; Tao, X.; Du, J.; Fang, J.; Gan, Y.; Zhang, W. *J. Mater. Chem.* **2012**, *22*, 10452–10456.
- (107) Suslick, K. S.; Price, G. J. *Annu. Rev. Mater. Sci.* **1999**, *29* (1), 295–326.
- (108) Farhat, S.; Scott, C. D. *J. Nanosci. Nanotechnol.* **2006**, *6* (5), 1189–1210.
- (109) Subrahmanyam, K. S.; Panchakarla, L. S.; Govindaraj, a.; Rao, C. N. R. *J. Phys. Chem. C* **2009**, *113* (11), 4257–4259.
- (110) Chen, Y.; Zhao, H.; Sheng, L.; Yu, L.; An, K.; Xu, J.; Ando, Y.; Zhao, X. *Chem. Phys. Lett.* **2012**, *538*, 72–76.
- (111) Shen, B.; Ding, J.; Yan, X.; Feng, W.; Li, J.; Xue, Q. *Appl. Surf. Sci.* **2012**, *258* (10), 4523–4531.

- (112) Tung, V. C.; Allen, M. J.; Yang, Y.; Kaner, R. B. *Nat. Nanotechnol.* **2009**, *4* (1), 25–29.
- (113) Schafheutl, C. *J. für Prakt. Chemie* **1840**, *21*, 129–157.
- (114) Schafheutl, C. *Philos. Mag.* **1840**, *16*, 570–590.
- (115) Brodie, B. C. *Philos. Trans. R. Soc. London* **1859**, *1859*, 249–259.
- (116) Staudenmaier, L. *Berichte der Dtsch. Chem. Gesellschaft* **1898**, *31*, 1481–1487.
- (117) Hummers, W. S.; Offeman, R. E. *J. Am. Chem. Soc.* **1958**, *80*, 1339.
- (118) Dreyer, D. R.; Park, S.; Bielawski, C. W.; Ruoff, R. S. *Chem. Soc. Rev.* **2010**, *39* (1), 228–240.
- (119) Lerf, A.; He, H.; Forster, M.; Klinowski, J. *J. Phys. ...* **1998**, *5647* (97), 4477–4482.
- (120) He, H.; Klinowski, J.; Forster, M.; Lerf, A. *Chem. Phys. Lett.* **1998**, 287 (April), 98–101.
- (121) Szabó, T.; Berkesi, O.; Forgó, P. *Chem. ...* **2006**, *18* (11), 2740–2749.
- (122) Stankovich, S.; Dikin, D. a.; Piner, R. D.; Kohlhaas, K. a.; Kleinhammes, A.; Jia, Y.; Wu, Y.; Nguyen, S. T.; Ruoff, R. S. *Carbon N. Y.* **2007**, *45* (7), 1558–1565.
- (123) Fernandez-Merina, M. J.; Guardia, L.; Paredes, J. I.; Villar-Rodil, S.; Solis-Fernandez, P.; Martinez-Alonso, A.; Tascon, J. M. D. *J. Phys. Chem. C* **2010**, *114*, 6426–6432.
- (124) Shin, H.-J.; Kim, K. K.; Benayad, A.; Yoon, S.-M.; Park, H. K.; Jung, I.-S.; Jin, M. H.; Jeong, H.-K.; Kim, J. M.; Choi, J.-Y.; Lee, Y. H. *Adv. Funct. Mater.* **2009**, *19* (12), 1987–1992.
- (125) Periasamy, M.; Thirumalaikumar, M. *J. Organomet. Chem.* **2000**, *609* (1-2), 137–151.
- (126) Gao, W.; Alemany, L. B.; Ci, L.; Ajayan, P. M. *Nat. Chem.* **2009**, *1* (5), 403–408.
- (127) Pei, S.; Zhao, J.; Du, J.; Ren, W.; Cheng, H.-M. *Carbon N. Y.* **2010**, *48* (15), 4466–4474.
- (128) Moon, I. K.; Lee, J.; Ruoff, R. S.; Lee, H. *Nat. Commun.* **2010**, *1* (6), 73.

- (129) Wang, G.; Yang, J.; Park, J.; Gou, X.; Wang, B.; Liu, H.; Yao, J. *J. Phys. Chem. C* **2008**, *112* (22), 8192–8195.
- (130) Fan, X.; Peng, W.; Li, Y.; Li, X.; Wang, S.; Zhang, G.; Zhang, F. *Adv. Mater.* **2008**, *20* (23), 4490–4493.
- (131) Zhou, X.; Zhang, J.; Wu, H.; Yang, H.; Zhang, J.; Guo, S. *J. Phys. Chem. C* **2011**, *115* (24), 11957–11961.
- (132) Pei, S.; Cheng, H.-M. *Carbon N. Y.* **2012**, *50* (9), 3210–3228.
- (133) Zhou, T.; Chen, F.; Tang, C.; Bai, H.; Zhang, Q.; Deng, H.; Fu, Q. *Compos. Sci. Technol.* **2011**, *71* (9), 1266–1270.
- (134) Chua, C. K.; Ambrosi, A.; Pumera, M. *J. Mater. Chem.* **2012**, *22* (22), 11054.
- (135) Williams, G.; Seger, B.; Kamat, P. V. **2008**, *2* (7), 1487–1491.
- (136) Williams, G.; Kamat, P. V. *Langmuir* **2009**, *25* (24), 13869–13873.
- (137) Ng, Y. H.; Iwase, A.; Kudo, A.; Amal, R. *J. Phys. Chem. Lett.* **2010**, *1* (17), 2607–2612.
- (138) Zhang, H.; Lv, X.; Li, Y.; Wang, Y.; Li, J. *ACS Nano* **2010**, *4* (1), 380–386.
- (139) Yang, N.; Zhai, J.; Wang, D.; Chen, Y.; Jiang, L. *ACS Nano* **2010**, *4* (2), 887–894.
- (140) Kim, S. R.; Parvez, M. K.; Chhowalla, M. *Chem. Phys. Lett.* **2009**, *483* (1-3), 124–127.
- (141) Zhou, M.; Wang, Y.; Zhai, Y.; Zhai, J.; Ren, W.; Wang, F.; Dong, S. *Chemistry* **2009**, *15* (25), 6116–6120.
- (142) Wang, Z.; Zhou, X.; Zhang, J.; Boey, F.; Zhang, H. *J. Phys. Chem. C* **2009**, *113* (32), 14071–14075.
- (143) An, S. J.; Zhu, Y.; Lee, S. H.; Stoller, M. D.; Emilsson, T.; Park, S.; Velamakanni, A.; An, J.; Ruoff, R. S. *J. Phys. Chem. Lett.* **2010**, *1* (8), 1259–1263.
- (144) Ramesha, G. K.; Sampath, S. *J. Phys. Chem. C* **2009**, *113* (19), 7985–7989.
- (145) Pressions, I. H.; Supe, E. N. **1998**, No. 1, 24–26.
- (146) Sun, X.; Li, Y. *Angew. Chem. Int. Ed. Engl.* **2004**, *43* (5), 597–601.
- (147) Luo, L.; Yu, S.; Qian, H.; Zhou, T. *J. Am. Chem. Soc.* **2005**, *127* (10), 2822–2823.

- (148) Zhou, Y.; Bao, Q.; Tang, L. A. L.; Zhong, Y.; Loh, K. P. *Chem. Mater.* **2009**, *21* (13), 2950–2956.
- (149) Wang, H.; Robinson, J. T.; Li, X.; Dai, H. *J. Chem. Soc.* **2009**, *131* (29), 9910–9911.
- (150) Dubin, S.; Gilje, S.; Wang, K.; Tung, V. C.; Cha, K.; Hall, A. S.; Farrar, J.; Varshneya, R.; Yang, Y.; Kaner, R. B. *ACS Nano* **2010**, *4* (7), 3845–3852.
- (151) Schniepp, H. C.; Li, J.-L.; McAllister, M. J.; Sai, H.; Herrera-Alonso, M.; Adamson, D. H.; Prud'homme, R. K.; Car, R.; Saville, D. a; Aksay, I. a. *J. Phys. Chem. B* **2006**, *110* (17), 8535–8539.
- (152) Kudin, K. N.; Ozbas, B.; Schniepp, H. C.; Prud, R. K.; Aksay, I. A.; Car, R. **2008**, No. Figure 1, 1–6.
- (153) Becerril, H. a; Mao, J.; Liu, Z.; Stoltenberg, R. M.; Bao, Z.; Chen, Y. *ACS Nano* **2008**, *2* (3), 463–470.
- (154) Mattevi, C.; Eda, G.; Agnoli, S.; Miller, S.; Mkhoyan, K. A.; Celik, O.; Mastrogiovanni, D.; Granozzi, G.; Garfunkel, E.; Chhowalla, M. *Adv. Funct. Mater.* **2009**, *19* (16), 2577–2583.
- (155) Yang, D.; Velamakanni, A.; Bozoklu, G.; Park, S.; Stoller, M.; Piner, R. D.; Stankovich, S.; Jung, I.; Field, D. a.; Ventrice, C. a.; Ruoff, R. S. *Carbon N. Y.* **2009**, *47* (1), 145–152.
- (156) Wang, X.; Zhi, L.; Mullen, K. *Nano Lett.* **2008**, *8* (1), 323–327.
- (157) Pan, D.; Zhang, J.; Li, Z.; Wu, M. *Adv. Mater.* **2010**, *22* (6), 734–738.
- (158) Wu, Z.-S.; Ren, W.; Gao, L.; Liu, B.; Jiang, C.; Cheng, H.-M. *Carbon N. Y.* **2009**, *47* (2), 493–499.
- (159) Wu, Z.-S.; Ren, W.; Gao, L.; Zhao, J.; Chen, Z.; Liu, B.; Tang, D.; Yu, B.; Jiang, C.; Cheng, H.-M. *ACS Nano* **2009**, *3* (2), 411–417.
- (160) Li, X.; Wang, H.; Robinson, J.; Sanchez, H.; Diankov, G.; Dai, H. *J. Am. Chem. Soc.* **2009**, *131* (13), 15939–15944.
- (161) Gengler, R. Y. N.; Veligura, A.; Enotiadis, A.; Diamanti, E. K.; Gournis, D.; Józsa, C.; van Wees, B. J.; Rudolf, P. *Small* **2010**, *6* (1), 35–39.
- (162) Su, Q.; Pang, S.; Alijani, V.; Li, C.; Feng, X.; Müllen, K. *Adv. Mater.* **2009**, *21* (31), 3191–3195.

- (163) Zhu, Y.; Murali, S.; Stoller, M. D.; Velamakanni, A.; Piner, R. D.; Ruoff, R. S. *Carbon N. Y.* **2010**, *48* (7), 2118–2122.
- (164) Hassan, H. M. a.; Abdelsayed, V.; Khder, A. E. R. S.; AbouZeid, K. M.; Turner, J.; El-Shall, M. S.; Al-Resayes, S. I.; El-Azhary, A. a. *J. Mater. Chem.* **2009**, *19* (23), 3832.
- (165) Cote, L.; Cruz-Silva, R.; Huang, J. *J. Am. Chem. Soc.* **2009**, *131* (17), 11027–11032.
- (166) Zhang, Y.; Guo, L.; Wei, S.; He, Y.; Xia, H.; Chen, Q.; Sun, H.-B.; Xiao, F.-S. *Nano Today* **2010**, *5* (1), 15–20.
- (167) Lin, Y.; Dimitrakopoulos, C.; Jenkins, K. A.; Farmer, D. B.; Chiu, H.; Grill, A.; Avouris, P. *Science (80-.)*. **2010**, *327*, 100.
- (168) Tzalenchuk, A.; Lara-Avila, S.; Kalaboukhov, A.; Paolillo, S.; Syväjärvi, M.; Yakimova, R.; Kazakova, O.; Janssen, T. J. B. M.; Fal'ko, V.; Kubatkin, S. *Nat. Nanotechnol.* **2010**, *5* (3), 186–189.
- (169) Bae, S.; Kim, H.; Lee, Y.; Xu, X.; Park, J.-S.; Zheng, Y.; Balakrishnan, J.; Lei, T.; Kim, H. R.; Song, Y. Il; Kim, Y.-J.; Kim, K. S.; Ozyilmaz, B.; Ahn, J.-H.; Hong, B. H.; Iijima, S. *Nat. Nanotechnol.* **2010**, *5* (8), 574–578.
- (170) Dato, A.; Frenklach, M. *New J. Phys.* **2010**, *12* (12), 125013.
- (171) Lotya, M.; Hernandez, Y.; King, P. J.; Smith, R. J.; Nicolosi, V.; Karlsson, L. S.; Blighe, F. M.; De, S.; Wang, Z.; McGovern, I. T.; Duesberg, G. S.; Coleman, J. N. *J. Am. Chem. Soc.* **2009**, *131* (11), 3611–3620.
- (172) Lotya, M.; King, P. J.; Khan, U.; De, S.; Coleman, J. N. *ACS Nano* **2010**, *4* (6), 3155–3162.
- (173) Khan, U.; O'Neill, A.; Lotya, M.; De, S.; Coleman, J. N. *Small* **2010**, *6* (7), 864–871.
- (174) MatWeb
<http://www.matweb.com/search/datasheettext.aspx?matguid=5d84c510a8a243faa8d2a9caec5837ba> (accessed Jun 15, 2015).
- (175) Henderson, B. G. MS Thesis: Investigation of Graphenol as a Nanofiller, Texas State University, 2015.
- (176) Tuinstra, F.; Koenig, L. *J. Chem. Phys.* **1970**, *53* (1970), 1126–1130.

- (177) Elias, D.; Nair, R.; Mohiuddin, T.; Morozov, S.; Blake, P.; Halsall, M.; Ferrari, A.; Boukhvalov, D.; Katsnelson, M.; Geim, A.; Novoselov, K. *Science* (80-.). **2009**, *323* (January), 610–613.
- (178) Al-Hazmi, F. S.; Al-Harbi, G. H.; Beall, G. W.; Al-Ghamdi, a. a.; Obaid, a. Y.; Mahmoud, W. E. *Synth. Met.* **2015**, *200*, 54–57.
- (179) Stankovich, S.; Dikin, D. A.; Dommett, G. H.; Kohlhaas, K. M.; Zimney, E. J.; Stach, E. A.; Piner, R. D.; Nguyen, S. T.; Ruoff, R. S. *Nature* **2006**, *442* (7100), 282–286.
- (180) Cui, P.; Lee, J.; Hwang, E.; Lee, H. *Chem. Commun.* **2011**, *47* (45), 12370.
- (181) Zhang, J.; Yang, H.; Shen, G.; Cheng, P.; Zhang, J.; Guo, S. *Chem. Commun. (Camb)*. **2010**, *46* (7), 1112–1114.
- (182) Beall, G. W.; Powell, C. E. *Polymer-Clay Nanocomposites*; Cambridge Univ Press: New York, 2011.
- (183) Pham, V. H.; Dang, T. T.; Hur, S. H.; Kim, E. J.; Chung, J. S. *ACS Appl. Mater. Interfaces* **2012**, *4* (5), 2630–2636.
- (184) Cai, D.; Yusoh, K.; Song, M. *Nanotechnology* **2009**, *20* (8), 085712.
- (185) Song, P.; Cao, Z.; Cai, Y.; Zhao, L.; Fang, Z.; Fu, S. *Polymer (Guildf)*. **2011**, *52* (18), 4001–4010.
- (186) Halpin, J. C. *J. Compos. Mater.* **1969**, *3*, 732–734.
- (187) Halpin, J. C.; Kardos, J. L. *Polym. Eng. Sci.* **1976**, *16* (5), 344–352.
- (188) Fornes, T. D.; Paul, D. R. *Polymer (Guildf)*. **2003**, *44* (17), 4993–5013.
- (189) Jiang, J.-W.; Wang, J.-S.; Li, B. **2009**, 15–18.
- (190) Bayer MaterialScience. Bayhydrol 124 - Product Information. *Online*, 2004, 1–2.
- (191) Webmineral Webpage - Graphite Mineral Data
<http://webmineral.com/data/Graphite.shtml#.VYR9z0ZWJnl> (accessed Jun 19, 2015).